AD-A114 771 GEORGIA INST OF TECH ATLANTA SCHOOL OF AEROSPACE ENG--ETC F/G 21/9.2
ROCKET RESEARCH AT GEORGIA TECH.(U)
NOV 81 E W PRICE, W C STRAHLE, B T ZINN F49620-78-C-0003
UNCLASSIFIED AFOSR-TR-82-0368 NL

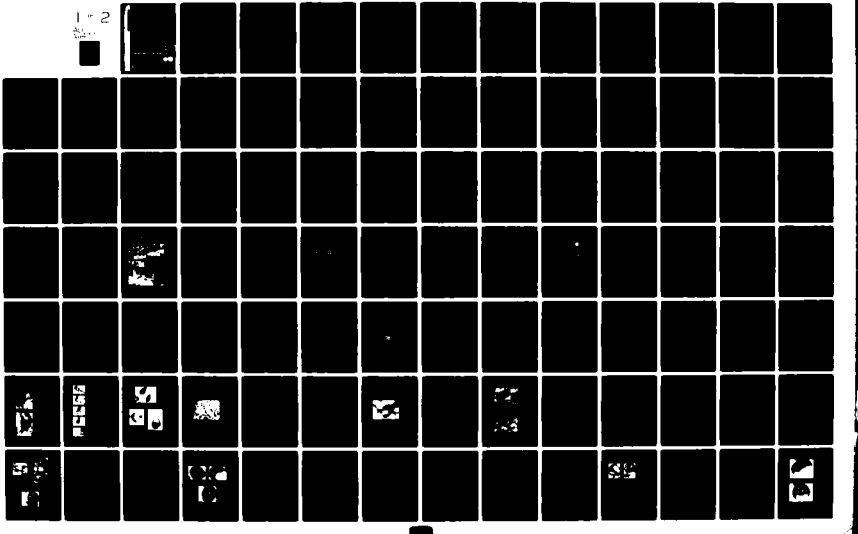

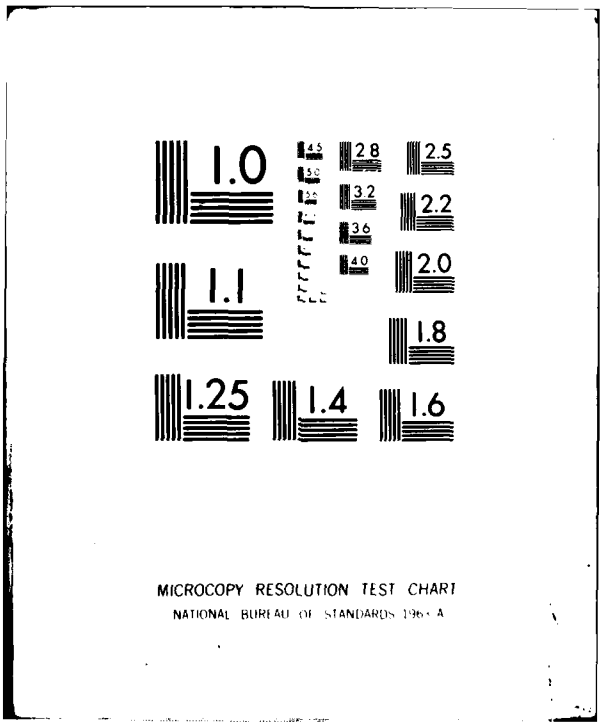
1.0
1.1
1.25
1.4
1.6
1.8
2.0
2.2
2.5
2.8
3.2
3.6
4.0
4.5
5.0
MICROCOPY RESOLUTION TEST CHART
NATIONAL BUREAU OF STANDARDS 1963 A

AFOSR-TR- 82-0368

AFOSR FINAL SCIENTIFIC REPORT

ROCKET RESEARCH AT GEORGIA TECH

Co-Principal Investigators

E. W. Price
W. C. Strahle
B. T. Zinn
J. E. Hubbartt
R. K. Sigman
B. R. Daniel

Prepared for

AIR FORCE OFFICE OF SCIENTIFIC RESEARCH
AEROSPACE SCIENCES DIRECTORATE
BOLLING AIR FORCE BASE, D.C.

Under

Contract No. F49620-78-C-0003

November 1981

GEORGIA INSTITUTE OF TECHNOLOGY
A UNIT OF THE UNIVERSITY SYSTEM OF GEORGIA
SCHOOL OF AEROSPACE ENGINEERING
ATLANTA, GEORGIA 30332

UNCLASSIFIED

SECURITY CLASSIFICATION OF THIS PAGE *(When Data Entered)*

REPORT DOCUMENTATION PAGE		READ INSTRUCTIONS BEFORE COMPLETING FORM
1. REPORT NUMBER AFOSR-TR-82-0368	2. GOVT ACCESSION NO.	3. RECIPIENT'S CATALOG NUMBER
4. TITLE *(and Subtitle)* ROCKET RESEARCH AT GEORGIA TECH		5. TYPE OF REPORT & PERIOD COVERED FINAL 1 OCT 77 - 30 SEPT 81 6. PERFORMING ORG. REPORT NUMBER
7. AUTHOR(s) E. W. Price, W. C. Strahle, B. T. Zinn, J. E. Hubbartt, R. K. Sigman, B. R. Daniel		8. CONTRACT OR GRANT NUMBER(s) [redacted]F49620-78-C-0003
9. PERFORMING ORGANIZATION NAME AND ADDRESS GEORGIA INSTITUTE OF TECHNOLOGY SCHOOL OF AEROSPACE ENGINEERING ATLANTA, GA 30332		10. PROGRAM ELEMENT, PROJECT, TASK AREA & WORK UNIT NUMBERS 61102F 2308 A1
11. CONTROLLING OFFICE NAME AND ADDRESS AIR FORCE OFFICE OF SCIENTIFIC RESEARCH/NA BLDG. 410 BOLLING AIR FORCE BASE, D.C. 20332		12. REPORT DATE NOV. 1981 13. NUMBER OF PAGES 163
14. MONITORING AGENCY NAME & ADDRESS*(if different from Controlling Office)*		15. SECURITY CLASS. *(of this report)* UNCLASSIFIED 15a. DECLASSIFICATION/DOWNGRADING SCHEDULE

16. DISTRIBUTION STATEMENT *(of this Report)*

Approved for public release; distribution unlimited.

17. DISTRIBUTION STATEMENT *(of the abstract entered in Block 20, if different from Report)*

18. SUPPLEMENTARY NOTES

19 KEY WORDS *(Continue on reverse side if necessary and identify by block number)*

SOLID PROPELLANT COMBUSTION, ALUMINUM AGGLOMERATION, ALUMINUM COMBUSTION, COMBUSTION INSTABILITY, COMBUSTION OSCILLATION, RESPONSE FUNCTION, IMPEDANCE TUBE, TURBULENCE NOISE, TURBULENT COMBUSTION, EXTERNAL BURNING PROPULSION, BASE FLOW, SUPERSONIC FLOW.

20. ABSTRACT *(Continue on reverse side if necessary and identify by block number)*

Progress is reported on four investigations of fundamentals of rockets and reaction propulsion.

TASK I: Measurement of the dynamic response of solid propellant combustion to flow oscillations, using an impedance tube method. Measurements were made of pressure-coupled combustion response and bulk damping of aluminized and nonaluminized propellants, and the

DD FORM 1 JAN 73 1473 EDITION OF 1 NOV 65 IS OBSOLETE

UNCLASSIFIED

SECURITY CLASSIFICATION OF THIS PAGE *(When Data Entered)*

develop of an apparatus for measurement of velocity coupled response is near completion.

~~TASK II~~ (2): Use of external base burning as a means of producing reduced drag or positive thrust on a supersonic bluff base flight vehicle. Flow field and surface measurements were made in cold flow simulation and in hydrogen fueled tests in a Mach 3 test duct.

~~TASK III~~ (3): Combustion of powdered aluminum as a fuel ingredient in solid propellants. A variety of tests were developed and used to clarify and control the agglomeration-combustion behavior of aluminum that usually compromises its effectiveness as a fuel.

~~TASK IV~~ (4): Turbulence-generated noise in the interior flow of rocket motors. Measurements were made in cold flow simulat ors of solid rocket combustors, and results were compared with predictions based on adaptation of the Bernoulli enthalpy theory of aeroacoustics.

These tasks are continuing.

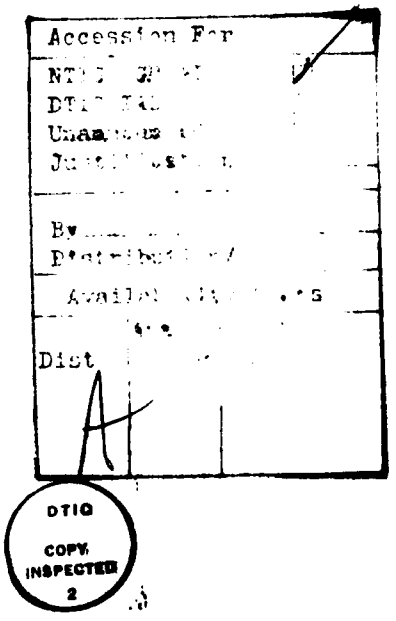

TABLE OF CONTENTS

GENERAL INTRODUCTION

Activities and progress are summarized for the four years of contract AFOSR F49620-78-6-0003, with emphasis primarily on progress not reported in the previous annual reports and publications. The project consists of four interrelated tasks that are reported individually in this report and described below.

Task I is concerned with measurement of the characteristics of combustion of solid rocket propellants that are important to motor combustion instability. The approach is to adapt and apply the impedance tube method to measure the dynamic response of the combustion zone and product flow to imposed gas oscillations typical of rocket combustion chambers. As the methods were perfected they were extended to increasingly more difficult measurements dictated by observed rocket motor instabilities. In the process, the experimental method and facility, and supporting analysis and data reduction systems, were progressively improved to provide a basis for routine measurements and for comparison with those made by other experimental methods.

Task II is concerned with external and base burning as a means for reducing base drag or providing base thrust with minimum weight and and volume demands on the propulsion system. The investigation involved development of a properly instrumented flow facility to simulate base flow of a cylindrical body with fuel flow and combustion in the base region. A series of studies was carried out starting with cold flow simulation, and progressing to increasingly complex situations aimed at clarifying details of the flow field and efficiently increasing the base pressure. Mach 3 external flow and radial and base injection was evaluated, with hydrogen fuel, diluted hydrogen, and combustion pre-heated hydrogen.

Task III is concerned with achieving improved combustion of the aluminum ingredient in solid propellant. The approach is to clarify understanding of the complex detailed processes exhibited by aluminum and relate them to control of propellant burning rate, combustion stability, combustion efficiency and two phase flow behavior in the motor. A series of experiments were contrived to elucidate the microscopic details of aluminum behavior and their relation to microscopic details of the propellant, and to behavior of the other propellant ingredients.

Task IV is concerned with prediction of turbulence-induced pressure fluctuations in rocket motors, particularly as they pertain to production of vibrations in the motor structure. The approach combines analytical developments

and cold flow experiments, using each as a means to validate or guide improvement of the others. The analysis indicates what measurements and data analysis are necessary to interpret the experiments, and the measurements indicate the ability of the theory to predict the real behavior. The experiment involved development of a suitable cold flow simulator for combustion chamber flow, and measurement of velocity and pressure fluctuations at appropriate locations.

The above Tasks are continuing under AFOSR Contract No. F49620-82-C-0013.

TASK I

INVESTIGATION OF THE UNSTEADY BURNING CHARACTERISTICS OF SOLID PROPELLANTS

B. T. ZINN
B. R. DANIEL

TASK I

INVESTIGATION OF THE UNSTEADY BURNING CHARACTERISTICS OF SOLID PROPELLANTS

A. Objectives

This task was generally concerned with the experimental determination of the burn rate response of different classes of solid propellants under various conditions simulating those encountered in unstable solid propellant rocket motors. Specifically, this task pursued the following objectives:

(1) Adaptation of the impedance tube technique for the measurement of the pressure coupled response of solid propellants under different oscillatory flow conditions.

(2) Utilization of the developed impedance tube setup to determine the pressure coupled response functions of aluminized and unaluminized solid propellants under a variety of oscillatory flow conditions.

(3) Development of an impedance tube experiment for the determination of the velocity coupled response of solid propellants under different oscillatory flow conditions.

(4) Investigation of the feasibility of using piezoelectric quartz and ceramic crystals in the direct measurement of the unsteady burn rate of solid propellants.

B. Progress and Significant Accomplishments.

Introduction

The detrimental effects associated with the occurrence of combustion instability are well known and they will not be repeated in this

discussion. Instead, the importance of knowing the unsteady propellant burn rate under different engine operating conditions will be briefly considered. The amplification of a small amplitude disturbance in a rocket combustor into combustion instability depends upon its interactions with the various engine processes that affect its growth and decay. Interaction between a combustor disturbance and the combustion processes on various portions of the propellant may result in a positive feedback leading to disturbance energy gain and amplitude growth. In contrast, disturbance energy dissipation by such processes as viscosity, heat transfer and acoustic radiation and convection through the nozzle generally results in disturbance amplitude decay. Instability occurs when the disturbance energy gains outweigh the disturbance energy losses while stable engine operation is assured when the reverse is true.

Since the energy feedback between the combustion process and the disturbance is responsible for the disturbance growth, the ability to quantitatively describe this feedback or interaction process in terms of the conditions that prevail in the rocket motor or experimental setup is of utmost practical importance. In general, combustion in solid rockets is assumed to be concentrated at the propellant surface and its effect upon rocket stability is described by specifying the boundary condition at the burning surface. When describing the effect of the pressure oscillations, this boundary condition is expressed either as the complex ratio of the local burn rate perturbation to the local pressure oscillation (i.e., the propellant response function) or as the complex ratio of the local velocity perturbation normal to the propellant surface to the local pressure perturbation (i.e., the propellant admittance). Similar boundary conditions are being used to describe the propellant response to a velocity oscillation parallel to its surface and the resulting response function is known as the velocity coupled response function.

To evaluate the <u>total</u> amplification of a given disturbance in a combustor the sum of its interactions with various parts of the burning propellant surface must be evaluated. To evaluate this sum, the nature of the interaction of the disturbance with various parts of the propellant

surface need to be known. For example, the propellant in an unstable rocket motor experiencing an axial instability of its fundamental mode is exposed to regions of primarily velocity oscillations (e.g., near the center of the motor) and regions that experience both velocity and pressure oscillations. The interactions between the combustion processes and the combustor disturbance occurring at each of these regions may be fundamentally different and, in addition, they may depend upon the frequency, the amplitude of the oscillation and the local operating conditions (i.e., the steady state pressure, velocity, etc.). Thus, it is of utmost importance to develop experimental techniques that would enable engineers to determine the propellant response in terms of the flow conditions near its burning surface.

The majority of the experimental efforts to date have concentrated on the measurement of the pressure coupled response of solid propellants. These efforts utilized the T-burner[1,2], the rotating valve[3], the microwave technique[4] and the impedance tube[2,5]. Much of what has been done to date in this area is reviewed in a paper by Levine and Andrepont[6]. In recent years some attention has been given to the development of capabilities for determining the velocity coupled response of solid propellants. Notable among these are the works of Beckstead et al[7], Micheli[8], Micci et al[9] and Brown et al[10]. Considering the importance of having reliable propellant response data, it is important that the burn rate response data generated by the various measurement techniques under the same conditions agree with one another.

In the present study, the classical impedance tube technique has been modified for application in the measurements of the pressure and velocity coupled response functions of solid propellants. In addition, the feasibility of utilizing crystals in the direct measurement of the unsteady propellant burn rate has been investigated. In what follows, the major accomplishments under this program are summarized.

Pressure Coupled Propellant Response Measurements

This section describes the application of the impedance tube technique in the measurement of the pressure coupled response of solid propellants. The development of this impedance tube experiment had been inspired by earlier investigations[11,12] in which the classical impedance tube setup had been used in the determination of admittances of sound absorbing materials. Impedance tube experiments generally consist of a long tube with a sound source at one end and a surface whose admittance is to be measured at the other end. The sound source is used to establish a longitudinal standing wave of a desired frequency in the tube. The structure (i.e., amplitude and phase) of this standing wave is affected by the wave's interaction with the surface whose admittance is being measured. The resulting standing wave structure is measured by using one or more microphones and the measured data is input into an appropriate data reduction computer program to determine the unknown admittance.

A schematic of the impedance tube developed under this program to measure the pressure coupled response of solid propellants is described in Fig. 1. The application of this setup in the measurement of the pressure coupled response function involved the following steps:

(1) Modification of the classical impedance tube theory to account for the effects of a steady flow, steady state temperature gradient and gas phase losses that are present in the solid propellant experiment. These efforts are described in detail in Refs. 13 through 16.

(2) Development of the experimental setup, multi microphone measurement system and the analog-to-digital data acquisition system.

(3) Development of a data reduction computer program that Fourier analyzes the measured data and then uses it to determine the values of the complex, pressure coupled propellant admittance, the steady state temperature gradient and the gas phase losses that provide the best fit

between the measured acoustic pressure data (obtained under (2) above) and the solutions of the impedance tube wave equations (derived under (1) above).

The above described facility has been utilized in the determination of the frequency dependence of the admittances and gas phase losses of various aluminized and nonaluminized propellants and the results of these studies showed that:

(1) The developed impedance tube setup can indeed measure the pressure coupled admittances of both aluminized and nonaluminized propellants at different frequencies. Furthermore, at a given frequency, the impedance tube setup can determine the time variations of both the real and imaginary parts of the propellant admittance and the gas phase losses.

(2) The conduct of the experiment and associated data reduction are easier with aluminized propellants.

(3) Measured frequency dependence of the real part of the admittance of nonaluminized propellants indicate the existence of multiple peaks (see Fig 2). This result is in agreement with results obtained with the microwave technique but they contradict T-burner data.

(4) The measured data indicates that in some instances both the propellant admittance and the gas phase losses may vary with time during the course of a given experiment.

Velocity Coupled Propellant Response Measurements

In view of the success achieved with the application of the impedance tube technique in the measurement of the pressure coupled propellant response function, a decision had been made to further modify the developed impedance tube setup for applications in solid propellant

velocity coupled response measurements. Subsequently, a number of potential impedance tube setups were considered before settling on the experimental configuration shown in Fig. 3. In this case the objective of the experiment is to measure the velocity coupled response of the "test" propellant that is placed at some distance downstream of the "driver" propellant that provides a flow of hot combustion products past the test propellant surface. An acoustic driver at the other end of the tube is utilized to excite a standing acoustic wave of a given frequency in the tube. In this configuration the "driver" propellant surface is subjected to acoustic pressure oscillations only while the "test" propellant surface is subjected to both pressure and acoustic velocity (parallel to the propellant surface) oscillations. Thus, the "driver" propellant interacts with the tube oscillation via a pressure coupled response only while the "test" propellant interacts with the tube oscillation via both pressure and velocity coupled responses. With this configuration one is faced with the problem of determining both of these responses under the conditions of the experiment. The approach chosen toward the resolution of this problem is outlined in Fig. 3 and it involves the utilization of the existing impedance tube to determine the pressure coupled response of the propellant and the newly developed setup for the determination of the velocity coupled response of the "test" propellant.

In order to describe the developed data reduction procedure for the determination of the velocity coupled response function R_v, the impedance tube wave equations need to be considered. These equations are presented in Fig. 4 where m_b' represents the burn rate perturbation of the test propellant and the quantity $b/A\ \bar{m}_b \bar{E} \left[\frac{E'}{\bar{E}} + \frac{m_b'}{\bar{m}_b} \right]$ represents the perturbation in the energy addition to the flow from the test propellant. Figure 4 also presents the relationships that relate this quantity to R_p and R_v, the pressure and velocity coupled response functions. One should note that the developed relationships are somewhat arbitrary and that they imply linear dependence upon $p'/\bar{p}$ and $\bar{u}/\bar{a}$, which may not be the case in reality. The objective of the developed experiment is to find the values of R_p and R_v that will produce the

"best" agreement between the solutions of the wave equations in Fig. 4 and the acoustic pressure data measured during a given test.

In reviewing the equations presented in Fig. 4 one should note that the unknowns R_p and R_v appear in the differential equations while in the previously developed impedance tube the unknown R_p only appeared in the boundary conditions of the problem. Consequently, a new data reduction procedure that will allow for the determination of R_v from measured acoustic pressure data had to be developed. Since a discussion of this data reduction procedure that utilizes the actual impedance tube wave equations may become too cumbersome, this method will be discussed utilizing a simpler example, as shown in Fig. 5. In reviewing this example it may be convenient to think of the dependent variable y and the parameter k as being analogous to the acoustic pressure p' and the response function R_v, respectively. One should also note that the method utilizes the method of quasilinearization and that the determination of k at each iteration involves the solution of linear equations only.

The accuracy and numerical efficiency of the developed data reduction procedure has been investigated utilizing a number of hypothetical cases. For a given case, values of R_p and R_v were assumed and the impedance tube wave equations were solved to determine the corresponding impedance tube wave structure. Next, utilizing the computed wave structure, values of the calculated acoustic pressure (i.e., amplitude and phase) were modified by the addition of arbitrary errors to simulate measured data, and the resulting amplitudes and phases were input into the data reduction procedure in order to compute the "unknown" R_p and R_v. Results of some of these calculations are summarized in Fig. 6. In this case four transducers, whose locations are shown in the figure, were utilized in the computation. The results are summarized in the table and they demonstrate that the developed data reduction procedure is indeed capable of utilizing measured acoustic pressure data in the determination of velocity coupled response functions.

Finally, in order to optimize the design of the developed impedance tube, a study aimed at the determination of the dependence of the "new" impedance tube wave structure upon the length and location of the tested propellant samples was conducted and some results obtained in this study are presented in Figs. 7 through 10. Examination of these figures clearly indicates that the length and location of the tested propellant sample can be optimized in a sense that differences in the propellant response function produce measurable changes in the resulting acoustic pressure wave structure in the impedance tube. These studies will continue in the near future as the determination of the optimum impedance tube configuration is expected to result in more accurate determination of the velocity coupled response function.

Using the results of the above described analysis, the impedance tube shown in Fig. 11 has been designed and it is currently in the fabrication stage. To obtain maximum flexibility, the designed impedance tube offers the possibility of changing the distance between the test propellant and driver propellant from one experiment to another, thus providing an opportunity to investigate the effect of "positioning" the test propellant at different parts of the impedance tube standing wave. Furthermore, the lengths of the two test propellant samples can be varied between four and eight inches and the shown stepping motor will be utilized to "push" the test propellants inward at a rate equal to their burning rate. This will be done in an attempt to maintain the burning test propellants surfaces flush with the impedance tube walls. A square impedance tube cross sectional area has been chosen for this study in order to simplify the installation of the acoustic pressure transducers and optical windows that will be used in order to investigate the unsteady flow conditions inside the impedance tube during the course of various experiments.

Direct Measurements of Solid Propellant Burn Rates

In a separate study, Mr. Peter Erbland, an M. S. student, investigated the feasibility of utilizing crystals in the "direct" measurement of solid propellant mass loss during burning in steady and unsteady flow environments. The experimental setup investigated by Mr. Erbland is shown on the bottom of Fig. 12 and a related experimental setup utilized by the Russians[17] is shown at the top of Fig. 12. The basic idea of the experiment is to measure the changes with time of the natural frequency of a crystal loaded with a burning solid propellant sample. Loading a crystal with a solid propellant sample was expected to change its natural frequency and since the amount of loading changes during burning, the natural frequency of the loaded crystal would also change. If one could measure these frequency changes, then one could , in principle, relate these changes to the mass lost due to burning. The objective of Mr. Erbland's study was to determine whether (1) available crystals would respond while loaded with typical solid propellant samples and (2) whether these crystals possessed the necessary sensitivity. The results of Mr. Erbland's study are described in his M. S. Special Project report and they are summarized in Figs. 13 and 14. These figures indicate that the properties of both quartz and ceramic crystals were investigated and that the results of these studies showed that while the tested quartz crystals possessed the necessary sensitivity (i.e., $\Delta f/\Delta m$) they would not respond when loaded with even the smallest possible samples of solid propellants. In contrast, the tested ceramic crystals would respond when loaded with masses comparable to those of burning solid propellant but they did not possess the necessary sensitivity. While these results are discouraging, they do not nullify the original concept as it is quite possible that there may be other crystals available which do possess the desired properties. Thus, it is still quite possible that the suggested measurement technique may produce the desired results when appropriate crystals are found.

Investigation of the Dependence of the Propellant Response Function and Gas Phase Losses upon the Propellant Aluminum Content

Since the developed impedance tube setup is capable of the simultaneous determination of the propellant pressure coupled admittance and the gas phase acoustic losses, a study aimed at the determination of the effect of aluminum addition upon the propellant admittance and gas phase losses was undertaken. Due to lack of a propellant mixing facility at Georgia Tech, the needed test propellants were kindly supplied by AFRPL. To isolate the effect of aluminum addition, three different propellant formulations differing only in their aluminum content were to be tested; that is, the formulations of the nonaluminized fraction of each of the tested propellants was to be the same. Such propellant formulations could be ideally obtained by replacing different weight fractions of a given propellant formulation with equivalent weights of aluminum. In the planned tests, the three propellant formulations were going to have zero, five and eighteen percent of aluminum by weight. While this approach was agreed upon with AFRPL personnel, propellant processing difficulties resulted in variations of the developed propellants compositions from those that had been originally agreed upon. The discrepancy is illustrated in Table I where the actual and "planned" formulations of the three propellants are compared. Obviously, the amount of binder remained constant in all three formulations and the added aluminum replaced some of the AP particles. Thus, the three propellants formulations varied from one another both in their aluminum content and in the formulation of their nonaluminized fractions.

The three propellants formulations were tested in the impedance tube over the frequency range 400 to 1200 Hz. Some of the measured data is summarized in Table II where the driving of the three propellants (i.e., Y_r) and their gas phase damping (i.e., G) are compared at different frequencies. An examination of these data suggests that aluminum addition increases both the propellant driving and the gas phase damping. Since increasing both of these factors in a practical situation would exert

countering effects upon the stability of a rocket motor, it remains to determine which of the two increases is dominant at the various frequencies as this may indicate whether aluminum addition to the tested propellant would stabilize or destabilize in actual rocket motors. Furthermore, it remains to establish that the observed effects are due to the aluminum addition only and not due to the differences in the compositions of the nonaluminized fractions of the tested propellants.

Finally, samples of the propellants tested in this study have been given to Professor Price who will further investigate their burning characteristics. The results of his studies will be compared with the impedance tube data to determine whether any correlations between the results of the two studies can be established.

C. References

1. T-Burner Manual, CPIA Publication No. 191, Nov. 1969.

2. Brown, R. S., Culick, F. E. C., Zinn, B. T., "Experimental Methods for Combustion Admittance Measurements," AIAA Series "Progress in Astronautics and Aeronautics," Vol. 63, "Experimental Diagnostics in Combustion of Solids," pp. 191-220, 1978.

3. Brown, R. S., "Development and Evaluation of Rotating Valve/Combustion Response Test Technique," AFRPL-TR-76-72, Chemical System Division, United Technologies, Oct. 1976.

4. Strand, L. D., Magiawala, K. R., McNamara, R. P., "Microwave Measurement of the Solid Propellant Pressure Coupled Response Function," AIAA/SAE/ASME, 15th Joint Propulsion Conference, Paper No. 79-1211, June 1979.

5. Baum, J. D., Daniel, B. R. and Zinn, B. T., "Determination of Solid Propellant Admittances by the Impedance Tube Method," AIAA Paper No. 80-0281, January 1980. Also, AIAA Journal, Vol. 19, No. 2, pp. 214-220, February 1981.

6. Levine, J. N. and Andrepont, W. C., "Measurement Methods of Transient Combustion Response Characteristics of Solid Propellant - An Assessment," AIAA Paper No. 79-1209, June 1979.

7. Beckstead, M. W., Horton, M. D., Kraskin, M., Butcher, A. G., "Velocity Coupling Combustion Instability," Final Technical Report, AFRPL-TR-73-73, July 1973, Hercules, Bacchus Works, Magna, UT.

8. Micheli, P. L., "Investigation of Velocity Coupled Combustion Instability," AFRPL-TR-76-100, January 1977. Aerojet Solid Propulsion Co., Sacramento, California.

9. Micci, M. M., Caveny, L. H. and Sirignano, W. A., "Linear Analysis of Forced Longitudinal Waves in Rocket Motor Chambers," AIAA Paper No. 79-1210, June 1979.

10. Brown, R. S., Willoughby, P. G., and Kelly, V. L., "Rotating Valve for Velocity Coupled Combustion Response Studies," AIAA Paper 77-975, presented at AIAA 13th Propulsion Conference, July 1977, Orlando, FL.

11. Scott, R. A., "An Apparatus for Acoustic Measurement of the Acoustic Impedance of Sound Absorbing Materials," Proceedings of the Physical Society, 58, p. 253, 1946.

12. Lippert, W. K. R., "The Practical Representation of Standing Waves in an Acoustic Impedance Tube," Acustica, 3, p. 153, 1953.

13. Salikuddin, Mohammed, "Application of Impedance Tube Technique in the Measurement of Burning Solid Propellant Admittances," Ph.D. Thesis, School of Aerospace Engineering, Georgia Institute of Technology, April, 1978.

14. Baum, J. D., "Experimental Determination of the Admittances of Solid Propellants by the Impedance Tube Technique," Ph.D. Thesis, School of Aerospace Engineering, Georgia Institute of Technology, May, 1980.

15. Salikuddin, M. and Zinn, B. T., "Adaptation of the Impedance Tube Technique for the Measurement of Combustion Process Admittances," AIAA Paper No. 79-0167, 1979 and Journal of Sound and Vibration (68)(1), 1980.

16. Baum, J. D., Daniel, B. R. and Zinn, B. T., AIAA Paper No. 80-0281, January 1980. AIAA Journal, Vol. 19, No. 2, pp. 214-220, February 1981.

17. Mikheev, V. F., Zarko, V. E., Borin, S. M., Kutsenogli, K. P. and Simonenko, V. N., "Measurement of Burning Rates in Transient Combustion Processes Under the Influence of External Radiation," AIAA Series Progress in Astronautics and Aeronautics," Vol. 63, "Experimental Diagnostics in Combustion of Solids," pp. 173-187, 1978.

D. Publications

The following are publications that resulted from the research efforts conducted under this task.

A. Ph.D. Theses

1. Salikuddin, Mohammed, "Application of Impedance Tube Technique in the Measurement of Burning Solid Propellant Admittances," School of Aerospace Engineering, Georgia Institute of Technology, April 1978.

2. Baum, J. D., "Experimental Determination of the Admittances of Solid Propellants by the Impedance Tube Technique," School of Aerospace Engineering, Georgia Institute of Technology, May 1980.

B. Papers

1. Brown, R. S., Culick, F. E. C., Zinn, B. T., "Experimental Methods for Combustion Admittance Measurements," AIAA Series "Progress in Astronautics and Aeronautics," Vol. 63, "Experimental Diagnostics in Combustion of Solids," pp. 191-220, 1978.

2. Salikuddin, M. and Zinn, B. T., "Adaptation of the Impedance Tube Technique for the Measurement of Combustion Process Admittances," AIAA Paper No. 79-0167, 1979. Also Jr. of Sound & Vibration (1980)68(1).

3. Baum, J. D., Daniel, B. R. and Zinn, B. T., "Determination of Solid Propellant Admittances by the Impedance Tube Method," AIAA Paper No. 80-0281, January 1980. Also AIAA Journal, Vol. 19, No. 2, pp. 214-220, February 1981.

4. Zinn, B. T. and L. Narayanaswami, "Application of the Impedance Tube Technique in the Measurement of the Driving Provided by Solid Propellants during Combustion Instabilities," accepted for publication in Acta Astronautica, 1981.

5. Zinn, B. T., Daniel, B. R., Bell, W. A., and Meyer, W. L., "Determination of the Acoustic Responses of Solid Propellants by the Impedance Tube Method," Proceedings of the 12th JANNAF Combustion Meeting, CPIA Report No. 273, Vol. II, pp. 83-98, December 1975.

6. Zinn, B. T., Salikuddin, M., Daniel, B. R., and Bell, W. A., "Measurements of the Response Factors of Burning Solid Propellants by the Driven Tube Method," Proceedings of the 13th JANNAF Combustion Meeting, CPIA Report No. 281, Vol. II, pp. 113-114, December 1976.

7. Baum, J. D., Daniel, B. R., and Zinn, B. T., "Experimental Determination of Solid Propellant Admittances by the Impedance Tube Method," Proceedings of the 16th JANNAF Combustion Meeting, CPIA Report No. 308, , pp. 325-341, December 1979.

8. Salikuddin, M. and Zinn, B. T., "Experimental Observations of the Dependence of the Impedance Tube Behavior upon Gas Phase Losses and Propellant Self-Noise," AIAA Paper No. 80-1020, June 1980.

9. Baum, J. D., Daniel, B. R. and Zinn, B. T., "Experimental Determination of the Admittances of Aluminized Propellants by the Impedance Tube Method," 17th JANNAF Combustion Meeting, CPIA Report No. 329, Vol. I, pp. 133-148, November 1980.

10. Zinn, B. T. and L. Narayanaswami, "Experimental Determination of the Velocity Coupled Response of Solid Propellants," Proceedings of the 18th JANNAF Combustion Meeting, October 1981.

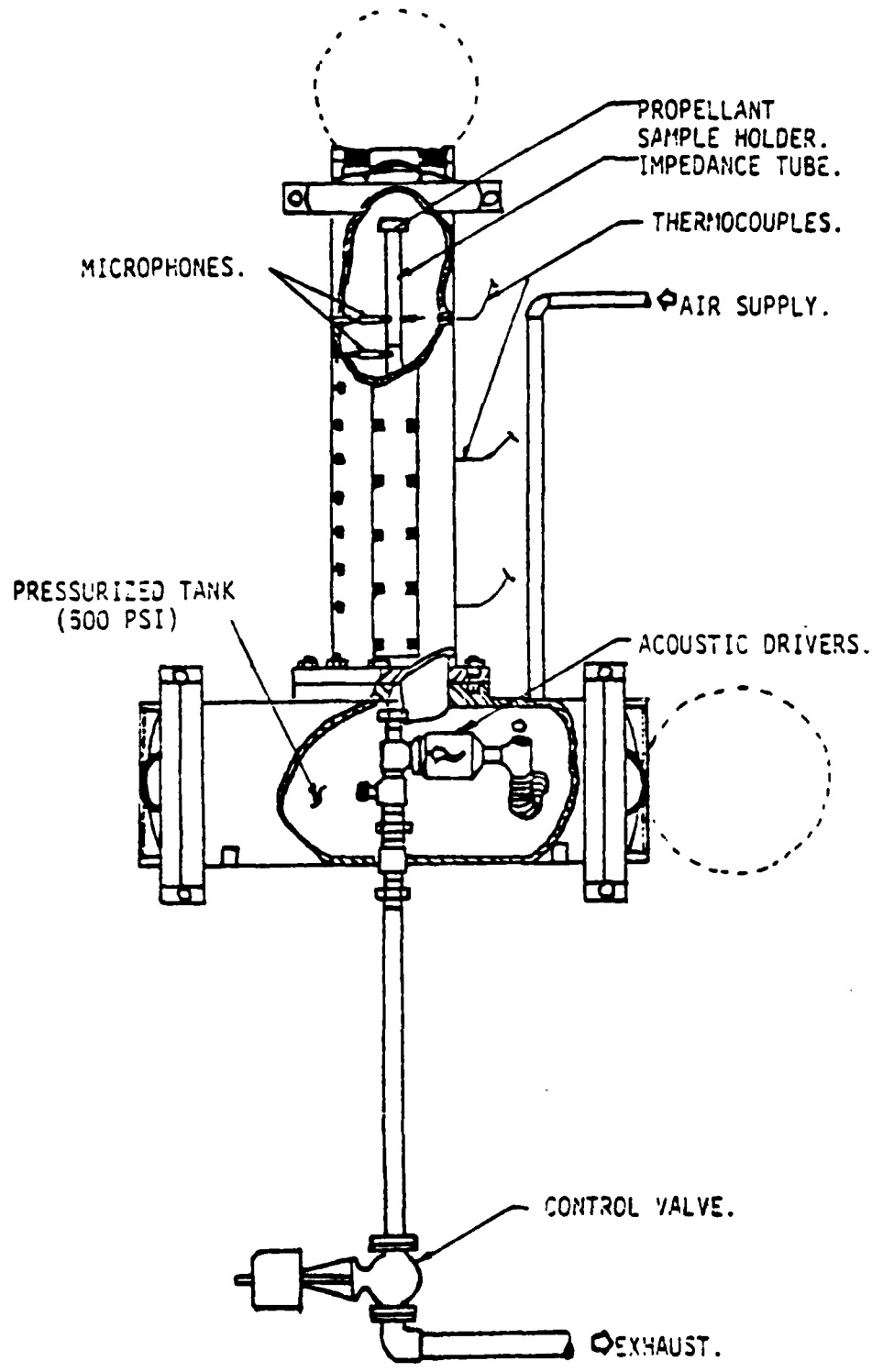

Fig. 1. Schematic Diagram of the Pressurized Impedance Tube Facility.

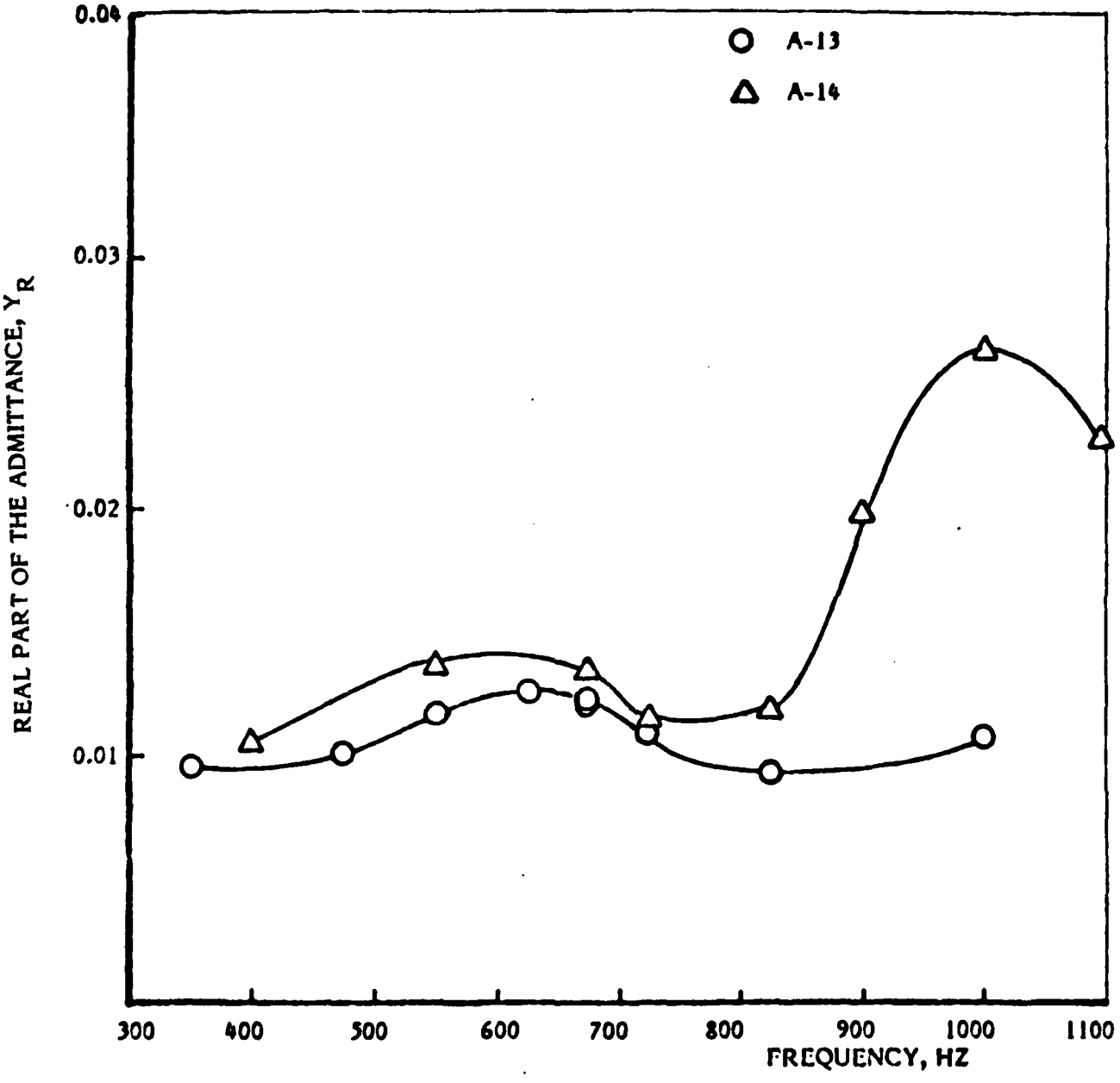

Fig. 2. Real Part of the Admittance vs. Frequency for A-13 and A-14 Propellants, 300 psig.

MODIFIED IMPEDANCE TUBE SETUP

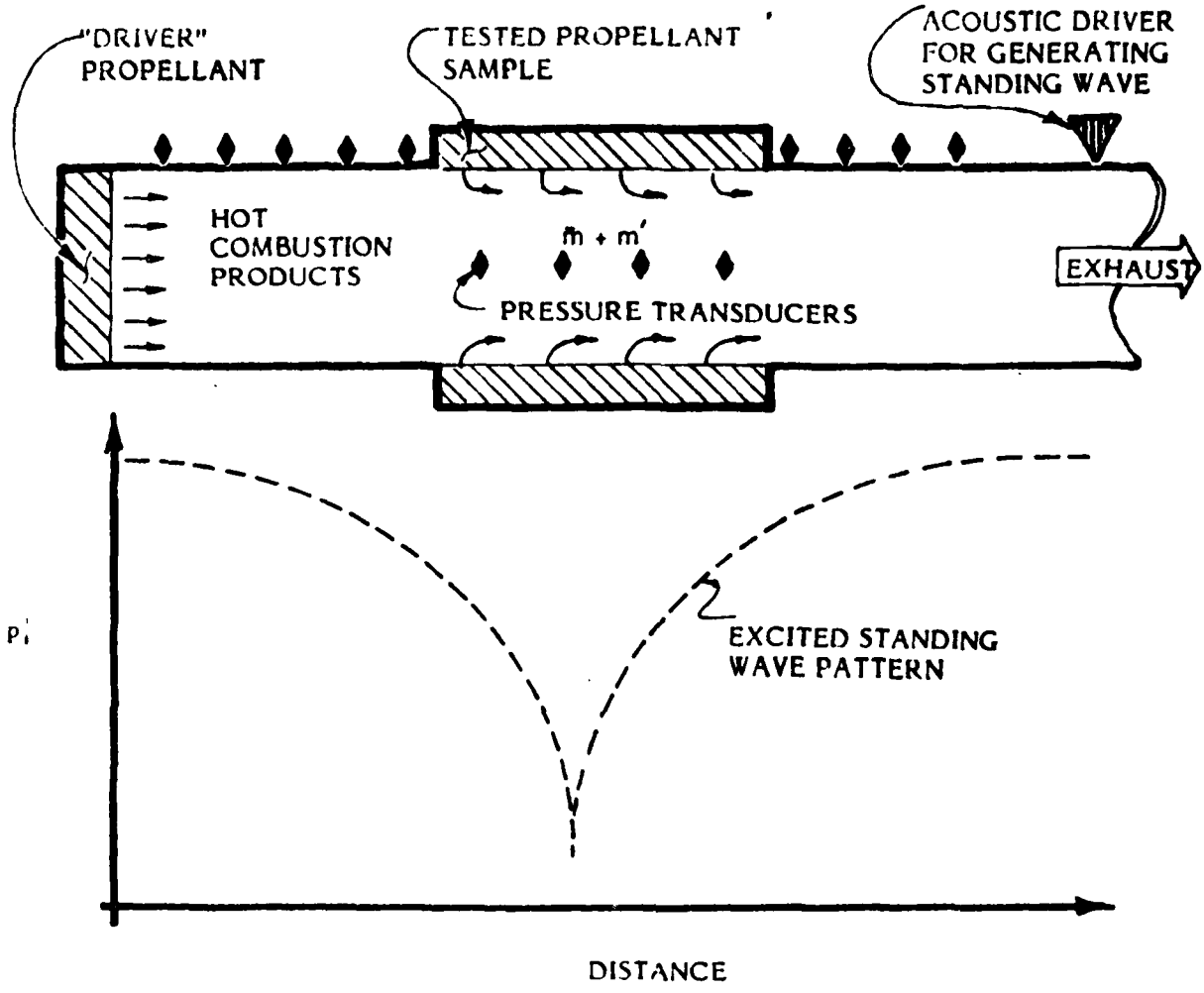

EXPERIMENTAL PROCEDURE

(1) Utilize the available impedance tube to determine the pressure coupled response function R_p of the tested propellant.

(2) Use the acoustic driver to generate a standing acoustic wave in the modified impedance tube setup. Ignite both propellant samples and use the pressure transducers to measure the acoustic pressures at the indicated locations.

(3) Input data obtained under (1) and (2) above into the newly developed data reduction computer program to determine the velocity coupled response function R_v of the tested propellant sample.

FIGURE 3. MAIN FEATURES OF EXPERIMENTAL APPROACH.

IMPEDANCE TUBE WAVE EQUATIONS

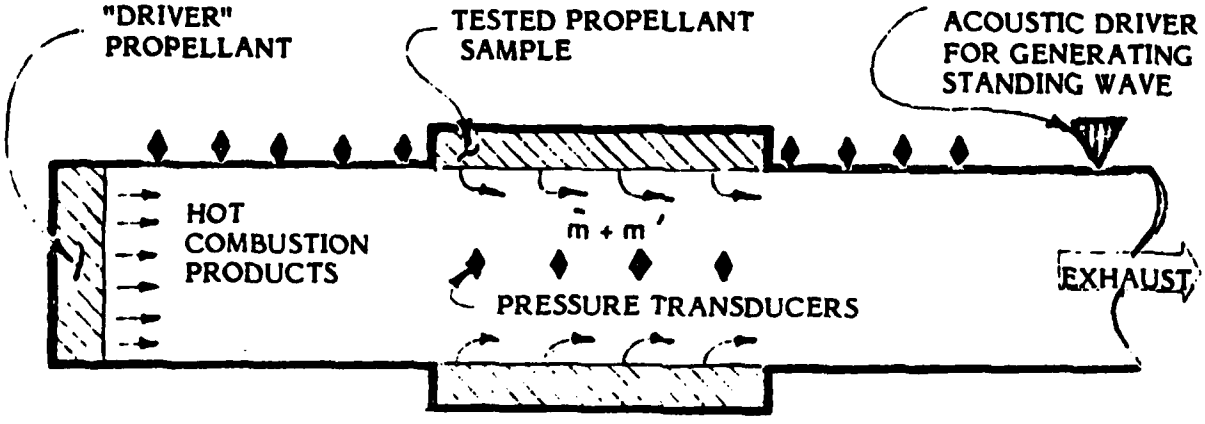

CONTINUITY: $$i\omega\rho' + \frac{d}{dx}(\bar{u}\rho' + \bar{\rho}u') = \frac{b}{A}m_b'$$

MOMENTUM: $$i\omega\bar{\rho}u' + \bar{\rho}\bar{u}\frac{du'}{dx} + \bar{\rho}\frac{d\bar{u}}{dx}u' + \frac{dp'}{dx} + \frac{b}{A}\bar{m}_b u' + F' = 0$$

ENERGY: $$i\omega p' + \bar{u}\frac{dp'}{dx} + \frac{d\bar{p}}{dx}u' + \gamma\bar{p}\frac{du'}{dx} + \gamma\frac{d\bar{u}}{dx}p' = \frac{b}{A}\bar{m}_b\bar{E}\left(\frac{E'}{\bar{E}} + \frac{m_b'}{\bar{m}_b}\right) + (\gamma-1)\,G\bar{u}u'$$

WHERE $$E = \gamma RT_F + \gamma R\Delta T + (R/2C_v)(u^2 + u_b^2)$$

THE VELOCITY AND PRESSURE COUPLED RESPONSE FUNCTIONS ARE INTRODUCED BY LETTING

$$R_p = \frac{\left(\frac{E'}{\bar{E}} + \frac{m_b'}{\bar{m}_b}\right)}{\left(\frac{p'}{\bar{p}}\right)} \quad ; \quad R_v = \frac{\left(\frac{E'}{\bar{E}} + \frac{m_b'}{\bar{m}_b}\right)}{\gamma(u'/\bar{a})}$$

OR

$$\frac{m_b'}{\bar{m}_b} + \frac{E'}{\bar{E}} = R_p\frac{p'}{\bar{p}} + R_v\frac{u'}{\bar{a}}$$

Figure 4. Impedance Tube Wave Equations

Consider the following differential equation that models the behavior of a measurable quantity $y(x,k)$

$$\frac{dy}{dx} = g(x,y,k) = kxy \quad ; \quad y(0) = A \tag{1}$$

Where k is an as yet unknown constant parameter that needs to be determined. Let:

$$E = \sum_{i=1}^{N} \left(y_t(x_i,k) - y_m(x_i) \right)^2$$

and determine k by solving

$$\frac{\partial E}{\partial k} = 2 \sum_{i=1}^{N} \left(y_t(x_i,k) - y_m(x_i) \right) \left(\frac{\partial y_t}{\partial k} \right)_{x=x_i} = 0 \tag{2}$$

Step 1: Assume a value for k, say $k = k_0$, and solve (1) above to get the first approximation $y_0(x,k_0)$

Step 2: To obtain an improved value of y_0, expand Eq. (1) about the y_0 solution to get

$$\frac{dy}{dx} = g_0 + \left(\frac{\partial g}{\partial y} \right)_0 (y - y_0) + \left(\frac{\partial g}{\partial k} \right)_0 (k - k_0) \tag{3}$$

where

$$y(x) = y(0)\, e^{\left(\frac{\partial g}{\partial y} \right)_0 x} + \int_0^x \left(g_0 - \left(\frac{\partial g}{\partial y} \right)_0 y_0 \right) e^{-\left(\frac{\partial g}{\partial y} \right)_0 (x' - x)} dx'$$

$$+ (k - k_0) \int_0^x \left(\frac{\partial g}{\partial k} \right)_0 e^{-\left(\frac{\partial g}{\partial y} \right)_0 (x' - x)} dx' \tag{4}$$

Note

(1) $y(x)$ is linear in the unknown parameter k

(2) $$\left(\frac{\partial y_t}{\partial k} \right)_{x=x_i} = \int_0^{x_i} \left(\frac{\partial g}{\partial k} \right)_0 e^{-\left(\frac{\partial g}{\partial y} \right)_0 (x' - x_i)} dx' \tag{5}$$

Substitute (5) into (2) and solve for the new $k = k_1$

Step 3: If $k_1 \neq k_0$, repeat Step 2 until convergence occurs.

Figure 5. An Example of the Developed Data Reduction Procedure.

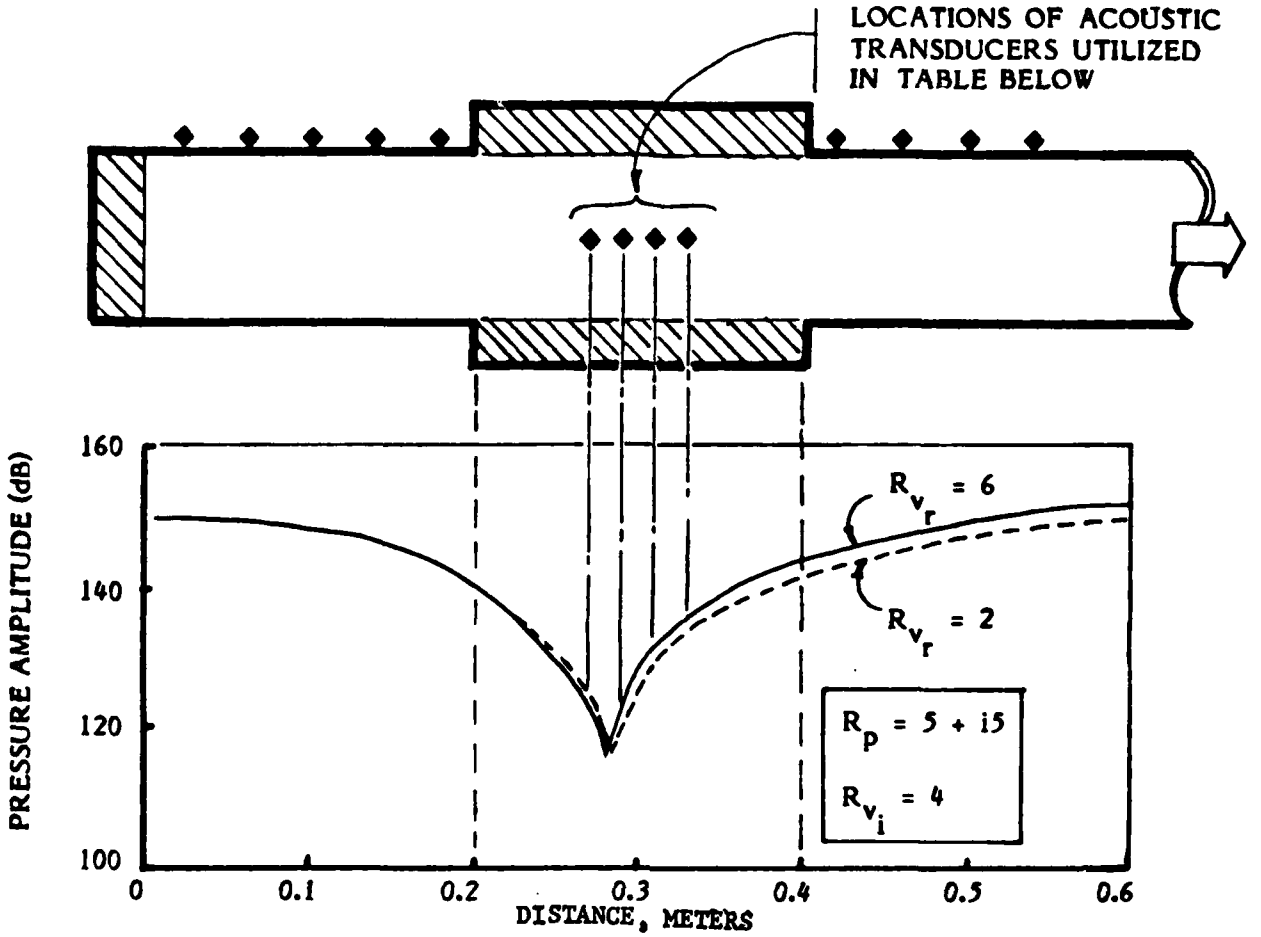

PREDICTED ACOUSTIC PRESSURE WAVE PATTERN FOR DIFFERENT REAL PARTS OF THE VELOCITY COUPLED RESPONSE FACTOR R_{v_r}

TRANSDUCER LOCATION, m	EXACT VALUES		ASSUMED ERRORS		ASSUMED ERRORS		ASSUMED ERRORS	
	dB	Phase	dB	Phase	dB	Phase	dB	Phase
0.27	121.7	+ 61.	+ 1.0	0	0	+ 2	+ 1.0	+ 2
0.29	123.3	- 63.	+ 1.0	0	0	+ 2	+ 1.0	+ 2
0.31	131.6	- 78.	- 0.5	0	0	- 1	- 0.5	- 1
0.33	135.9	- 81.	+ 0.5	0	0	+ 1	+ 0.5	+ 1
R_{v_r} (Computed)	6.00 +	14.00	6.39 +	14.15	5.95 +	14.10	6.34 +	14.28

DEPENDENCE OF THE COMPUTED RESPONSE FUNCTION UPON EXPERIMENTAL ERRORS; SAMPLE COMPUTATION

FIGURE 6. SAMPLE RESULTS.

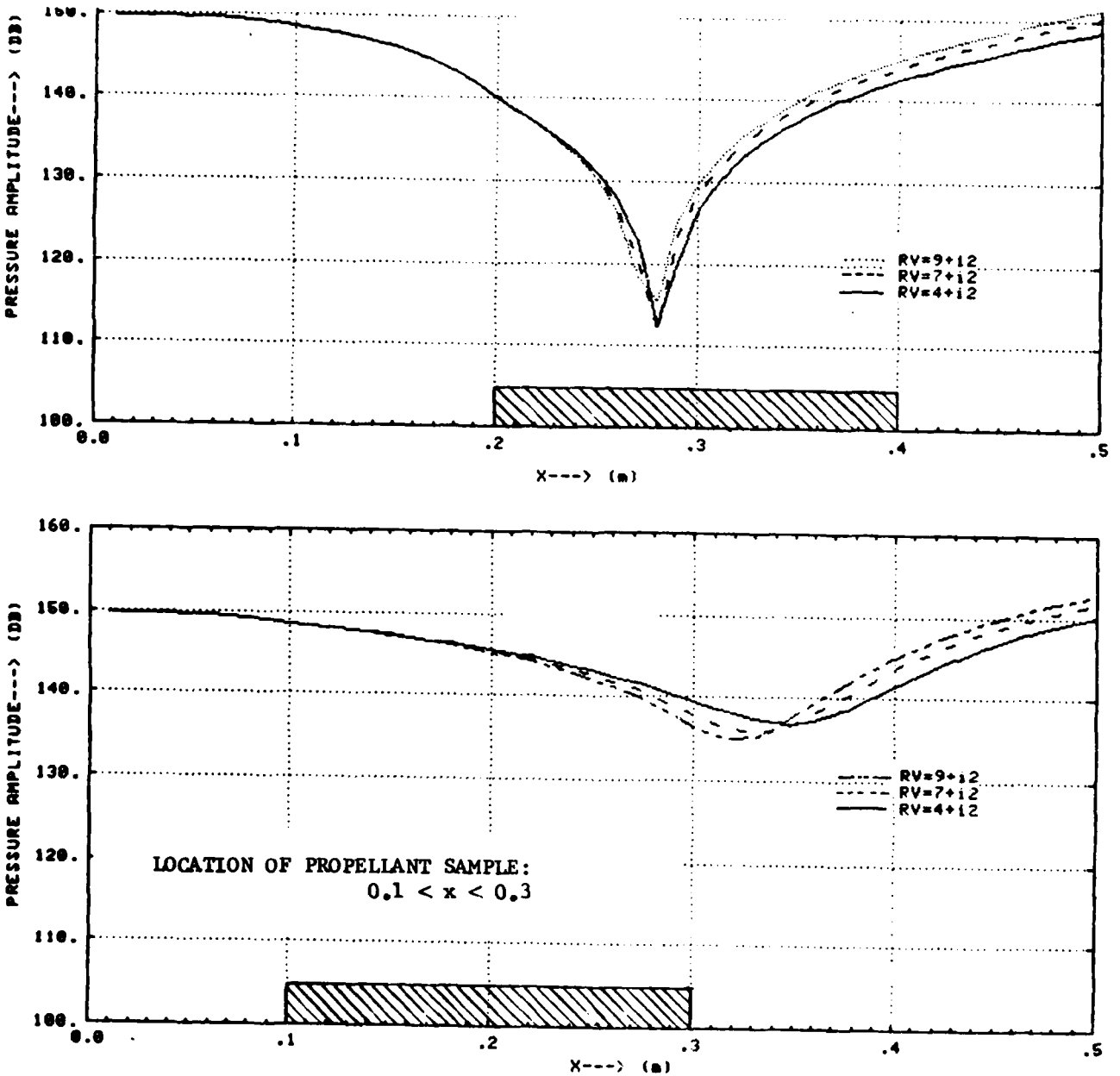

FIG. 7. THE DEPENDENCE OF THE ACOUSTIC PRESSURE AMPLITUDE UPON THE LOCATION OF THE TESTED PROPELLANT SAMPLE.

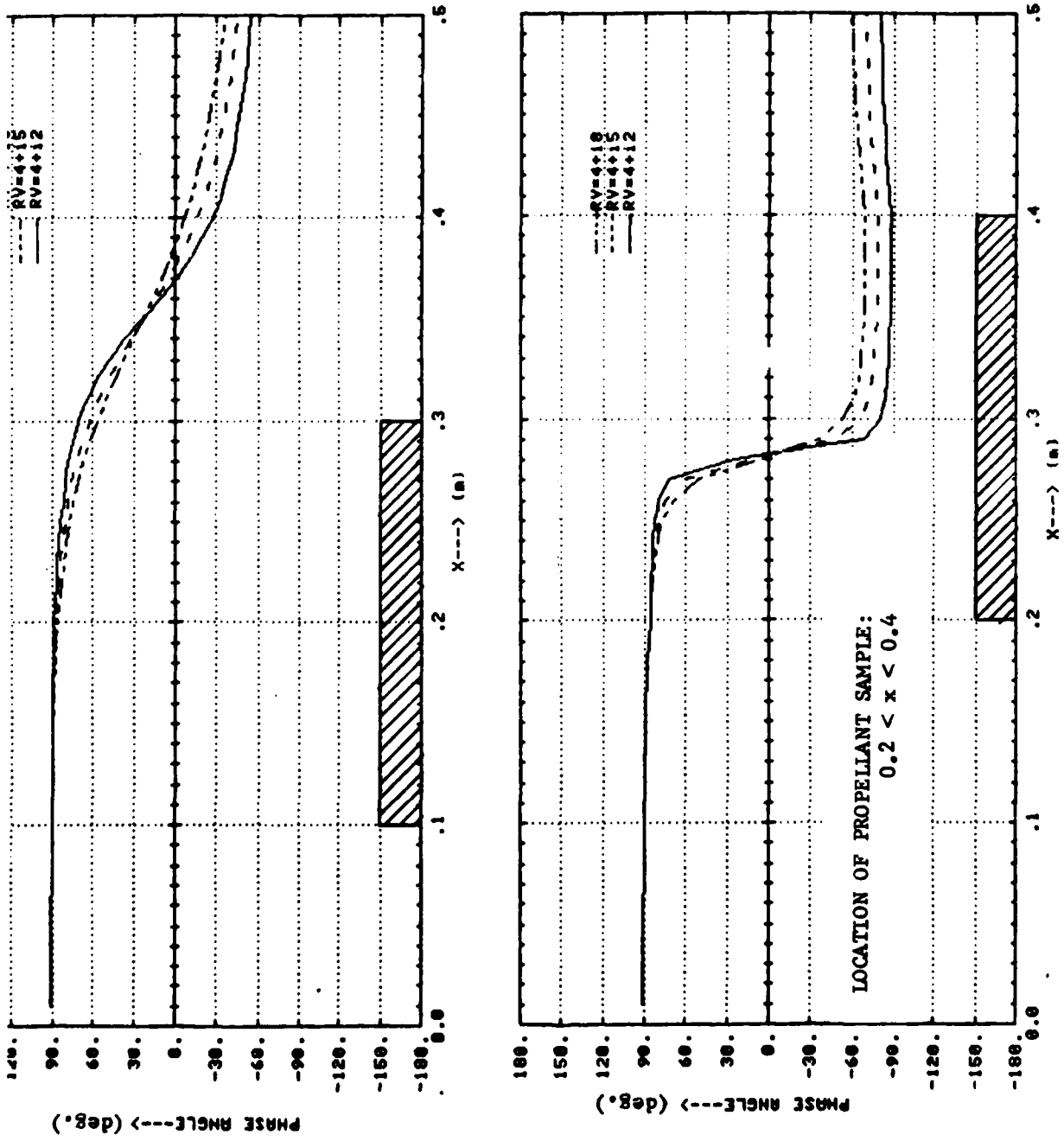

FIG. 8. THE DEPENDENCE OF THE ACOUSTIC PRESSURE PHASE UPON THE LOCATION OF THE TESTED PROPELLANT SAMPLE.

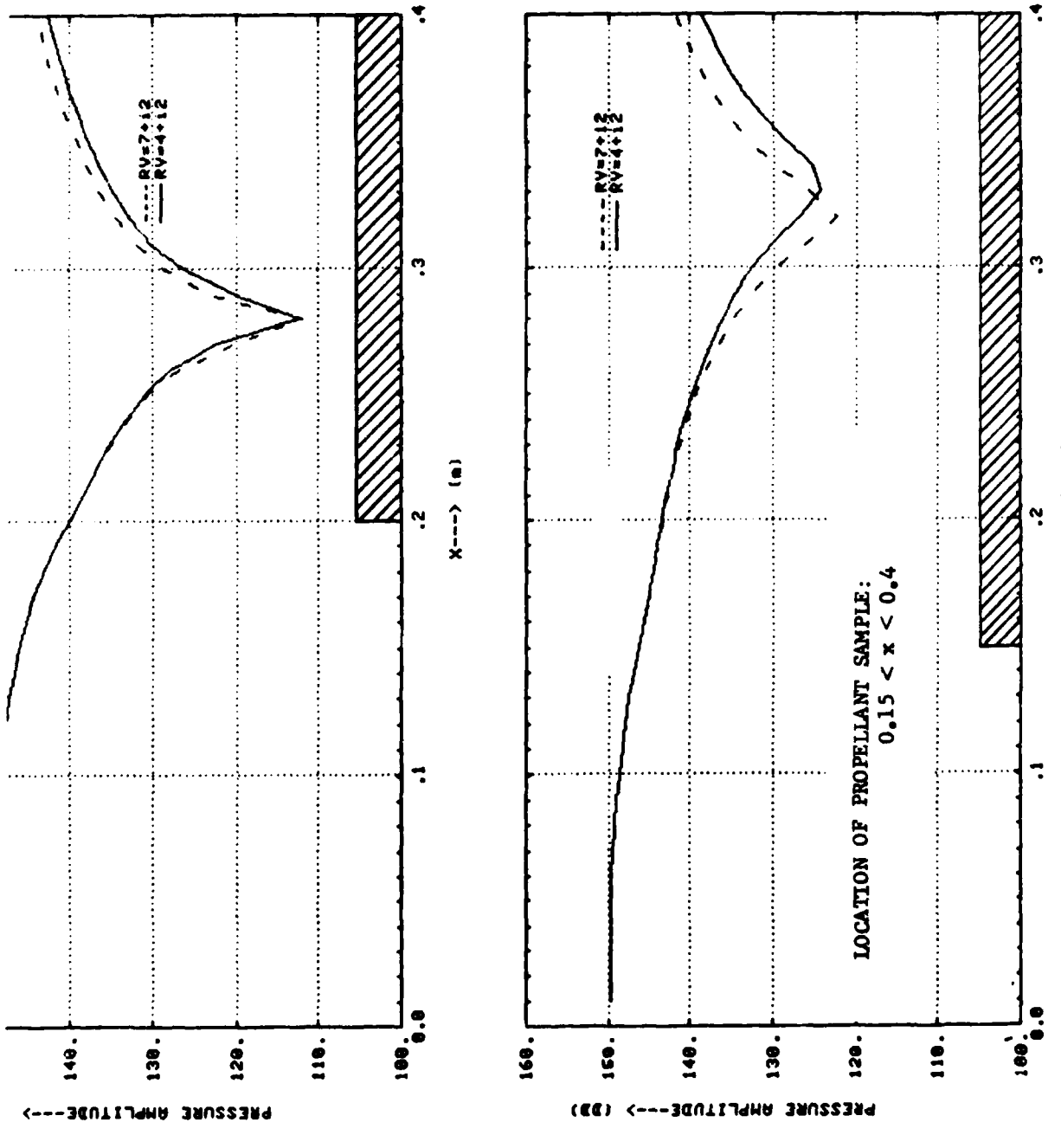

FIG. 9 . THE DEPENDENCE OF THE ACOUSTIC PRESSURE AMPLITUDE UPON THE LENGTH OF THE TESTED PROPELLANT SAMPLE.

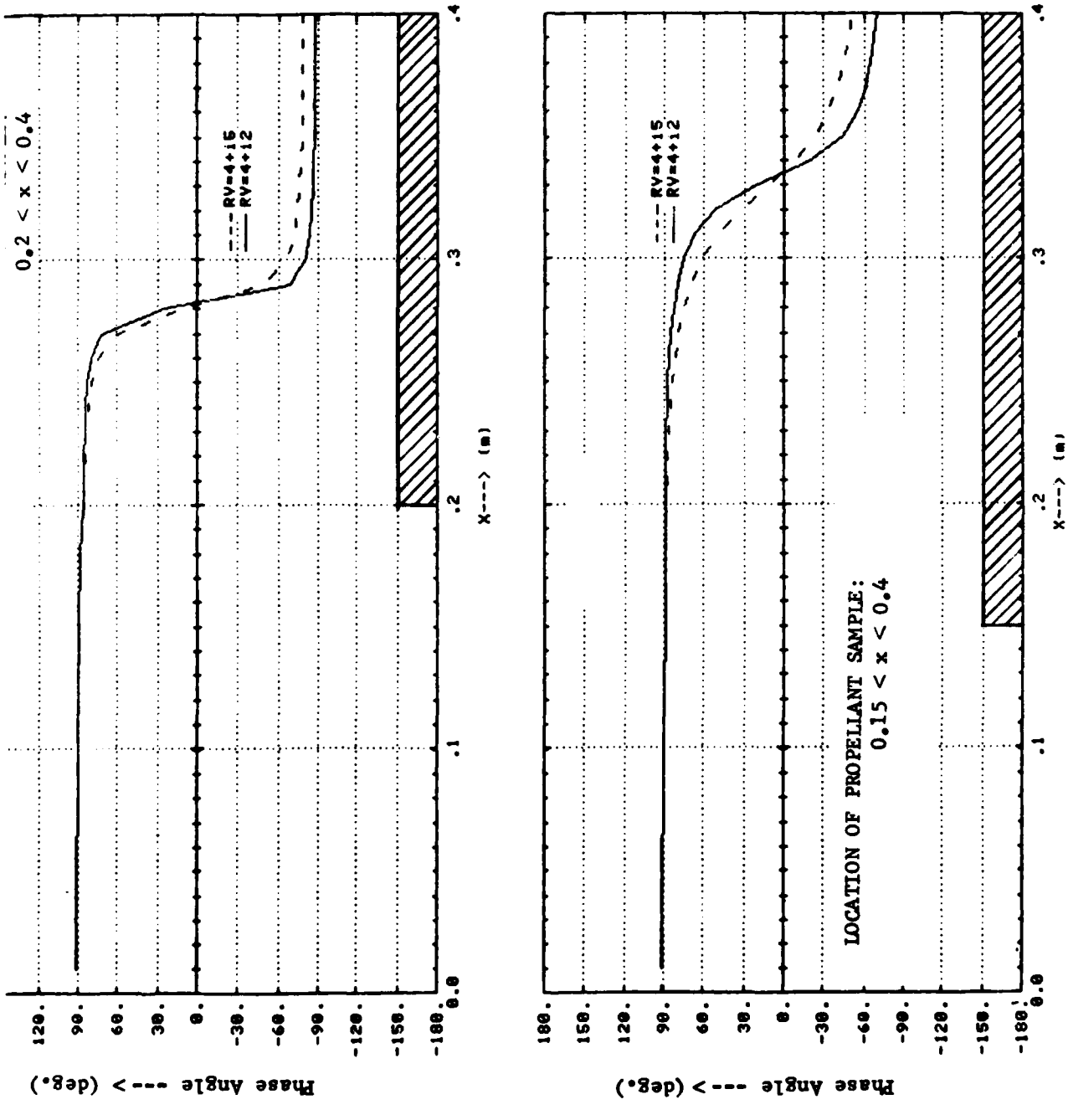

FIG.10. THE DEPENDENCE OF THE ACOUSTIC PRESSURE PHASE UPON THE LENGTH OF THE TESTED PROPELLANT SAMPLE.

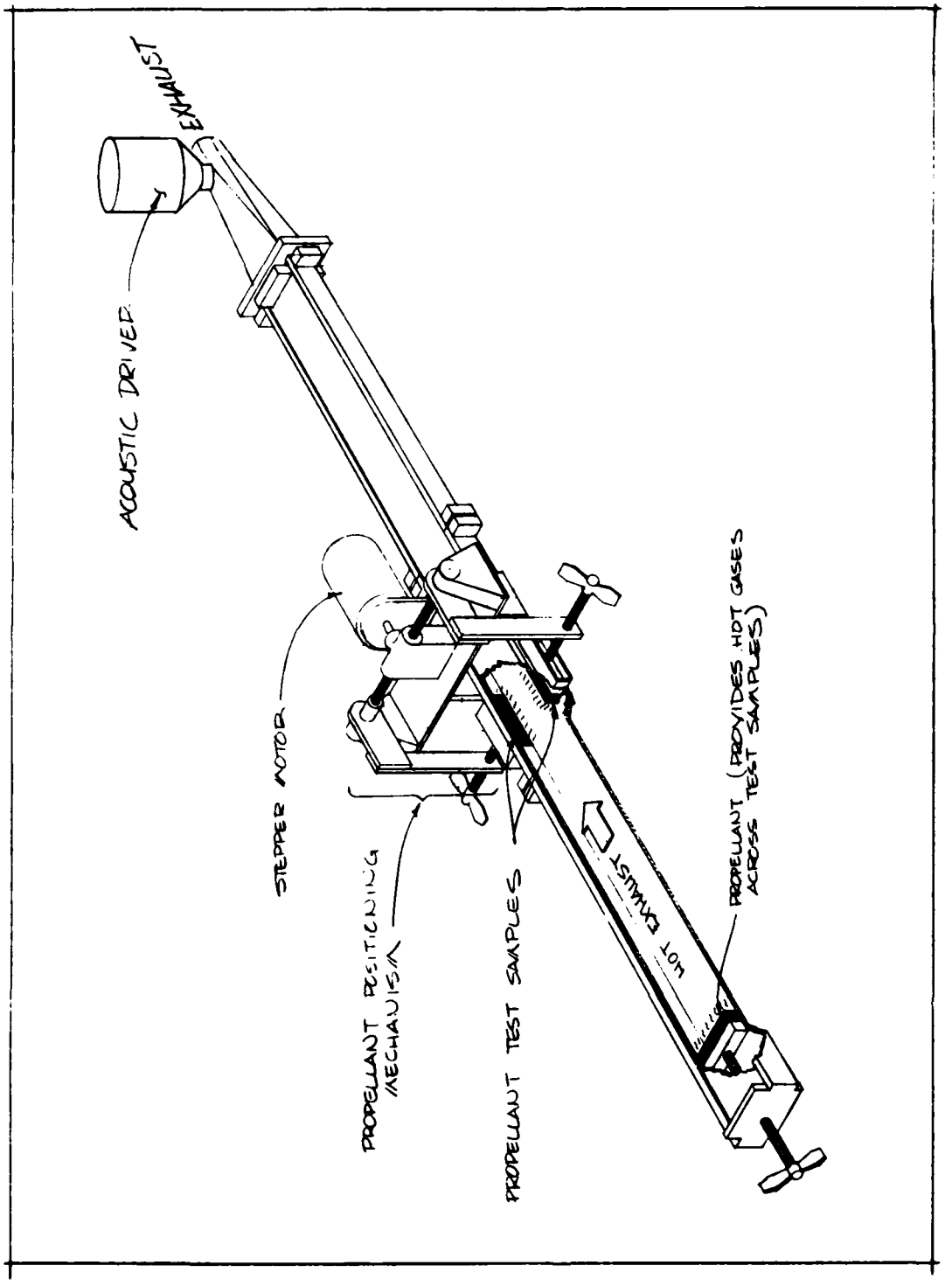

Figure 11. Modified Impedance Tube for Velocity Coupling Measurements.

SCHEMATICS FOR DIRECT MASS LOSS MEASUREMENTS

ROMANOV ET AL SETUP IS EQUIVALENT TO THE FOLLOWING

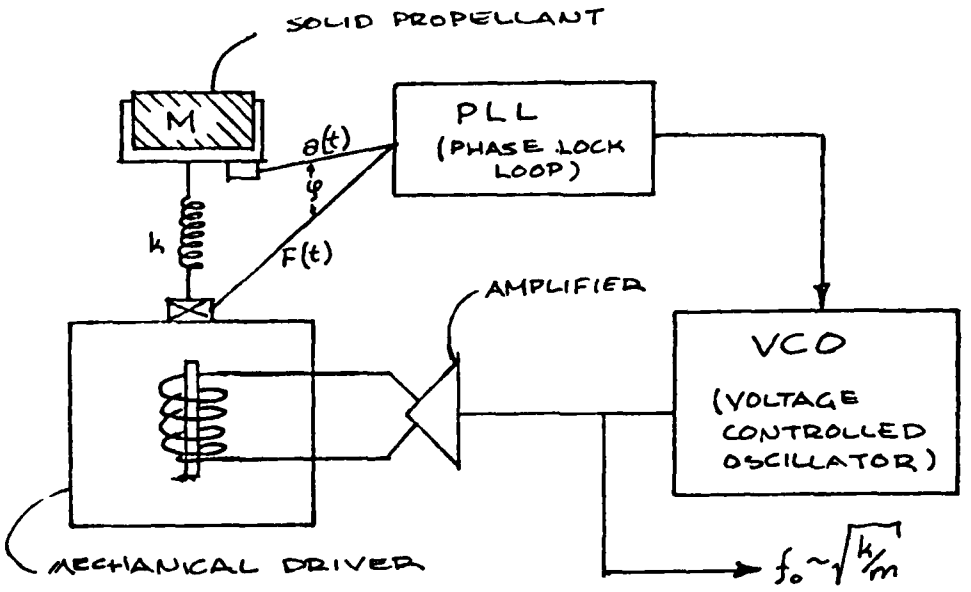

SETUP UNDER CONSIDERATION AT GEORGIA TECH

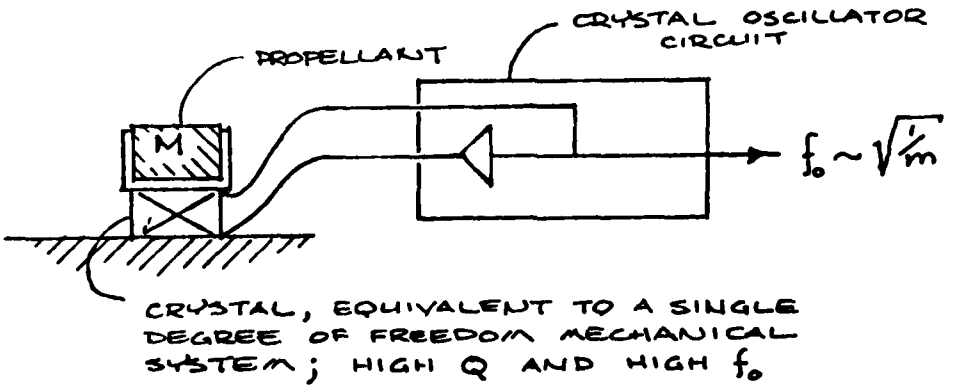

Figure 12. Schematics for Direct Mass Loss Measurement.

RESULTS OF "DIRECT" UNSTEADY MASS MEASUREMENT STUDIES

(I) OBJECTIVES

INVESTIGATE THE SUITABILITY OF USING PIEZOELECTRIC QUARTZ AND CERAMIC CRYSTALS IN THE MEASUREMENT OF THE UNSTEADY MASS LOSS OF BURNING SOLID PROPELLANTS.

(II) SUMMARY OF INVESTIGATION STEPS

(1) AN ELECTRICAL CIRCUIT CAPABLE OF DETERMINING THE NATURAL FREQUENCIES OF PIEZOELECTRIC CRYSTALS WAS DEVELOPED.

(2) THE DEPENDABILITY OF THE EXPERIMENTAL PROCEDURE WAS INVESTIGATED BY DETERMINING THE DEPENDENCE OF THE CRYSTAL RESPONSE UPON

(a) THE LOCATION OF THE ELECTRODES
(b) THE CRYSTAL SUPPORT SYSTEM AND
(c) THE SIZE OF THE ELECTRODE PLATING

(3) THE FREQUENCY RESPONSES OF EIGHT CERAMIC CRYSTALS AND ONE QUARTZ CRYSTAL WERE INVESTIGATED.

Figure 13. Objective and Summary of Direct Mass Measurement Study.

(III) RESULTS

(1) THE FREQUENCY MEASUREMENTS FOR THE CERAMIC CRYSTALS WERE ONLY REPEATABLE TO THE FIRST THREE DIGITS.

(2) THE LOADING OF THE CERAMIC CRYSTALS BY RUBBER-CEMENT TYPE MATERIAL DID NOT RESULT IN A DETECTABLE SHIFT IN THE CRYSTAL'S NATURAL FREQUENCIES

(3) THE LOADING OF A CERAMIC CRYSTAL WITH A LAYER OF SILVER PAINT DID PRODUCE A FREQUENCY SHIFT. HOWEVER, THE FREQUENCY SHIFT PRODUCED BY A 10^{-4} GRAM LOADING WAS SMALLER THAN THE FREQUENCY SHIFT THAT COULD BE ACCURATELY MEASURED DUE TO REPEATABILITY LIMITS.

(4) QUARTZ CRYSTALS CAN BE READILY OVERLOADED AND THEY STOP OSCILLATING WHEN LOADED WITH A MASS OF THE ORDER OF .1 GRAM.

(IV) CONCLUSIONS

(1) THE TESTED QUARTZ CRYSTALS CANNOT BE UTILIZED FOR THE INDICATED PURPOSE BECAUSE THEY WOULD NOT RESPOND WHEN LOADED WITH EVEN THE SMALLEST POSSIBLE SAMPLES OF SOLID PROPELLANTS.

(2) THE TESTED PIEZOCERAMIC CRYSTALS COULD NOT BE USED FOR THE INDICATED PURPOSE BECAUSE THEY DO NOT POSSESS THE RESPONSE CHARACTERISTICS THAT ARE REQUIRED TO DETECT THE MASS CHANGES THAT ARE EXPECTED TO OCCUR DURING UNSTEADY COMBUSTION OF SOLID PROPELLANTS.

Figure 14. Results and Conclusions of Direct Mass Measurement Study.

PROPELLANT COMPOSITION (%)

	UZ-7: Non-aluminized		UZ-8: 5% Aluminum		UZ-9: 18% Aluminum	
INGREDIENT	ACTUAL	DESIRED	ACTUAL	DESIRED	ACTUAL	DESIRED
R-45m	9.34	9.34	9.34	8.873	9.34	7.6588
INDOPOL	1.85	1.85	1.85	1.7575	1.85	1.517
TEPANOL	0.15	0.15	0.15	0.1425	0.15	0.123
AP-200 μ	51.00	51.00	51.00	48.45	38.00	41.82
AP-50 μ	15.00	15.00	12.00	14.25	13.00	12.3
AP-8 μ	22.00	22.00	20.00	20.90	19.00	18.04
ALUMINUM: 4.5 μ	0.00	0.00	5.00	5.00	18.00	18.
IDPI	0.66	0.66	0.66	0.627	0.66	0.5412

Table I. Comparison of desired and actual compositions of tested propellants.

Real Part of the Propellant Non-Dimensional Admittance

FREQUENCY (Hz)	UZ - 7	UZ - 8	UZ - 9
400	0.6686×10^{-2}	0.1928×10^{-1}	0.2821×10^{-1}
600	0.1498×10^{-1}	0.121×10^{-1}	0.3336×10^{-1}
800	0.7941×10^{-2}	0.233×10^{-1}	0.4821×10^{-1}
1000		0.1187×10^{-1}	0.2841×10^{-1}

Gas Phase Loss Coefficient x 10^6 (lbm/in^3-s)

FREQUENCY (Hz)	UZ - 7	UZ - 8	UZ - 9
400	2	20	41
600	7	27	60
800	0	52	114
1000		49	126

Table II. Frequency dependence of measured admittances and gas phase losses of the propellants described in Table I.

TASK II

EXTERNAL/BASE BURNING FOR PROPULSION

J. E. HUBBARTT
W. C. STRAHLE

TASK II

EXTERNAL/BASE BURNING FOR PROPULSION

JAMES E. HUBBARTT WARREN C. STRAHLE

A. Research Objectives

This research employed scale-model, simulation tests to systematically evaluate the use of external/base burning to reduce base drag or provide base thrust for axisymmetric, blunt-base bodies at Mach 3. The specific objectives were to determine performance potentials, flowfield features, and effects of fuel properties.

B. Results and Discussions

The following six major tasks were completed under this research program:

1. Modification of the test facility for combustion tests.
2. Cold flow tests with base injection.
3. Base burning tests with subsonic base and radial injection.
4. Combined base and external burning tests using supersonic radial injection.
5. Base burning tests with diluted fuel injection.
6. Combined preburning and base burning tests.

All of the goals initially set down for this program were successfully completed except for external burning with base thrust (i.e., with base pressure greater than the freestream pressure). External burning with base thrust was accomplished but it was established that the results vere biased by wind tunnel interference effects which cannot be eliminated in a small scale test facility. The program has yielded a vast amount of data important to assessing the application of burning for elevating the base pressure of blunt base bodies. All results have been reported in the open literature[1]-[5]. The major accomplishments and results are summarized in the following sections. The reader is referred to these references for more details.

1. Test Facility.

Figures 1 and 2 present schematics of the test facility and test section. Photographs of the test section and the probe actuator system are shown in Figure 3. This is a blowdown type wind tunnel designed to simulate the flow in the base region of an axisymmetric projectile with a fineness ratio of about 6. The freestream Mach number at the base plane is 2.98 and most tests were conducted at a Reynolds number, based on the model diameter, of about 4.5×10^6. During a typical test the freestream stagnation temperature drifted downward from about 10 to 20°C. The cylindrical model is supported in the low-speed flow upstream of the supersonic nozzle to eliminate support effects. Injection gases and instrumentation leads are ducted into the model cavity through these support struts. The wake is surveyed with small scale pilot-static and thermocouple probes supported downstream of the base by the two-degree-of-freedom actuator. Tests are controlled and data are retrieved by a computer-based data acquisition system.

The basic facility was originally designed for cold flow tests which simulated the compression imposed on the near wake by external burning. During the current program it was modified for fuel injection and actual burning tests. This required the addition of three gas systems fed by bottled gases and including metering and safety devices. Hydrogen was used as the fuel because of its high reaction rate. Either pure hydrogen or hydrogen diluted with an inert species, reducing the effective fuel heating value, could be supplied to the model base region. Simultaneously, pure oxygen could be ducted to the base region, permitting tests with combined preburning and wake burning, simulating the decomposition and subsequent base burning for a solid propellant. Also, several different base configurations were fabricated for the various burning tests.

2. Cold Flow Tests with Base Injection.

Cold-flow, base injection tests were made using several gases to determine the effect of injectant molecular weight and specific heat ratio on base pressure rise due to blowing. The model was fitted with a porous sintered-metal base plate for uniform base injection and tests were run injecting air, nitrogen, helium, and hydrogen. The gases were injected axially into the near wake at ambient temperature, at subsonic speed, and with negligible momentum flow rates. The results are summarized in Figure 4. The top plot presents the

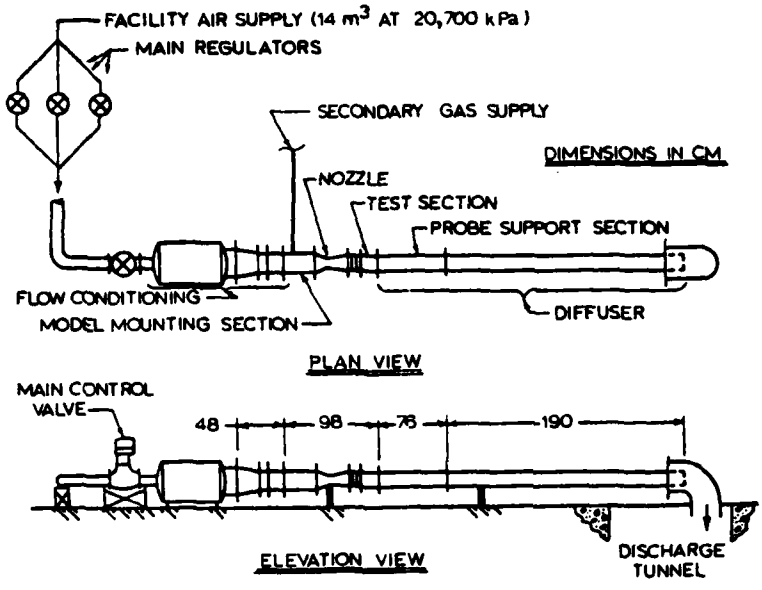

FIGURE 1. EXTERNAL/BASE BURNING TEST FACILITY SCHEMATIC

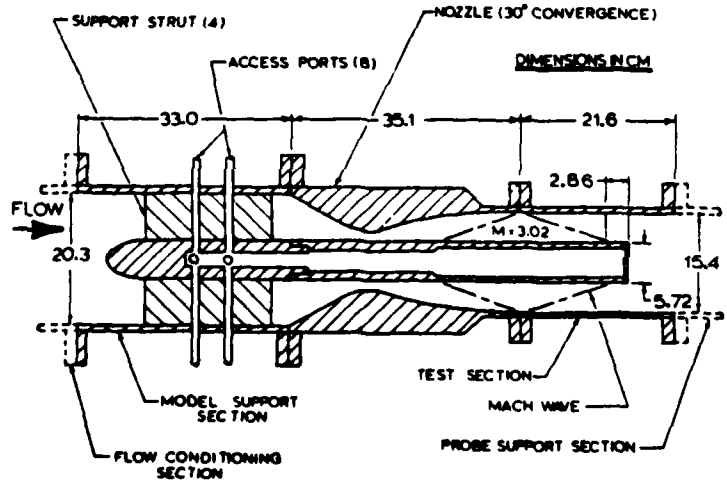

FIGURE 2. TEST SECTION DETAILS

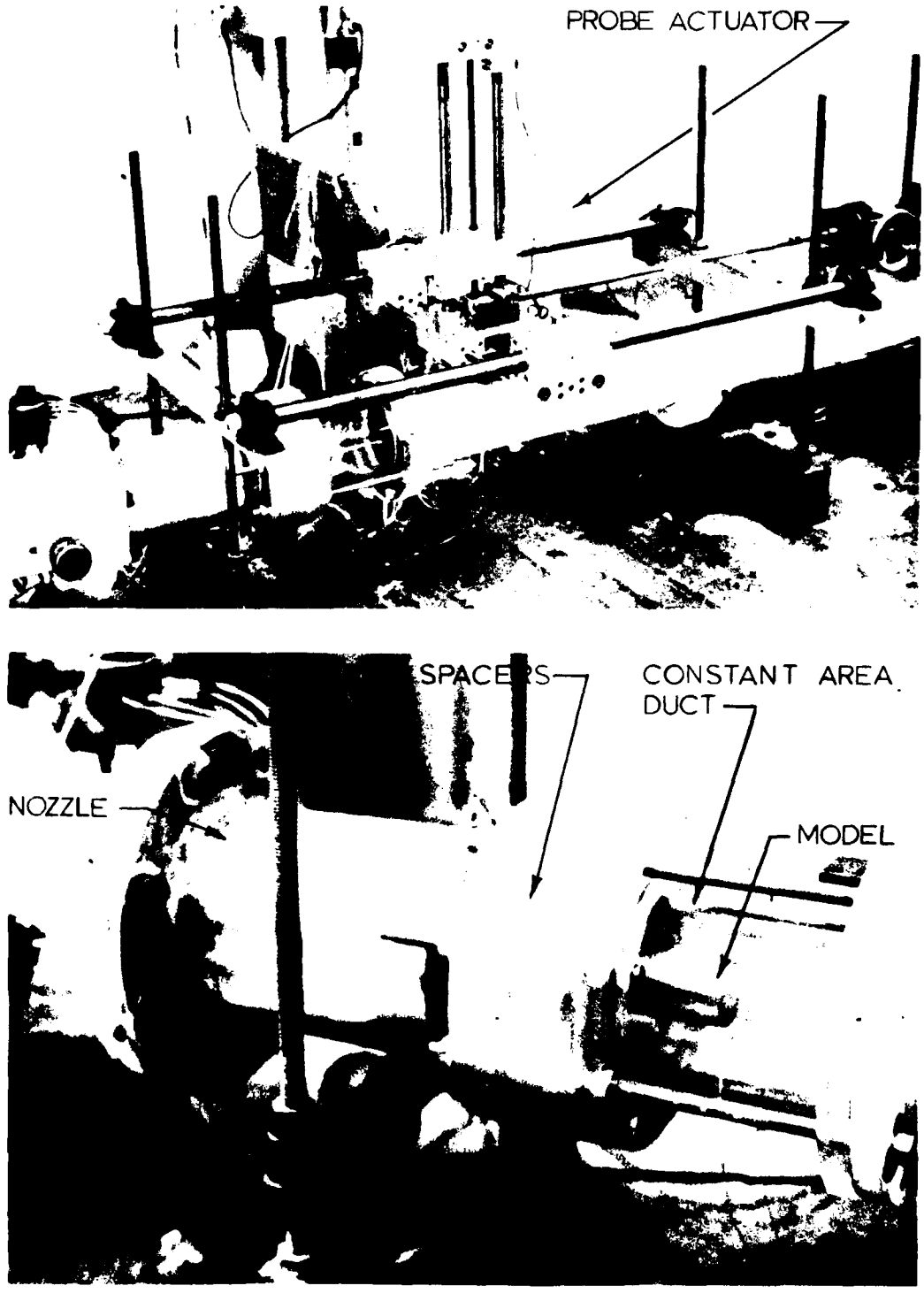

FIGURE 3. PHOTOGRAPHS OF TEST SECTION AND PROBE ACTUATOR

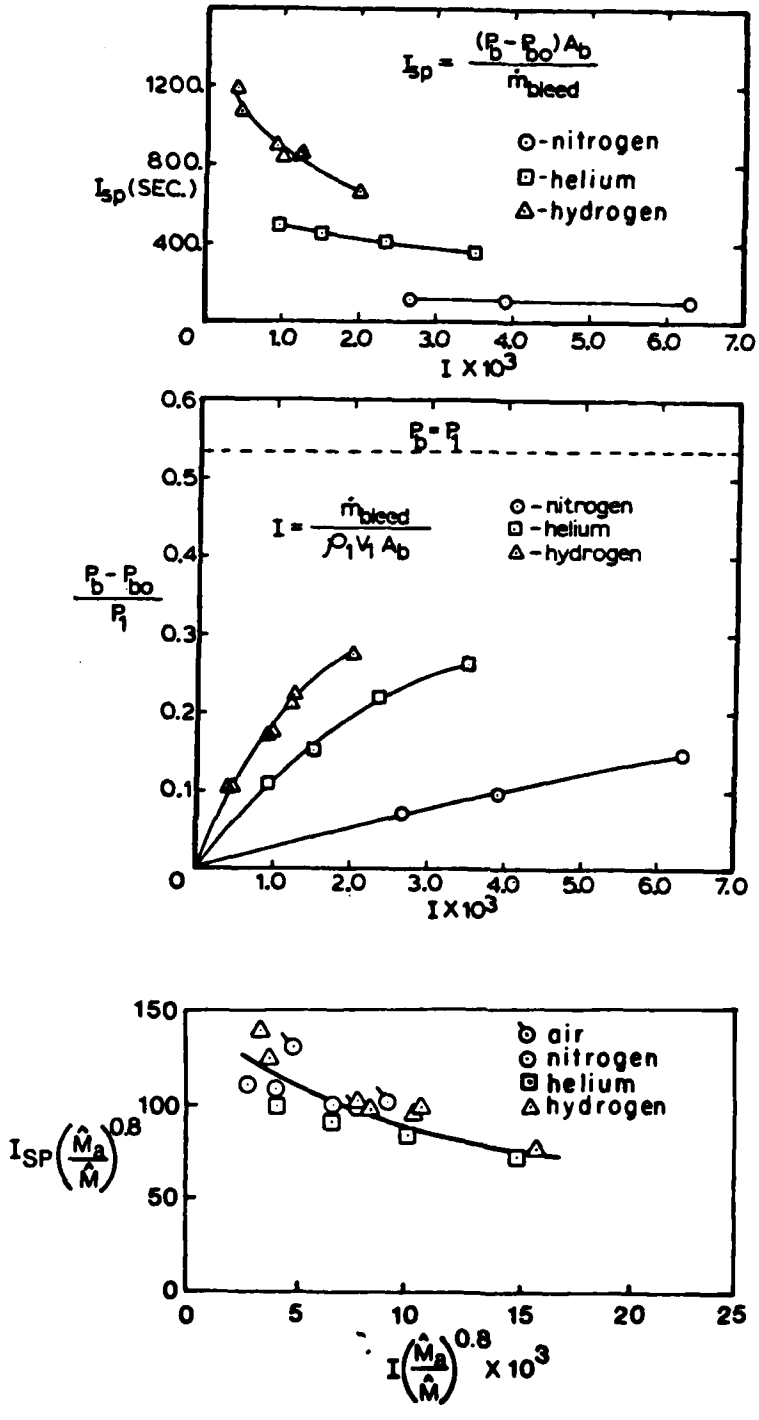

FIGURE 4. RESULTS FOR COLD GAS INJECTION

specific impulse I_{SP} (i.e., the increase in base force due to injection divided by the injectant mass flow rate) versus the injectant flow rate parameter I (i.e., the injectant mass flow rate divided by the freestream mass flow rate through an area equal to the base area) for nitrogen, helium, and hydrogen injection. The middle plot shows the effect of I on the ratio of the base pressure rise with injection to the freestream pressure P_1. As shown, the specific impulse and base pressure elevation increases with decreasing molecular weight or gas density. Correlation of the data is shown in the bottom plot of Figure 4. The scatter of the data from the mean line is probably within data accuracy. The relevant flow parameter is I divided by the molecular weight raised to the 0.8 power. (This presentation normalizes the molecular weight by that of air.) This is very nearly a volume flow rate parameter and was first suggested by Bowman and Clayden[6] and, later, by Freeman and Korkegi[7]. Also, in the present tests, the specific heat ratio slightly affected base pressure rise[2] but is not included in the correlation of Figure 4 since the change is nearly within the data accuracy. Wake surveys [2][3] showed that the length of the near wake increases markedly with injection rate and the recirculation bubble is blown off when about 80% of the base drag is eliminated.

3. Base Burning with Subsonic Base and Radial Injection.

Four fuel injection configurations were used for the base burning tests. Three of these are shown in Figure 5. The base injection configuration (top panel) uses a porous sintered-metal base plate for axial injection of a uniform stream of hydrogen. The radial injection configuration (lower left panel) uses six equally spaced radial ports recessed in an annular channel which serves as a flame holder. The combination configuration (base plate shown at lower right) uses the radial injection configuration with a porous base plate for combined radial and axial injection. The fourth configuration (not shown) provides for radial slot injection. Spacers were inserted between the plane base plate and the cylindrical forebody to yield a 0.64 cm wide peripheral slot immediately upstream of the base plane.

Ignition of the base flow was accomplished using cured pyrotechnic compound coated on a consumable igniter sting as illustrated with the base injection configuration of Figure 5. Also, the channel containing the six radial nozzles was lined with the pyrotechnic paste and was ignited separately. The pyrotechnics were ignited by resistance heating.

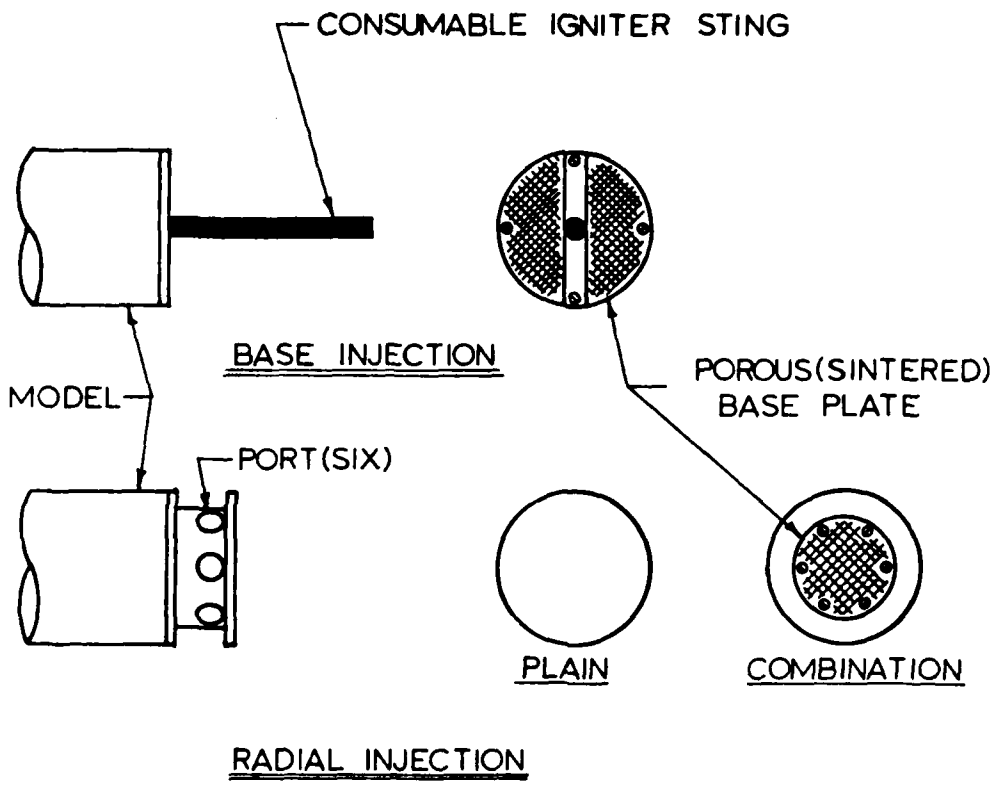

FIGURE 5. IGNITION AND FUEL INJECTION CONFIGURATIONS

Burning results for subsonic base injection, radial slot injection and radial jet injection of pure hydrogen are shown in Figure 6. For comparison the figure includes cold flow base injection results. Results are the same for radial slot injection and for base injection. Observation of the burning zone revealed that both of these modes of injection yield pure base burning. As shown in Figure 6, performance with subsonic radial injection through discrete nozzles is somewhat lower than that with base or radial slot injection. Observations of the flame indicated that this mode of operation more resembled base burning than external burning with discrete plume combustion in the freestream. Furthermore, analysis show that jet penetration into the freestream is very small. Hence, it is included here as base burning mode of operation. It is thought that the reduced performance with the jets is probably due to asymmetries in the mixing processes created by the discrete jets.

As shown in Figure 6, the base pressure rises with increasing hydrogen injection and asymptotically approaches freestream pressure. The diminishing returns of increased injection are reflected by the rapid decline of specific impulse. Nevertheless, significant reductions in base drag at impressive values of I_{SP} are demonstrated. For examples, the lower plot, which summarizes the results for base injection, shows an 80% reduction in base drag with I_{SP} of about 5000 and a 50% reduction with I_{SP} = 12,000. For comparison, the I_{SP} for a comparable ramjet engine would be about 5000 to 6000. Townsend and Reid[8] have also reported high values of I_{SP} for base burning at Mach 2.14.

The effect of superimposing external compression, simulating that due to external burning, and, base burning with axial injection is shown in Figure 7. Compression sections I, II, and IV, described in Reference 1, were used for these tests. Compression section I and II impose axisymmetric compressions on the near wake whereas compression section IV impose an asymmetric compression like that due to six combustion plumes in the freestream. The important point from these results is that the separate effects of base burning and external compression are additive. This is shown to be the case for high base thrust levels. Schadow and Chieze[9] also determined from two-dimensional tests that the base pressure rise with external burning of a solid propellant and base injection of an inert gas superimpose.

4. Combined Base and External Burning.

The two base configurations shown in Figure 8 were used for combined

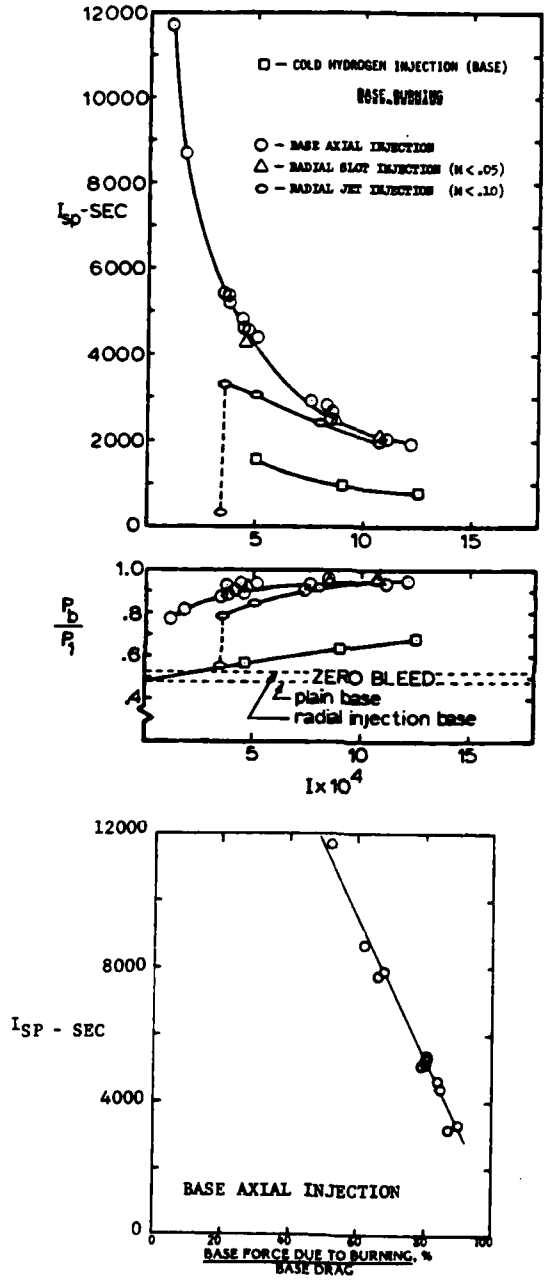

FIGURE 6. BASE BURNING RESULTS

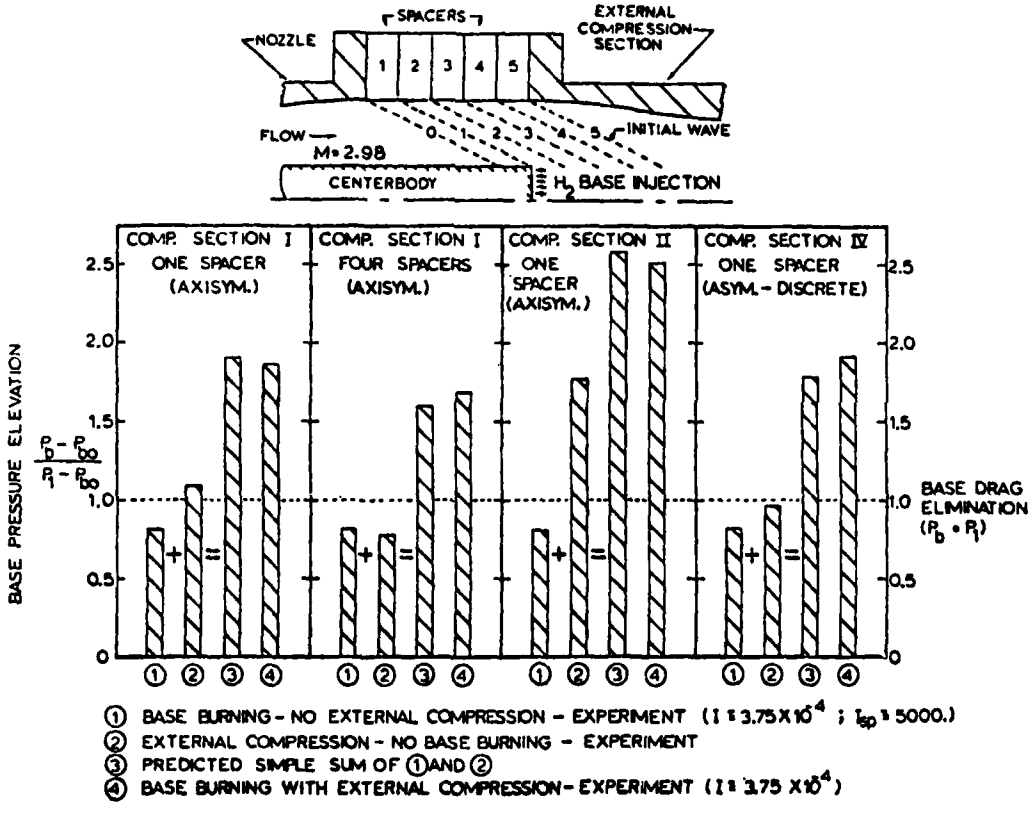

FIGURE 7. COMBINED BASE BURNING AND SIMULATED EXTERNAL BURNING

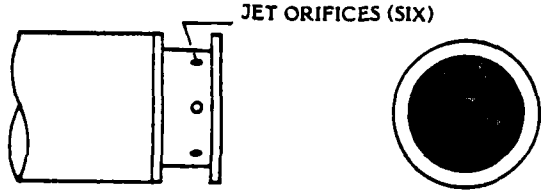

CHANNEL FLAMEHOLDER

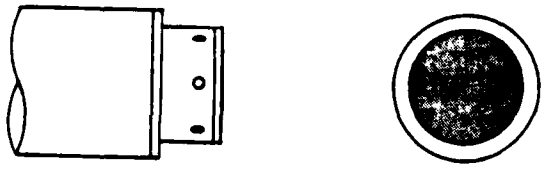

STEP FLAMEHOLDER

FIGURE 8. BASE CONFIGURATIONS FOR COMBINED BASE AND RADIAL INJECTION

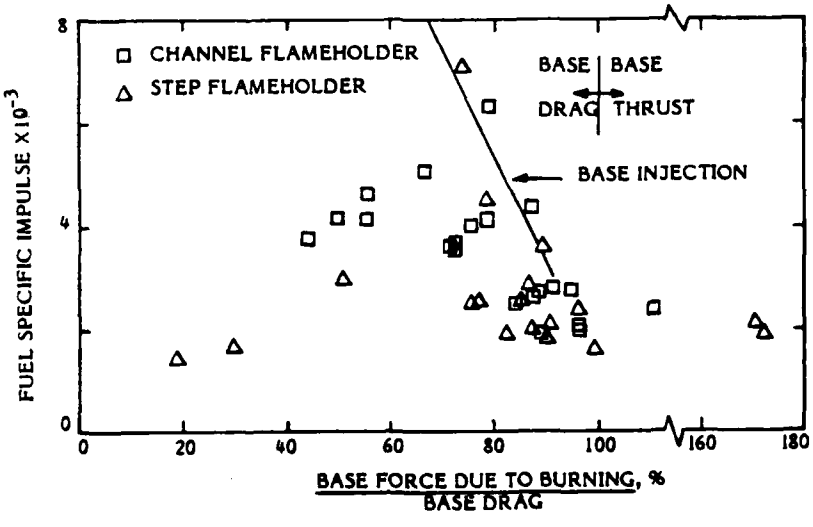

FIGURE 9. RESULTS FOR SUPERSONIC RADIAL INJECTION

base and external burning tests. Both configurations have six small jet orifices for radial injection and a porous base plate for axial injection at subsonic speeds. In contrast with the subsonic radial injection tests discussed in the previous section, supersonic injection results in deeper jet penetration into the freestream and, correspondingly, some external burning. The upper configuration employs a channel type flameholder around the jets while the lower configuration uses a step flameholder. Tests were made with two jet orifice diameters (1.0 and 1.9 mm) and ratios of jet-to-base mass flow rates from about 0.3 to 4.0. The ranges in jet Mach number and jet-to-freestream velocity ratio were from 1 to 3.1 and 2 to 4.2, respectively.

The results for combined subsonic base and supersonic radial injection are presented in Figure 9. It should be noted that only three of the data points are for base thrust conditions. Furthermore, no attempt is made to associate the data points with orifice diameter, mass flow ratio, or jet Mach number since the results are characterized more by scatter than specific trends. The line representing the base burning data of Figure 7 is included for reference.

The results for combined base and radial jet injection scatter significantly. In general, the specific impulse with a given base drag reduction is lower than that for base injection. Nevertheless, specific impulse values slightly higher than those for base injection were obtained. The large data scatter is associated with differences in combustion which was very marginal for the test environment. In fact, ignition and combustion were erratic and many tests were aborted because ignition was obviously not accomplished in the base, in the flameholder, or in both. However, the high performance points of Figure 9 were visually identified with good combustion and are thought to be most representative of the performance potential. Therefore, it is concluded that combined external and base burning can be competitive with base burning alone. This suggests that external burning coupled with base burning may also be practical for providing base thrust. However this needs further verification in a more favorable environment.

It has been determined that the three data points which provided base thrust have been biased by wind tunnel wall effects. Surveys along the wake showed that the wake was subsonic beyond the point where the reflected compression wave created by the elevated base pressure intersects the wake.

This compression wave would tend to increase the base pressure and, hence, make these results optimistic. Definitive tests for base thrust conditions will require a much larger wind tunnel.

On the other hand, it is important to realize that wind tunnel interference effects in the results of Figure 9 for base drag conditions (i.e., P_b less than P_1) could only decrease the base pressure and, hence, render the results pessimistic.

5. Base Burning with Diluted Fuel Injection.

Base burning tests were made using hydrogen diluted by inert gases to simulate practical propellants with low fuel heating value. Nitrogen, helium, and carbon dioxide were used as diluents. The diluents were premixed with the hydrogen before entering the test model. The mixtures were injected into the wake through the porous base plate.

Performance results are shown in Figure 10. The upper two plots show that the percent base drag reduction and the specific impulse based only on the hydrogen flow rate, $I_{SP_{H_2}}$, depends on the hydrogen flow rate parameter, I_{H_4} and is independent of the type and amount of diluent. In other words, base pressure rise is determined solely by the total heat release. Correspondingly, the specific impulse based on the total injectant flow rate I_{SP}, decreases directly with the fuel heating value of the injectant Q_R. Thus, a more useful presentation of the data is a plot of specific impulse scaled by the fuel heating value versus the base drag reduction, as shown in the lower of Figure 10. The line in this figure represents the results for pure hydrogen injection for which $Q_R = 1.21 \times 10^5$ J/g (i.e., the circular data points in the upper two figures). The data points are for the diluted mixtures and cover effective fuel heating values from 10,000 to 60,000 J/g. In the abscissa, Q_R is normalized by 20,000 J/g, a typical heating value for a practical solid propellant. In this presentation the performance with the diluted mixtures agrees well with that for pure hydrogen. For example, a propellant with Q_R = 20,000 J/g would yield a specific impulse of about 800 sec with 80% base drag reduction. The I_{SP} increases to about 2000 sec for a 50% base drag reduction.

Some temperature and Mach number profiles along the wake centerline downstream of the base are shown in Figure 11. The upper plot of Figure 11a presents temperature profiles for three base pressure levels (i.e., total heat dump rate). The hydrogen is diluted with CO_2 so as to yield Q_R = 25,000 J/g. As

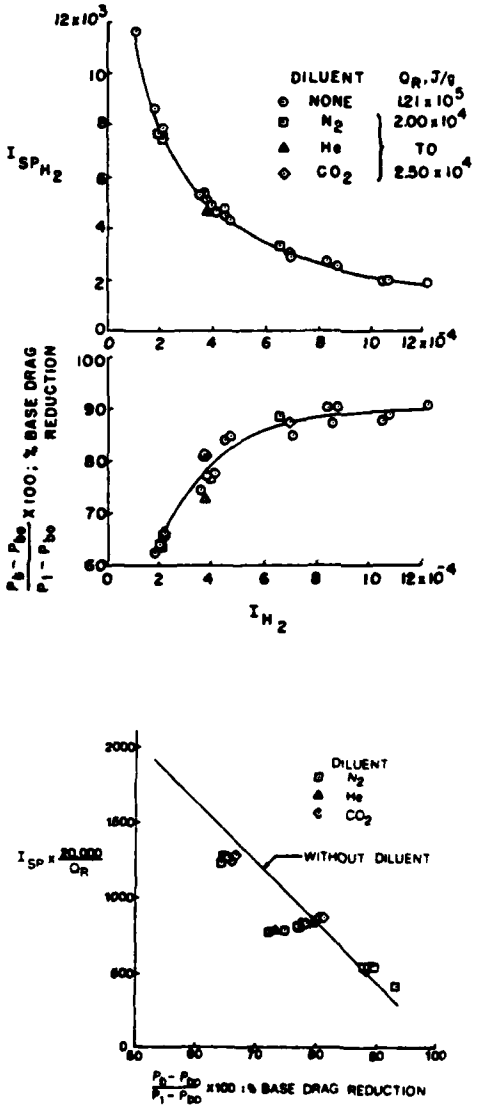

FIGURE 10. BASE BURNING RESULTS WITH DILUTED H_2

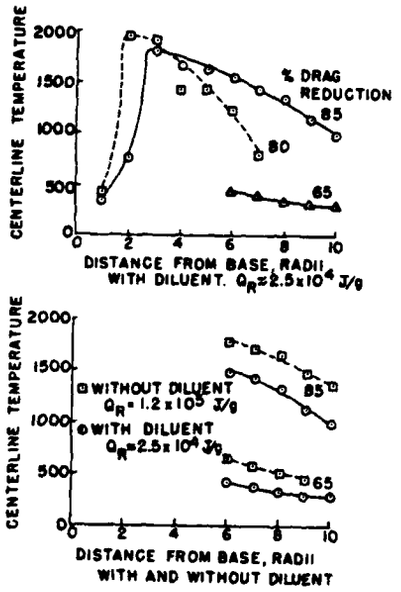

a. CENTERLINE TEMPERATURE PROFILES

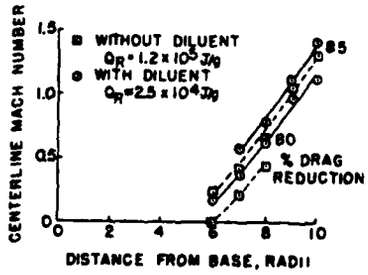

b. CENTERLINE MACH NUMBER PROFILES

FIGURE 11. WAKE CENTERLINE TEMPERATURE AND MACH NUMBER PROFILES FOR BASE BURNING WITH CO_2 DILUENT

shown, the maximum temperature on the centerline occurs close to the base plane even at the high base pressure levels. Oxygen must be supplied to this combustion zone by the forward flow induced by recompression. With increased hydrogen flow rate, the base pressure rises, the recompression weakens, and the location of the maximum temperature shifts downstream. Downstream of the temperature peaks the mixture is oxygen rich and the temperature drops rapidly due to mixing with the freestream. The lower plot of Figure 11a compares temperature profiles for pure and diluted hydrogen injection. The temperature reduction with diluent cannot be accounted for by the heat capacity of the diluent alone. Thus, it appears that the rates of mixing with the ambient air must be increased also because of the diluent.

Wake centerline Mach number profiles are shown in Figure 11b. For base drag reduction less than 80% and Q_R less than 25,000 J/g the wake becomes supersonic within 9.5 radii from the base. Since the expansion wave emanating from the base and reflecting from the wind tunnel wall will intersect the wake at this location this represents the boundary for interference free wake flow. For higher base drag reduction and Q_R the results are conservative since the expansion wave tends to reduce base pressure. However, the wave becomes weaker with increasing base pressure and the effect must be small.

6. Combined Preburning and Base Burning.

A solid propellant used for base drag reduction first decomposes into a hot gas mixture and then burns with the ambient air in the near wake. Thus, for a solid propellant there is combined preburning and base burning. The preburning component is equivalent to hot gas injection like that investigated by Clayden and Bowman[10]. To simulate the use of solid propellants tests were made in this program using combined preburning and base burning. Preburning was accomplished by injecting pure oxygen along with hydrogen diluted with nitrogen or carbon dioxide to reduce the effective heating value. The base configuration employed in these tests is shown in Figure 12. A hollow extension of the forebody is used as the preburner. Pure O_2 is supplied to the front of this preburner through four tubes passing through the center body and the porous base plates. H_2 premixed with N_2 or CO_2 is supplied separately through the centerbody and the porous base plate. This mixture is constrained to annular jets surrounding the oxygen jets by the solid metal base plate with four holes concentric with the oxygen supply tubes. The jets mix and burn within the

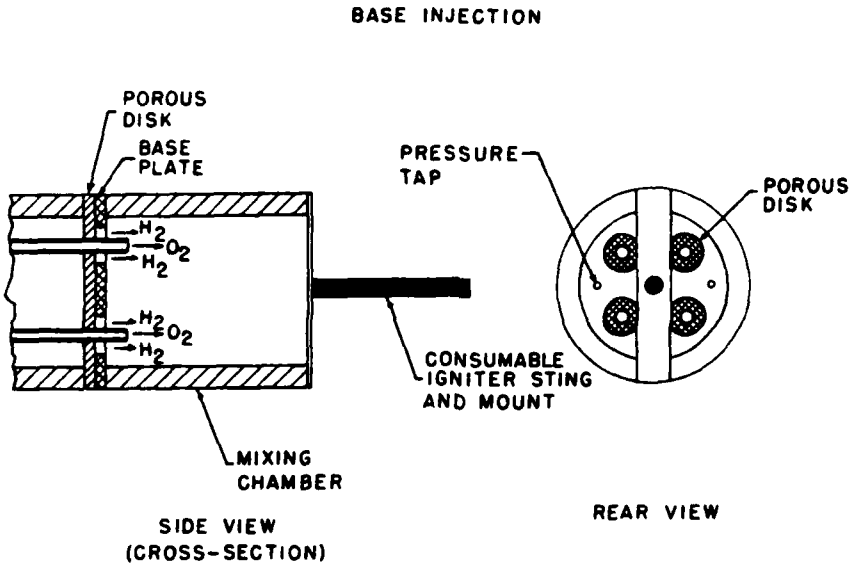

FIGURE 12. BASE CONFIGURATION FOR PREBURNING AND WAKE BURNING

preburner.

Performance results for combined preburning and base burning are shown in Figure 13. Figures 13a and 13b contain results obtained using N_2 as the diluent. Data are shown for runs distinguished by an increasing O_2 flow rate and a decreasing N_2 flow rate so as to maintain a nearly constant O_2 plus N_2 flow rate. Increasing I_{H_2} corresponds to increasing the effective fuel heating value. Increasing I_{O_2} corresponds to increasing the ratio of preburning to wake burning heat release. For comparisons, the curves representing pure base burning (Figure 10) are included. The exciting point of this comparison is that base pressure is increased significantly by preburning. The data for the two lowest O_2 flow rates show an optimum H_2 flow rate. The performance reduction after this optimum is apparently due to cooling of the preburned products as the excess H_2 absorbs heat. At the highest O_2 flow rate a maximum is not reached and the peak base pressure is nearly equal to the freestream pressure. Also it should be noted that the base pressure increase approaches a limit with increasing O_2 flow rate; that is, as the ratio of preburning to wake burning increases. The dashed line on Figure 13b indicates the approximate peak performance with this mode of operation. With base drag reductions greater than 80%, preburning can essentially double the I_{SP}. Impressive values of I_{SP} are obtainable with large drag reductions for practical total fuel heating values and splits between preburning and wake burning. In fact, the performance is as good as or better than performance with complex ramjets. The results of Figures 13a and 13b cover a range in effective fuel heating values from 17,000 to 35,000 J/g. The heat release ratio of preburning to wake burning at the lowest I_{H_2} varies from 0.35 to 2.4 and at the highest I_{H_2} varies from 0.15 to 0.5. The limiting base pressure is reached when this ratio is about 0.5 or higher.

Figure 13c compares results for preburning and wake burning using CO_2 and N_2 as diluents. These data again show that the type of diluent has no significant effect on performance.

Results of superimposing external compression on combined preburning and base burning are shown in Figure 14. The results cover preburning to wake burning heat release ratios of from zero to 3.0. Compression section IV[(1)] is used to impose external compression on the wake. As shown here, combined external compression with burning yields essentially the same base pressure rise as the

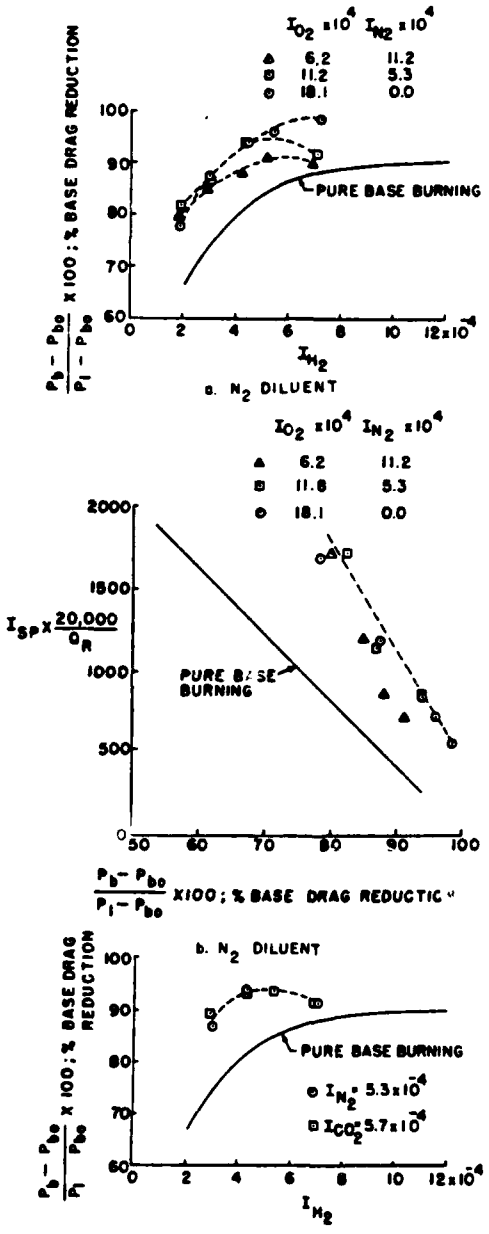

c EFFECT OF DILUENT ON PREBURNING AND BASE BURNING PERFORMANCE

FIGURE 13. PERFORMANCE RESULTS FOR COMBINED PREBURNING AND BASE BURNING

PREBURNING WAKE BURNING	$(P_b - P_{bo})/(P_1 - P_{bo})$ SUM OF SEPARATE CONTRIBUTIONS	COMBINED
0.52	2.06	2.18
3.0	1.95	1.83
2.9	2.00	2.07
0	1.79	1.92

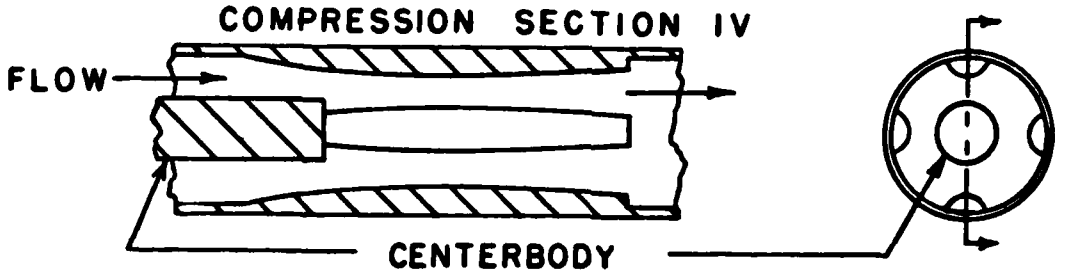

FIGURE 14. EFFECTS OF EXTERNAL COMPRESSION AND BASE BURNING

sum of the two separate contributions. This is shown to be the case for base thrust levels sufficient to overcome the forebody wave drag of a typical Mach 3.0 axisymmetric projectile. Thus, it is highly desirable that tests be made with real external burning and base burning combined. At the present time the efficiency of the external burning mode is unknown. However, as shown earlier, such tests must be conducted in a large scale wind tunnel or, perhaps, in free flight.

In concluding, Figure 15 is presented to show that base burning operates upon an exceedingly complex flow field which challenges analysts. This depicts the current understanding of the flow field as learned in this research from extensive probing of the hot and cold wakes and visual observations. Burning of the fuel or fuel rich gases injected through the base plane begins at the dashed line downstream of the base plane. Oxygen and heat diffuse into this combustion zone both from the freestream and the recirculation zone. The recirculation zone was always present at the injection rates used experimentally and this recirculation plays an important role in momentum, heat, and mass transport. Oxygen diffuses from the freestream into the dow stream portion of the recirculation zone and is then connected forward by the recirculation. Correspondingly, the stoichiometric line is distorted backward toward the base in the recirculation zone. The pressure at the rear stagnation point is determined by the base pressure, the flow Mach numbers, and momentum exchange rates. The Mach numbers and momentum exchange rates are decreased as a result of the high temperatures due to combustion. Thus, a temperture increase on the stagnating streamline as a result of combustion will yield a higher base pressure. Preburning a portion of the fuel with oxygen followed by wake combustion results in a higher temperature in the wake core and a higher temperature on the stagnating streamline. Hence, the base pressure is increased, in accordance with the experiments. On the other hand, an inert diluent added to the fuel, reducing the effective fuel heating value and slightly lowers the temperatures but this tends to be counterbalanced by increased diffusion and the higher mass addition which displaces the discriminating streamline outward. The experiments show that, in this case, the net effect is small.

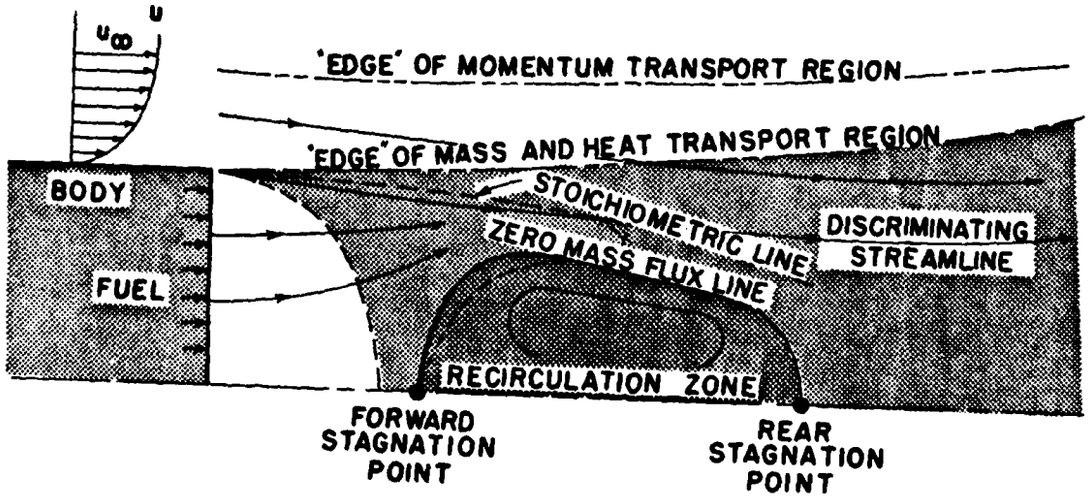

FIGURE 15. FLOW MODEL

C. Publications

1. Neale, D.H., Hubbartt, J.E., and Strahle, W.C., "Effects of Axial and Radial Air Injection on the Near Wake with and without External Compression," AIAA Journal, Vol. 17, Mar. 1979, pp. 301-303.
2. Hubbartt, J.E., Strahle , W.C., and Neale, D.H., "Mach 3 Hydrogen External/Base Burning, AIAA Journal, Vol. 19, June 1981, pp. 745-749. Also as Paper 80-0280, AIAA 18th Aerospace Science Meeting, Pasadena, Calif., Jan 14-16, 1980.
3. Hubbartt, J.E. and Strahle, W.C., "External/Base Burning for Base Drag Reduction at Mach 3," AIAA Journal, Vol. 19, Nov. 1981, pp. 1502-1504.
4. Strahle, W.C., Hubbartt, J.E., and Walterick, R., "Base Burning Performance at Mach 3," AIAA Paper 81-1469, AIAA/SAE/ASME 17th Joint Propulsion Conference, Colorado Springs, CO, July 27-29, 1981. Also accepted for publication in AIAA Journal.

D. Personnel

Principal Investigators - James E. Hubbartt and Warren C. Strahle.

Research Engineers - D.H. Neale (1977-78-79), R.N. Leary (1980), and R.E. Walterick (1981).

Graduate Research Assistants - J.C. Richardson (1979-80-81) and W.A. DeGroot (1980-81).

E. Professional Activities

1. Strahle, W.C., "Mach 3 External/Base Burning," Invited Seminar at NASA/Langley, July 1979.
2. Strahle, W.C., Hubbartt, J.E., and Walterick, R.E., "External/Base Burning for Propulsion," Paper presented by W.C. Strahle at 18th JANNAF Combustion Meeting, Jet Propulsion Laboratory, Pasadena, CA, Oct. 19-23, 1981.
3. Strahle, W.C. and Hubbartt, J.E., "Base and External Burning for Propulsion," AGARD Propulsion and Energetic Panel 58th Symposium, Ramjets and Ramrockets for Military Applications, London, U.K., Oct. 26-29, 1981.
4. Strahle, W.C.: a) Associate Editor for Combustion and Aeroacoustics, AIAA J., b) Member of AIAA Propellants and Combustion TC.

F. References

1. Neale, D.H., Hubbartt, J.E., Strahle, W.C., and Wilson, W.W., "Effects of External Compression on an Axisymmetric Turbulent Near Wake," AIAA Journal, Vol. 16, Sept. 1978, pp. 940-947.
2. Neale, D.H., Hubbartt, J.E. and Strahle, W.C., "Effects of Axial and Radial Air Injection on the Near Wake with and without External Compression," AIAA Journal, Vol. 17, Mar. 1979, pp. 301-303.
3. Hubbartt, J.E., Strahle, W.C. and Neale, D.H., "Mach 3 Hydrogen External/Base Burning," AIAA Journal, Vol. 19, June 1981, pp. 745-749. Also as Paper 80-0280, AIAA 18th Aerospace Sciences Meeting, Pasadena, Calif., Jan 14-16, 1980.
4. Hubbartt, J.E. and Strahle, W.C., "External/Base Burning for Base Drag Reduction at Mach 3," AIAA Journal, Vol. 19, Nov. 1981, pp. 1502-1504.
5. Strahle, W.C., Hubbartt, J.E., and Walterick, R., "Base Burning Performance at Mach 3," AIAA-81-1469, AIAA/SAE/ASME 17th Joint Propulsion Conference, Colorado Springs, Col., July 27-29, 1981. Also to be published in AIAA Journal.
6. Bowman, J.E. and Clayden, J.E., "Reduction of Base Drag by Gas Injection," Royal Armament Research and Development Establishment, Fort Halstead, U.K., RARDE Rept. 4169, Dec. 1969.
7. Freeman, L.M. and Korkegi, R.H., "Projectile Aft-Body Drag Recuction by Combined Boat-Tailing and Base Blowing," AFAPL-TR-75-112, February 1976.
8. Townsend, L.H. and Reid, J., "Some Effects of Stable Combustion in Wakes Formed in a Supersonic Stream," Supersonic Flows, Chemical Processes, and Radioactive Transfer, edited by D.B. Olfe and V. Zakkay, The Macmillan Co., New York, 1964, p. 137.
9. Schadow, K.C. and Chieze, D.J., "Experimental Investigation of Combined Base Injection and External Burning," AIAA Journal, Vol. 16, Oct. 1978, pp. 1084-1089.
10. Clayden, W.A. and Boeman, J.E., "Cylindrical Afterbodies at M = 2 with Hot Gas Injection," AIAA Journal, Vol. 6, Dec. 1968, pp. 2429-2431.

TASK III

BEHAVIOR OF ALUMINUM IN SOLID PROPELLANT COMBUSTION

E. W. PRICE
R. K. SIGMAN

TASK III
BEHAVIOR OF ALUMINUM IN SOLID PROPELLANT COMBUSTION

E. W. PRICE, R. K. SIGMAN

A. Research Objectives

The objectives of this task were to gain understanding and improved control of combustion of the aluminum ingredient in solid propellant, and of the aluminum effect in overall propellant combustion. In practical terms, this relates to attainment and assurance of desired burning rate, combustion efficiency, combustor stability and resistance to detonation while striving for high propellant density and high specific impulse.

Specifically, the objectives were to clarify the accumulation processes that set the stage on the propellant burning surface for formation of "large" agglomerates of aluminum, and clarify the conditions for ignition-agglomeration, the nature and combustion of agglomerates, and the nature of the oxide product population.

B. Progress and Significant Accomplishments

Much of the research conducted under this Task is reported in the publications listed under section C. In the following, a series of subsections report collectively on all phases of the research, in order to provide a complete summary. Those phases of the research that were not reported previously are covered in relatively greater detail for completeness.

INTRODUCTION

Metal powders are used as fuel components in solid propellants because of their high density, and high heat release when burned. The metals have other benefits as well, such as suppression of combustion instability, modification of burning rate, reduction of sensitivity to detonation, favorable supply, etc. These advantages are not all applicable to all metals in all rocket motors in all applications. Indeed, for rocket motor applications, only aluminum powder has seen widespread use. Even aluminum has been considered disadvantageous in some applications, particuarly those in which the smoky exhaust trail of aluminized propellants compromises system effectiveness too severely. However, aluminum (and possibly other metals) is a highly desirable ingredient in many applications, and is the second most plentiful ingredient in roughly 50% of all propellant manufactured.

The advantages and disadvantages of aluminum, both real and potential, depend to a significant degree on the details of combustion of the aluminum. Combustion behavior is in turn relatively complex compared to other propellant ingredients, a circumstance resulting from the low volatility of the metal and its oxide. The fine metal particles go through a complex accumulation-concentration-agglomeration on the propellant burning surface, yielding relatively large and slow-burning droplets. The combustion behavior, and nature of the oxide products, are sensitive to details of the propellant and motor, and are difficult to predict in advance of testing the all-up system. Because of this, a number of efforts have been mounted in the past to achieve better understanding and/or engineering characterization of aluminum behavior in propellant combustion, and its effect on system performance. The present study has been aimed at understanding the detailed processes that determine the behavior of aluminum in the rocket motor, using methods that provide information at the microscopic level of the aluminum particles, agglomerates and oxide product droplets. Such understanding provides the basis for more rational "design" of propellant formulation, prediction of performance, and manipulation of design to achieve best performance.

In the interests of perspective, the combustion "metabolism" of aluminum is outlined in Fig. 1, which shows the routes by which ingredient aluminum particles in propellants can progress to their final reaction products (the figure is based on the usual case where the products are molten Al_2O_3). For any given propellant,there is

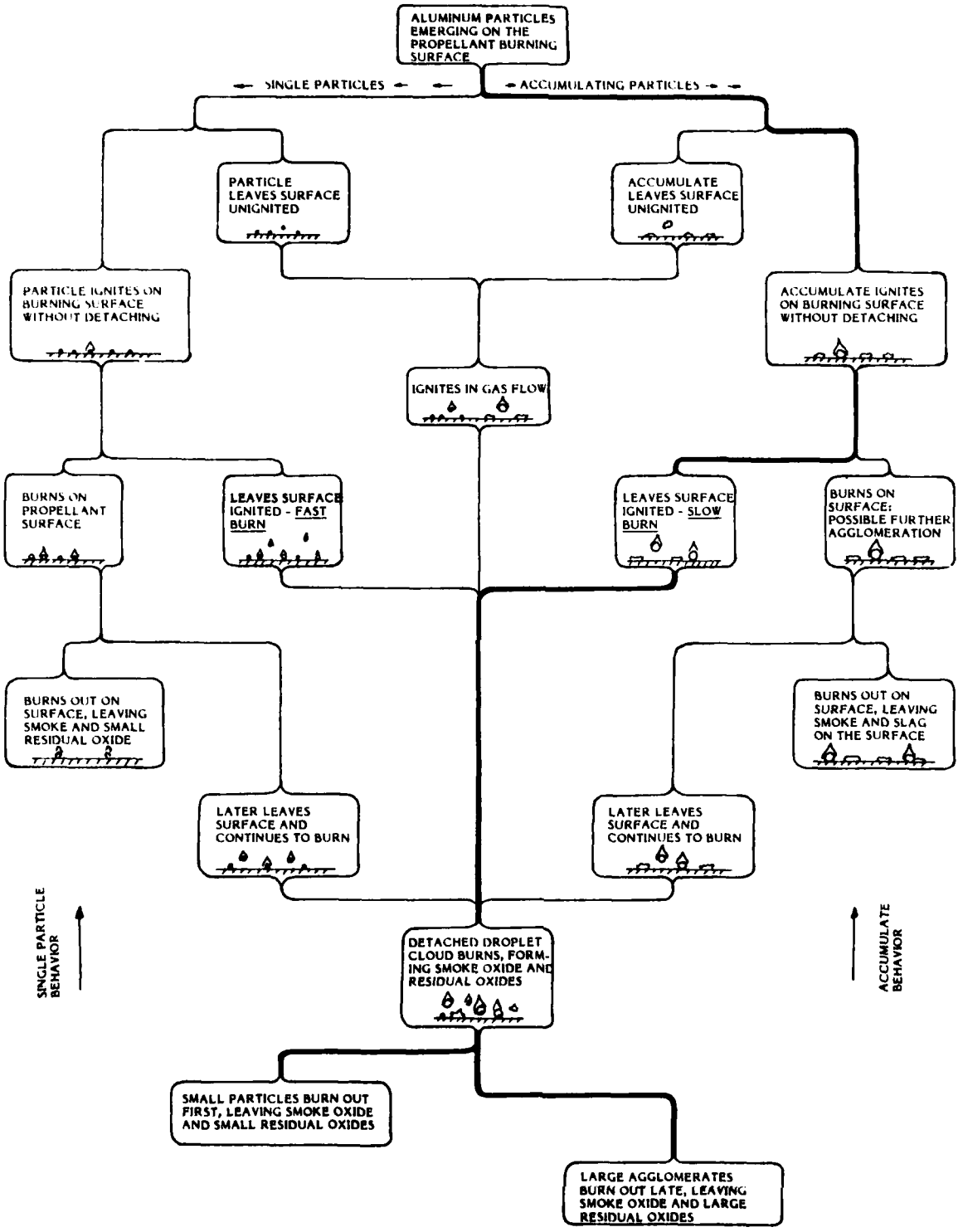

Fig. 1 Alternative paths of aluminum behavior in the combustion zone. The path emphasized by the heavy line is most typical with ammonium perchlorate-hydrocarbon binder propellants.

a "most typical" route, but some of the particles follow other routes, giving a statistical array of behavior. However under most conditions, aluminum concentrates on the burning surface (Fig. 2); agglomerates, ignites and detaches from the surface as a single complex event (Fig. 3); burns as 50 - 300 μm diameter agglomerates while moving away from the burning surface (Fig. 4); forms a fine Al_2O_3 smoke (< 2 μm) in a flame envelope about the agglomerate (Fig. 5); concurrently accumulates oxide on the surface of agglomerates that ends up as "residual" oxide droplets in the 5 - 100 μm range when the agglomerates burn out (Fig. 6). This sequence is noted by the heavy lines in Fig. 1.

It is this detailed behavior that determines the effect of aluminum on such combustion variables as

propellant burning rate
combustion stability
combustion efficiency
combustion quenching
aluminum slag residue

and such oxide product effects as

two-phase flow in the combustor and nozzle
thrust efficiency
component erosion
damping of combustor oscillations
oxide slag residue.

The combustion studies seek to understand the accumulation-concentration-agglomeration-ignition-detachment-agglomerate combustion sequence by studies that clarify these individual steps. This involves consideration of the original distribution of aluminum particles in the propellant microstructure; the relative dimensions of the combustion zone and the particulate ingredients; the forces conducive to retention and concentration of aluminum; the conditions that delay ignition during concentration; the processes that connect accumulated particles and set the stage for coalescence; the conditions that eventually break down sintered surface accumulations and cause agglomeration, ignition and detachment from the

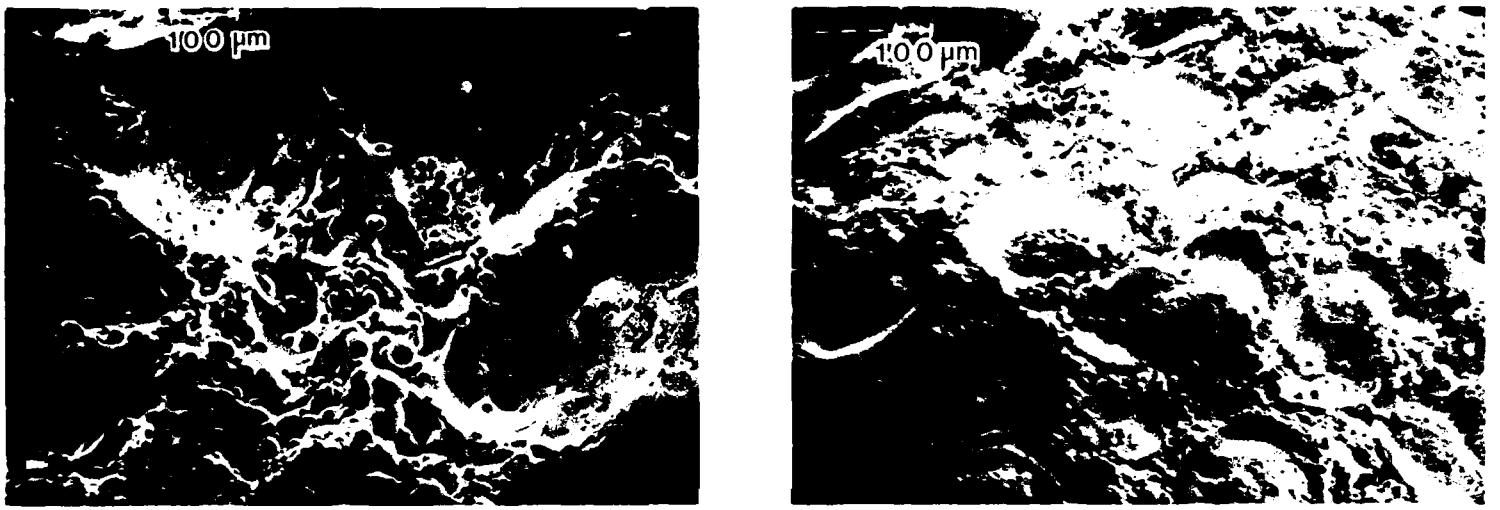

Fig. 2 Aluminum concentration on the burning surface. Scanning electron microscope pictures of surfaces quenched by rapid depressurization.
a) Aluminum concentration in a "pocket", with relatively visible evidence of binder melt (from 6.9 MPA test).
b) General pattern of aluminum concentration, selected to show also an example of relatively dry sintering of accumulated aluminum (from 0.7 MPa test).

Fig. 3 Formation of an agglomerate from a surface accumulation of aluminum particles (from high speed motion pictures by D. Zurn, Naval Weapons Center).

Fig. 4 Burning agglomerates, shortly after leaving the propellant burning surface.

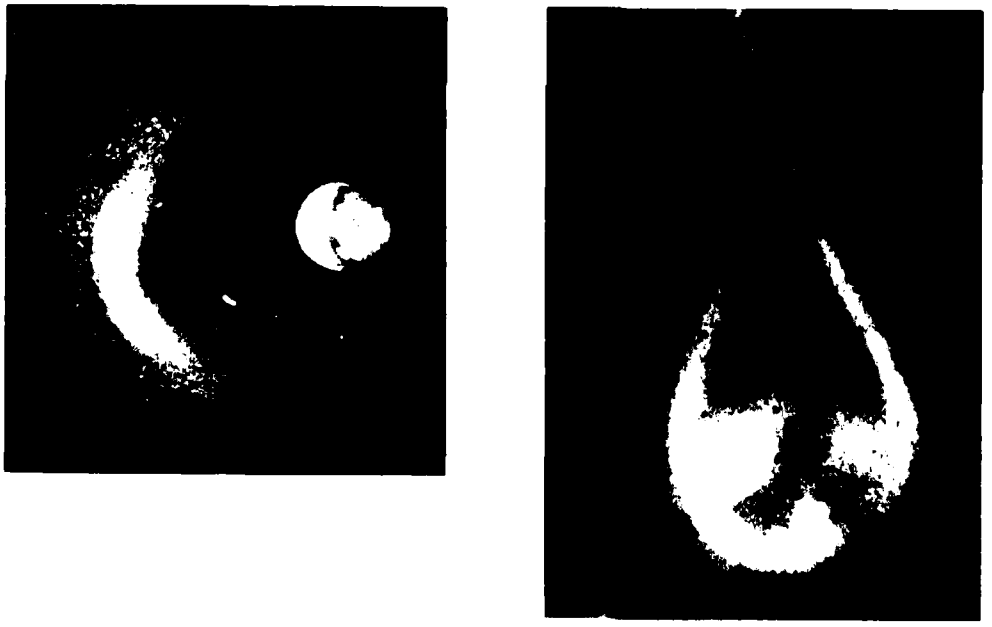

Fig. 5 Illustration of smoke oxide formation in the detached flame around the agglomerate.
a) Aluminum droplet with oxide lobe and smoke cloud deposited on a quench plate in an experiment burning single aluminum particles in air at 1 atm (photo by Prentice, NWC).
b) Burning aluminum agglomerate observed in high speed photography of propellant combustion.

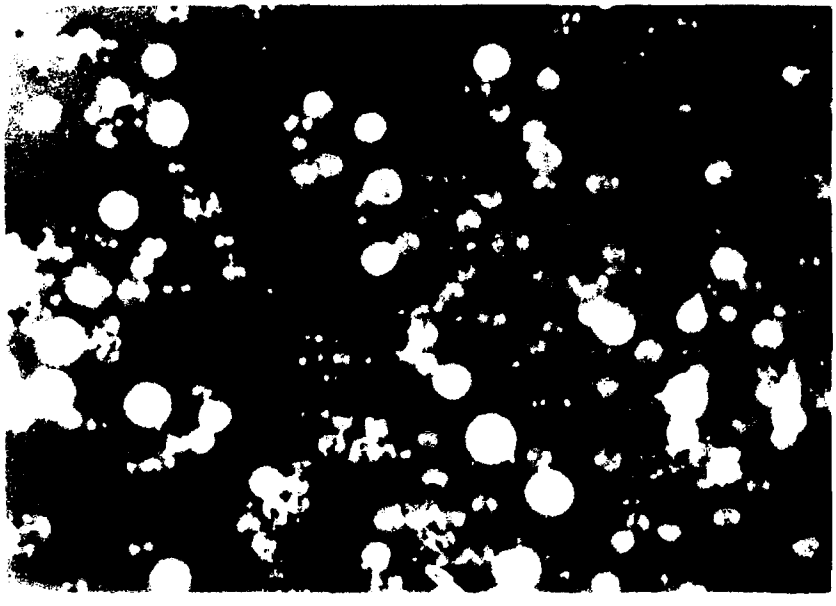

Fig. 6 Residual oxide, evolved from agglomerate oxide.

burning surface; and the combustion of agglomerates in the gas flow field. While it is not practical to seek complete understanding of all these complex processes, it is also not practical to ignore any of them because they are "branch points" for the alternative paths in Fig. 1, and each branch point can exercise decisive effects on combustion. The present investigations have sought to clarify these branch points, establish their roles at the microscopic level in real propellant combustion, and thus provide the basis for understanding the relation between conventional propellant variables (composition, particle size) and macroscopic combustion behavior (burning rate, stability, combustion efficiency, etc.). The discussion in the following seeks (in the first sections) to develop the arguments and summarize past results into a connected account of how aluminum behaves as it "moves through" the combustion wave. These sections are followed by accounts of several supporting studies that have not been reported previously. These studies were carried out as part of the basic study, and in part to explore potentially useful ideas emerging from the study (e.g., modifications of aluminum powder to control agglomeration, and use of high aluminum-content propellants).

PROPELLANT MICROSTRUCTURE

Typical composite propellants are made with oxidizer as a primary particulate ingredient (70 - 75% by weight for aluminized propellants), with particles ranging from 6 - 600 μ m (mass average 100 μm). Aluminum particles are typically 16% by weight, in the size range 5 - 40 μm. The balance of the mass (10 - 15%) is typically a polymeric material. In order to achieve a near-stoichiometric mixture, the binder content is made as low as possible consistent with acceptable processing characteristics and physical properties of the propellant. To achieve this, the size distribution of the particulate ingredients is normally chosen rather carefully so as achieve dense particle packing and minimize packing voids that that yield locally high concentrations of binder. On the other hand, it is required that the surface of all particles be "wetted" by binder in order to get acceptable mechanical properties, so all particles are surrounded by binder. In meeting all these requirements, propellant processors have to limit the "smallness" of particles (total surface area) to avoid processing problems (e.g., viscosity of the uncured mix). The net result is reflected in the typical figures noted above, but with oxidizer particle blends involving two to four different sizes, a substantial portion being in the coarse component (e.g., 200 - 400).

Given the foregoing practical realities and trade practices, a typical propellant looks like that shown in Fig. 7. An aggregate of coarse oxidizer particles is set in a "sponge" of binder and finer oxidizer and aluminum particles. In a low burning rate propellant, the coarse particles will be more densely packed (and possibly larger), with the "sponge" being correspondingly more tenuous and containing less fine oxidizer. Because the aluminum particles are normally relatively small in both size and total volume, they can be pictured as being part of the sponge. Thus the aluminum is not homogeneously distributed on the dimensional scale of the oxidizer particles, being located in that 30 - 50% of the volume occupied by the sponge. That volume is very fuel rich, containing only about 30% of the oxidizer in a propellant that is already fuel rich in overall formulation.

When a propellant burns, a burning front propagates through the matrix, with

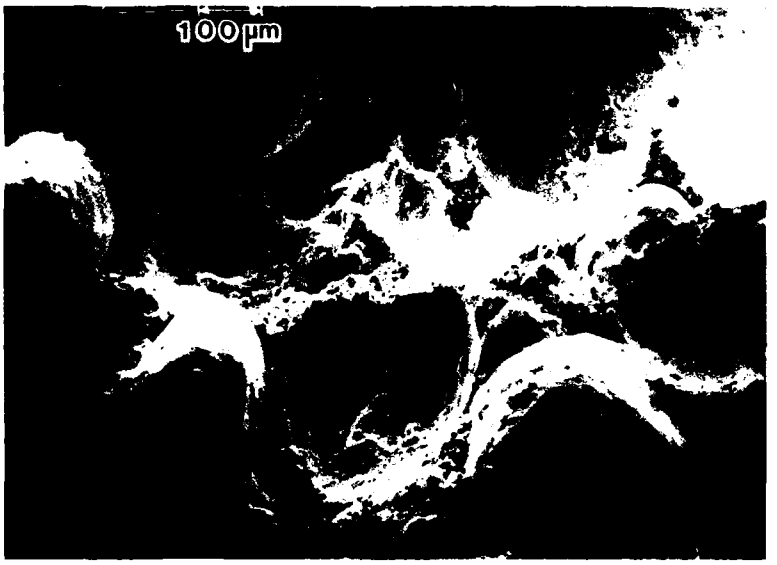

Fig. 7 Illustration of propellant microstructure. Scanning electron microscope picture of a surface produced by breaking the propellant (to show structure).

the burning surface representing a sort of "cross section" of the propel microstructure (Fig. 8). Oxidizer particles are readily visible, as is the "cross section" of the sponge (in Fig. 8 a nonaluminized propellant was used to enhance the visibility of sponge structure). The binder area of the surface is revealed as a tenuous, interconnected structure with occasional patches of larger dimensions corresponding to voids or "pockets" in the packing pattern of the larger oxidizer particles. These pockets may contain smaller oxidizer particles, which are often difficult to distinguish. A similar structure is revealed with aluminized propellants, but the sponge pattern is usually dominated on the burning surface by aluminum particles (Fig. 9). The aluminum presents an appearance of an interconnected array, which to some extent is a reflection of its actual distribution in the propellant (i.e., as part of the sponge). However, the distribution of the aluminum is critically dependent on its particle size relative to the coarser AP particles. Very fine aluminum can be uniformly dispersed in the sponge, but coarser aluminum particles will be isolated from each other because they will not fit in the thinner elements of the sponge structure. Thus aluminum may be localized in the thicker sponge components corresponding to oxidizer packing voids (referred to in this report as "binder pockets"). The degree of interconnectedness between these aluminum concentrations will depend on the size of aluminum particles and their corresponding ability to "fit" in the connective structure of the sponge between pockets. These circumstances are important because they affect the continuity of the aluminum's array on the burning surface, which in turn affects the opportunity for coalescence between pocket concentrations of aluminum.

As noted earlier, oxidizer is usually present as a blend of particle sizes. The smaller fraction typically has a particle size of the same order as the aluminum (this was the case for the propellant in Fig. 9). Thus arguments regarding the distribution of aluminum particles in the sponge apply also to the finer part of the oxidizer particle population. As noted earlier, this means that the aluminum containing part of the sponge contains also oxidizer, yielding a very fuel-rich propellant (which will ordinarily not burn unaided). Obviously the distributions of fine oxidizer and aluminum in the sponge are amenable to some delicate tailoring by careful particle size tailoring, but the size distributions ordinarily available are too broad for such "fine tuning" of microstructure, and the effects on combustion are consequently unevaluated.

In the present work, particle size has been one of the principal variables in experiments. The foregoing description of microstructure was evolved as a

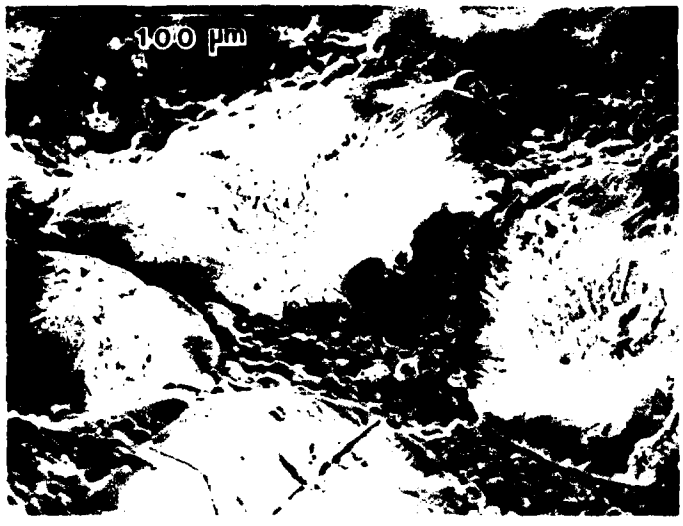

Fig. 8 Illustration of distribution of binder in a heterogeneous propellant. Scanning electron microscopc picture of a quenched surface (non aluminized sample used to enhance visibility of binder; test pressure 6.9 MPa; propellant contains fine AP, visible in the binder).

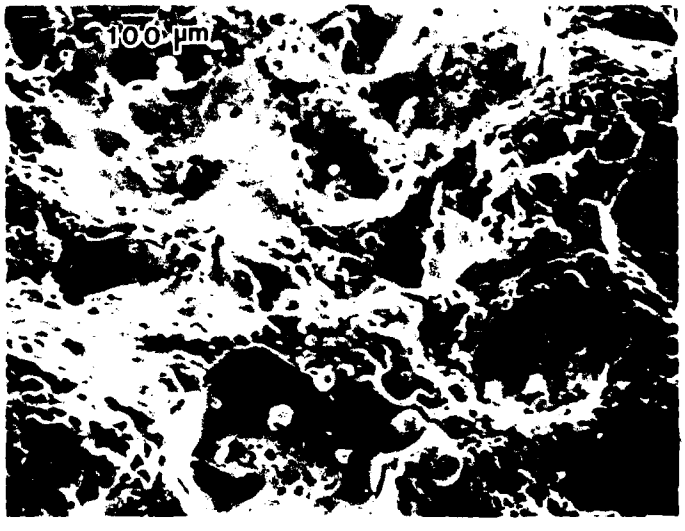

Fig. 9 Illustration of distribution of aluminum on the burning surface. SEM picture of a sample quenched from 6.9 MPa.

consequence of efforts to understand results of tests, and [illegible] basis for design of test experiments. In hindsight, the description is fairly obvious and a key element of the description (the concept of pockets) was presented by one of the authors earlier (Ref. 1). The more elaborate description presented here is designed to accomodate a more detailed understanding of aluminum behavior described in the following.

PRE-AGGLOMERATION BEHAVIOR OF ALUMINUM*

There is very little controversy over the thesis that aluminum forms agglomerates near the propellant burning surface, but there have been a variety of proposals as to what processes lead to agglomeration. These different proposals do not represent a controversy so much as divergent efforts to produce tractable idealized modeling schemes from which agglomeration behavior can be calculated (Ref. 2-4). The experimental evidence is largely in the form of combustion photography (which doesn't get published), and more controlled studies of response of aluminum powders to heating (available in diverse sources (Ref. 5)). In addition, some idea of intermediate steps leading to agglomeration can be gained from examination of quenched burning surfaces. These methods have all been used in one or more of past studies and the present study. The general interpretation is relatively unambiguous, and is summarized in the following.

Aluminum is seen to accumulate on the propellant burning surface, often residing there for much longer times than required for the burning surface to recede past the particles. In other words, particles typically adhere to the surface. Mobility is typically low, consistent with an "adhesive" surface retention. Knowing the propellant microstructure, it is evident that most adhering particles on a receding surface will be joined by underlying particles. This in turn implies that accumulation and concentration of aluminum particles will normally occur, an implication supported by countless observations by combustion photography and quenched sample studies. Low volatility of the metal, protective nature of the oxide skin, and initially low local concentration of oxidizing species prevent ignition of the metal during this surface accumulation (as seen later in this report, such accumulation occurs without ignition even on the burning surface of AP oxidizer). Finally, it is an observed fact that the accumulating particles eventually coalesce into agglomerates, implying that concentration proceeds to the point of contact between particles. Presence of relatively rigid structures of aluminum particles is manifested in combustion photography and quench tests; thus it is evident that particle contact progresses to a state of sintering, similar to that resulting from controlled heating of aluminum powder in oxidizing atmospheres. Indeed, acid etching of recovered accumulates shows them to consist of an

---

* This section is condensed from Ref. 7. See that reference for more extensive illustrations of relevant experimental results.

interconnected oxide shell structure filled with aluminum (Ref. 5 - 7).

In view of chaotic microstructure of the heterogeneous propellants, it is to be expected that some diversity and intermittency of behavior would occur. Some aluminum particles leave the surface without evident interaction with others. All aluminum eventually leaves the surface, and the extent of prior concentration and sintering can only be fully described with the aid of statistical language. Recalling the earlier discussion of the implications of propellant microstructure, the statistical language of accumulation, sintering and detachment must be linked to the statistical language of propellant microstructure, and concepts such as "pockets", "bridging" between pockets, and formation of "sintered filigrees" are terms used to connect propellant microstructure to the state of connectedness of accumulated aluminum on the burning surface. The ultimate size of an accumulate is thus dictated to some extent by the original concentration of aluminum in the propellant microstructure (pockets) and to some extent by the spatially nonuniform conditions that cause sintered structures to adhere to the propellant surface without ignition. Finally, ignition may precipitate detachment, and the ultimate size of the accumulate will in that case be determined by conditions necessary for ignition. Recalling the earlier reference to the reluctance of aluminum to ignite in the AP flame, it must be anticipated that ignition termination of surface accumulation may be as dependent on propellant microstructure as is the pattern of accumulation. This will be so when the ignition is induced by the local oxidizer-binder flamelets associated with oxidizer-binder interfacial regions of the burning surface microstructure. It is in or beyond these flamelets that high enough temperatures are reached to achieve ignition of sintered aluminum accumulates. The process of ignition and concurrent agglomeration is described in the following.

THE AGGLOMERATION EVENT

Agglomeration takes place when the progressive state of an accumulate reaches a point where the oxide containment of the molten aluminum breaks down. At this point, two processes come precipitously into dominance. The surface tension of the molten aluminum causes the metal to draw into a spherical configuration. Since the breakdown of the oxide containment does not occur simultaneously throughout the accumulate, this spheroidization is progressive. The second process that comes concurrently into dominance is the oxidation rate of the aluminum as it escapes the containment of the existing oxide shell. Thus it is typical in combustion photography, under conditions favorable for good resolution, to see areas of spheroidization in a surface accumulate, accompanied by onset of evidence of associated aluminum vapor flame and telltale oxide smoke trail.

The agglomeration event can be so rapid that it is not resolved in photography at a few thousand frames per second, or it can be fairly protracted and easy to observe (large accumulates at low pressure). The progressive nature of the event is obvious under favorable viewing conditions. Initiation appears to start at locations where the accumulate is best exposed to the high temperature of the diffusion flame elements (AP-binder flame). That region of the accumulate glows brightly, spheroidizes and develops darker reflective areas that are apparently molten metal. The smoke veil and trail develops over these areas when they appear. At this point, the oxide residue from the spheroidized portion is visible (at least in part) as a white glowing film over parts of the sphere, presumably molten. This is accompanied by increasing brightness of the neighboring portions of the accumulate. The molten portion starts to coalesce progressively into the rest of the accumulate, at the same time exhibiting a loss of any other attachment to the propellant surface. Under the conditions that give good resolution of these progressive features, the surface accumulation of aluminum is usually widely interconnected, so that the propagative aspect of a coalescence is relatively visible. Indeed, some investigators who observed the behavior without aid of the external illumination used to show the nonluminous part of the accumulate have interpreted the behavior as indicating a freely rolling droplet on the propellant surface (without accompanying rationale for the long delay before "lift-off" from the surface). In any case, the flaming agglomerate eventually burns itself free of surface attachment and moves away in a near spherical condition (Fig. 4), typically

showing burning metallic areas; bright molten oxide areas; and often darker or orange irregular areas of not yet melted material at the last point of contact of the droplet with the propellant surface. This is in effect the birth of an agglomerate, whose individual identity remains until burnout somewhere in the flow field. Such an agglomerate is typically 10 times the diameter of the original ingredient aluminum particles, implying an agglomeration of 1000 particles.

The foregoing description is based on interpretation of combustion photography, aided by a good deal of prior knowledge of the nature of surface accumulates, the propellant combustion zone, and aluminum combustion. It is basically a visualization of the agglomeration, seen from the outside. What's happening inside the coalescing mass, how does it affect the process, and what is the end effect on the fully developed agglomerate? This can be inferred from the nature of the situation, properties of materials involved, and the externally observable behavior.

When the accumulate first starts to break down and coalesce, it is a nonuniformly preheated structure consisting of an intricate solid oxide encasement of liquid aluminum. The metal of the original aluminum particles is probably mostly still unconnected, any contact points having oxidized to form the connected accumulate structure. Any localized breakdown of the oxide leading to onset of coalescence is initially insulated from the overall accumulate by the rigidity and low thermal conductivity of the oxide containment structure. However, the rise in local heat release due to the flame around the coalescing aluminum at the initial breakdown point melts the oxide locally, assuring continued and spreading reaction of aluminum.

As the oxide shell structure breaks down, it is swept up by the coalescing aluminum in the form of thin (sub micron) solid and melting sheets with varying degree of connectedness. Insoluble in the liquid aluminum, the oxide will be partly trapped in the interior of the agglomerate, and partly left as melting surface aggregations remaining after withdrawal of coalescing aluminum (Fig. 10 a). The quenched agglomerate in Fig. 10 b shows the tendency of the aluminum to spheroidize when the accumulate is not yet fully molten in the interior. Fig. 3 shows the tendency for much of the initial oxide to be left as a melting aggregate on the agglomerate surface. This external residue is the source of part of the oxide typically present as an oxide lobe on a fully burning agglomerate (Fig. 4). Acid etching of such agglomerates after quench-collection reveals the presence of a complex interior oxide structure (Fig. 11), probably evolved from the accumulate

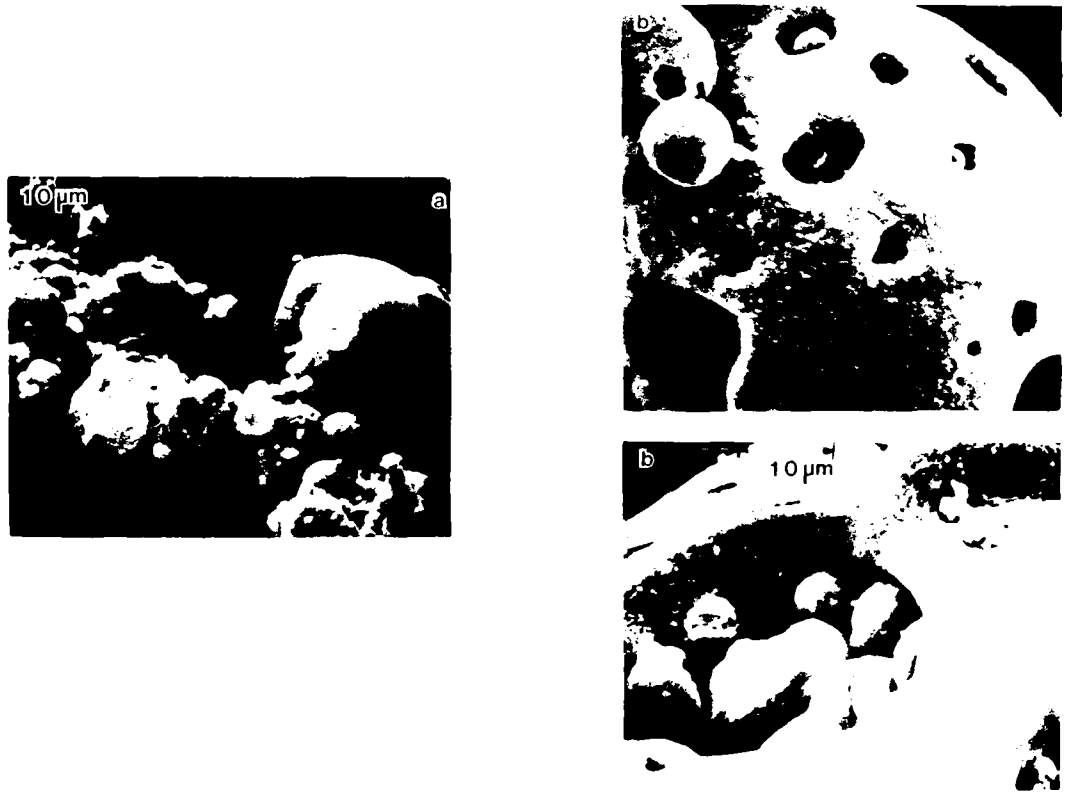

Fig. 10 Transition from accumulate to agglomerate.
a) Accumulate with sites where coalescence, burning and oxide lobe formation have occurred.
b) Spheroidization is largely complete, but not all original oxide has yet melted.

Fig. 11 Flake oxide in the interior of the aluminum portion of an agglomerate (revealed by acid etching). (From ethanol plume quench test at 1 atm.)

oxide that was trapped in the agglomerate during coalescence of the accumulate. Since the temperature of the burning agglomerates is above the melting point of the oxide, that oxide in the interior presumably survived as liquid sheets that solidified to the form in Fig. 11 during quenching. There is some evidence that the amount and structure of interior oxide is dependent on the abruptness of the agglomeration event, suggesting that the aluminum coalescence would exclude the oxide if it were completely free to flow. Thus agglomerates formed in the argon atmosphere in a hot stage microscope have little or no oxide trapped in the interior (Ref. 7,8). Combustion-produced agglomerates are observed in the present studies to have more interior oxide if formed in high pressure burning. The differences are conspicuous when one tries to cut the quenched agglomerate: "high pressure" agglomerates are brittle and give ragged cut surfaces, while "low pressure" agglomerates are soft, and cut smoothly. Thus it seems clear that the agglomeration is a dynamic event that yields a product that is dependent on a large complex of conditions. Indeed, the agglomerate may contain also carbon, nitrogen and/or chlorine and their compounds, probably only in small quantities.

A point of particular interest regarding the agglomeration event is its relation to ignition of the aluminum. Under most conditions, agglomerates are already burning at the moment of detachment from the propellant surface. When ingredient aluminum particles of agglomerate size are used in a propellant, they usually ignite some distance from the burning surface (and in some laboratory experiments, fail to ignite at all). This point may seem unimportant, since ingredient aluminum particles of a size comparable to that of typical agglomerates are usually not used in practical situations. The importance lies in the demonstration that the agglomeration process is an exothermic process, occurring in a loosely connected filigree on the propellant burning surface. Further, it is the initiation point of the sustained burning of the aluminum. Its responsiveness to combustor flow conditions (Ref. 9) and gas flow oscillations (Ref. 10) is likely to be a factor in erosive burning, g-force effects (Ref. 11), slag retention, combustor stability, propellant quench limits, combustion efficiency, and product oxide droplet size role in two-phase losses.

NATURE AND COMBUSTION OF AGGLOMERATES

The foregoing sections have described how aluminum agglomerates are formed in the propellant combustion. Much of that information was drawn from earlier research on this and other projects. A substantial part of recent effort on this project has been on the nature of the agglomerates and their combustion and (next section) on the nature of the oxide droplets formed during combustion. This work was reported in Ref. 7, and is presented here in summary form.

Test Methods

Experimental studies were based on analysis of samples collected in the outflow from the burning surface of real and model propellants. Collection was accomplished by directing the flow from the burning surface into a pool of ethanol. The method quenches burning agglomerates, and collects most of the condensed material in the flow except the fine oxide smoke formed in the flame envelope of the burning agglomerates (mass of that smoke is calculated from mass and composition of the original sample and collected sample). The collected samples were subjected to a variety of analyses, including: particle size analysis; determination of unreacted aluminum content; microscopic examination; and determination of interior structure by cleaving, breaking, acid etching and heat treatment. Such studies were made as a function of distance from the propellant surface, pressure, and propellant formulation variables. The objective was to reconstruct from quench sample data the combustion history of agglomerates.

Trends of Agglomerate Populations

When samples are quench-collected close to the propellant burning surface (1.5 cm), they are mostly aluminum (low pressure tests), consisting of a wide size range of agglomerates with small transparent oxide lobes. At greater distance from the propellant surface, the oxide lobe portion of each agglomerate becomes relatively large (Fig. 12), and a variety of small residual oxide particles appear in the collected samples (remnants of burnout of the initially small agglomerates). Figure 13 shows a typical sequence of agglomerate mass size distributions corresponding to quenches at increasing distances from the burning surface. The area under the curves is indicative of the total weight of the agglomerates in the quench sample (including oxide on the agglomerates, but excluding oxide particles).

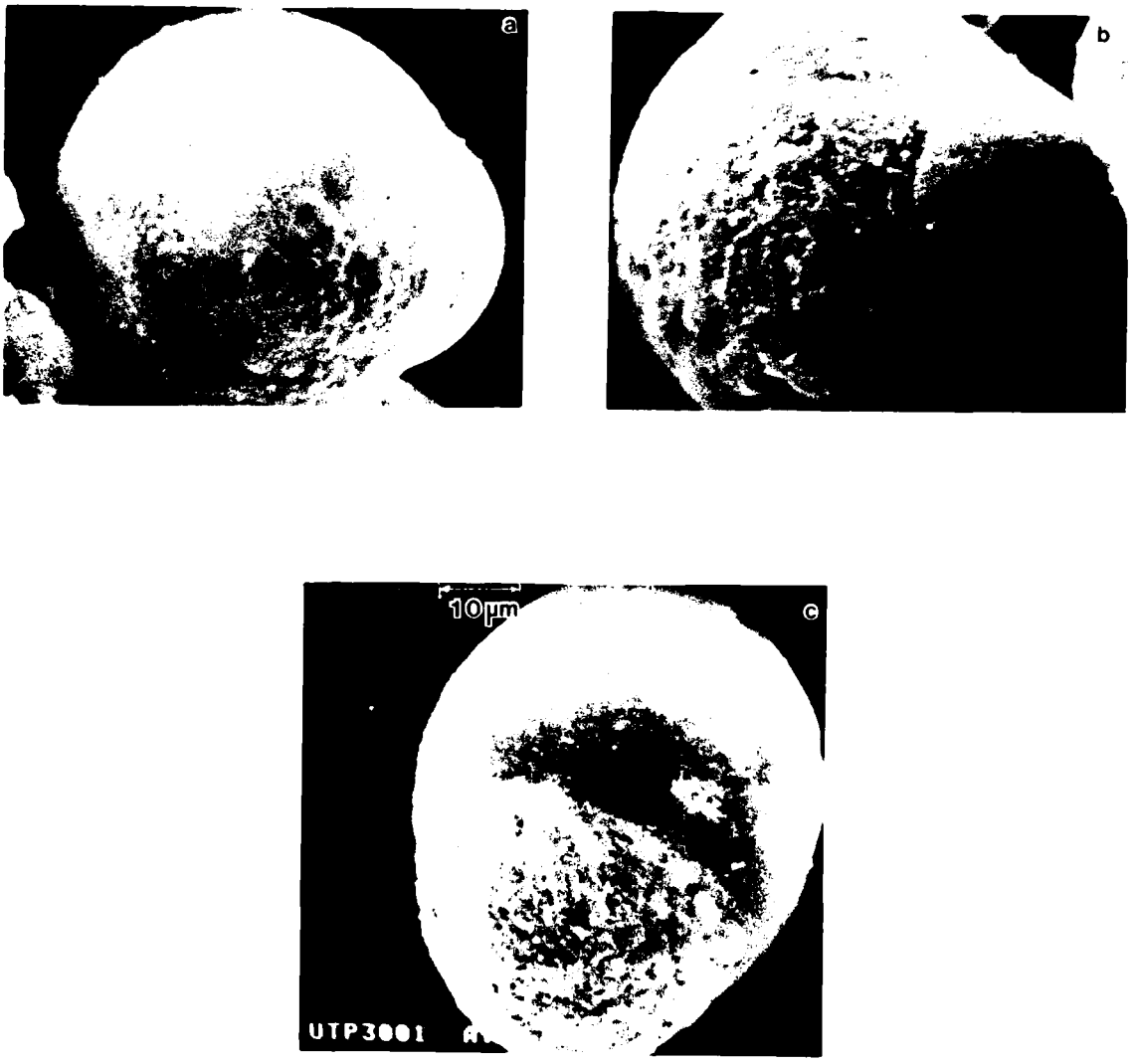

Fig. 12 Comparison of agglomerates at different quench distances, illustrating growth of relative size of the oxide lobe (test pressure 1 atm). The smooth lobe is oxide. a) 1.5 cm; b) 10 cm; c) 30 cm.

It is interesting to note that the size distribution doesn't change much with burning distance, although each particle is getting smaller and the total mass is decreasing. This relatively constant size distribution of the agglomerate population was noted earlier in an analytical study of burning agglomerate populations (Ref. 12), and is due in part to the nature of the original size distribution, and in part to the fact that some of the burned aluminum is retained on the agglomerate in oxide form, with weight gain due to the oxygen uptake. Some idea of agglomerate burning rate can be obtained from the curves in Fig. 13, in which the total agglomerate sample weight at a quench distance of 1.5 cm is about 40% of the original aluminum weight, so that a combustion efficiency of about 70% is reached at 1.5 cm from the propellant surface (0.7 MPa test). From estimates of flow velocity, this corresponds to 0.005 sec of burning, assuming the agglomerate started burning when it left the burning surface.

The actual aluminum combustion rate was determined by chemical analysis of the quenched samples obtained at different quench distances. The samples were analyzed by dissolving the unreacted aluminum in HCl, and comparing the weight of washed and dried samples before and after removal of the dissolved aluminum. Results of such tests are summarized in Fig. 14-16, which show the decrease in unburned aluminum with increasing quench distance in atmospheric pressure tests on several propellants. The principal features of these results are:

1. An initially rapid decrease in unburned aluminum (high aluminum consumption rate), which presumably reflects burn-up of the smaller agglomerates and unagglomerated particles.
2. A drop-off in combustion rate, to a rather low rate by 10 cm from the burning surface, reflected in quenched samples consisting of agglomerates that now have relatively large oxide lobes.
3. A significant dependence of the observed aluminum level on propellant and test variables (Fig. 15, 16), in the slow burning "tail off" phase.

Discussion of Results and Outstanding Issues Regarding Agglomerate Population

The foregoing results are qualitatively consistent with the agglomerate size distribution effects in Fig. 13 and with earlier calculations of burning of droplet populations (Ref. 12). However the results raise a number of questions that are the objects of continued study. Some of the questions relate to available experimental methods, which are only marginally adequate for quantitative work. These questions merit some discussion.

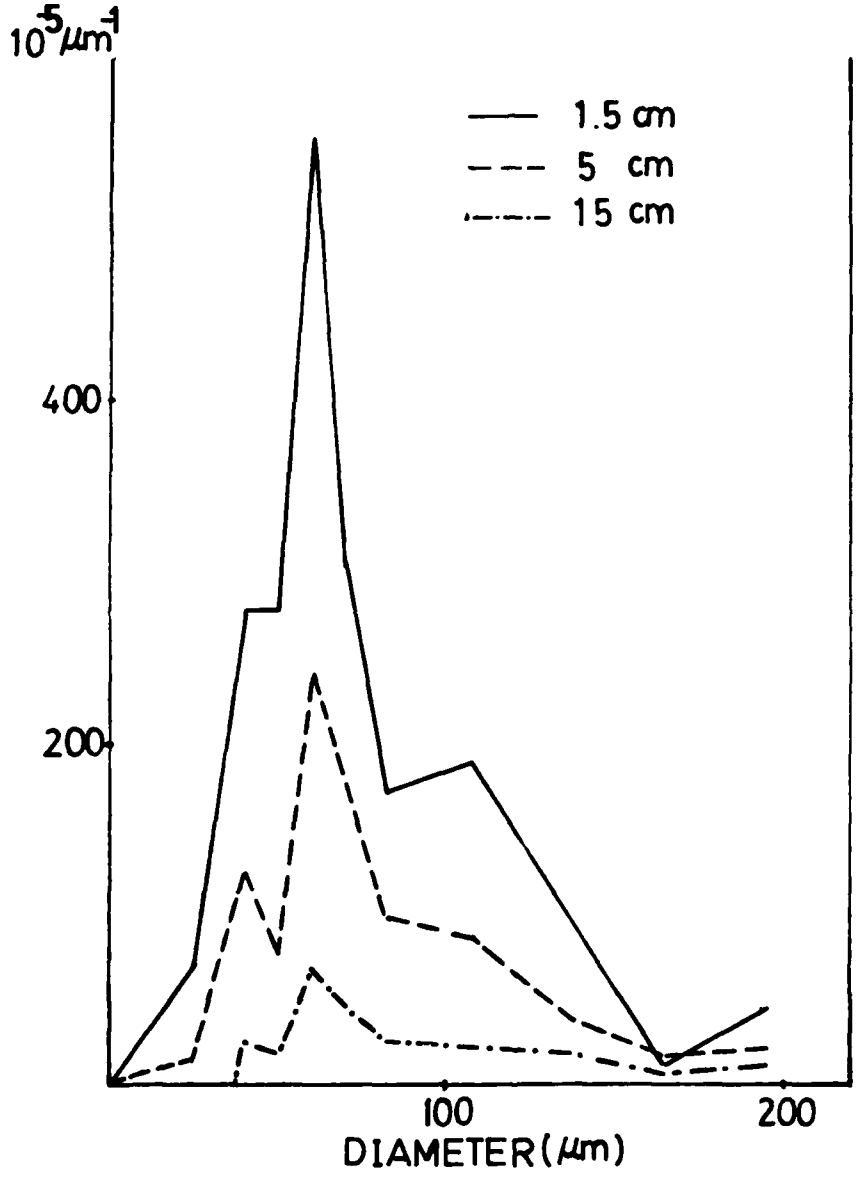

Fig. 13 Mass size distribution of agglomerates at three different quench distances (0.7 MPa test). The ordinate scale is mass per micron per initial aluminum mass.

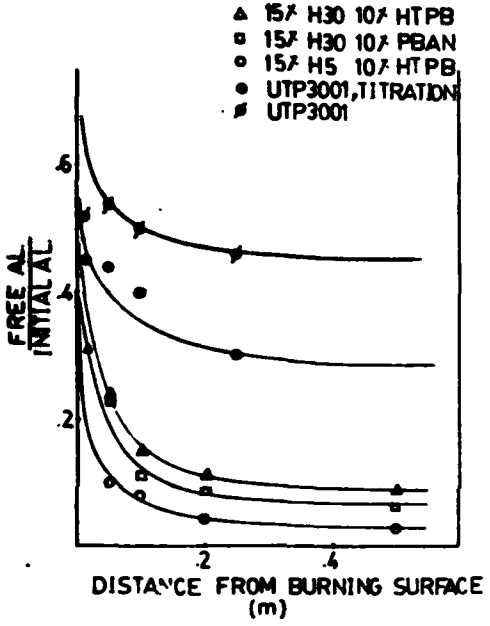

Fig. 14 Mass fraction of unreacted aluminum. Upper curve is for UTP 3001 propellant, lower curves are for a 10% binder, 15% Al, 75% 100 μm AP formulation. Atmospheric pressure tests.

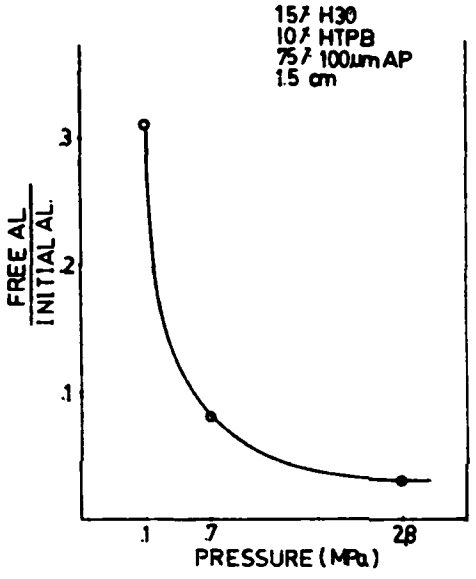

Fig. 15 Effect of pressure on mass fraction of unreacted aluminum for 1.5 cm quench, 10% HTPB, 15% H-30 Al, 75% 100 μm AP.

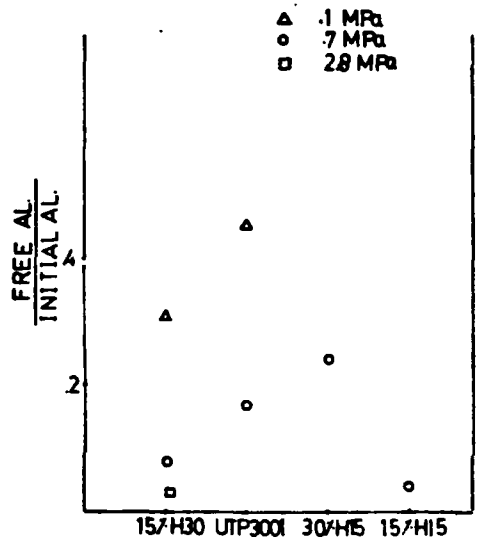

Fig. 16 Effect of formulation variables on mass fraction of unreacted aluminum for 1.5 cm quench distance. The hand-mixed propellants are 10% HTPB, indicated Al, balance 100 μm AP.

On the fundamental side, relatively little is known about the roles of the various oxidizing species present in the propellant combustion environment, and how they affect aluminum combustion. This means that the relevance of much past research on aluminum combustion is uncertain. Likewise, relatively little is known about the combustion of aluminum droplets with the large oxide accumulation present in the latter part of burning of agglomerates (e.g., beyond 5 cm quench distance in Fig. 14 a). Little is known about combustion of any aluminum droplets in the fuel-rich, high temperature conditions present in the propellant combustion environment at locations where the larger oxide-loaded agglomerates complete their burning. These conditions of oxide-burden and low oxidizer concentration are not very favorable for burnup of large agglomerates, and this is no doubt a factor in the "tail-off" of the curves in Fig. 14. It is also the key to the question of aluminum combustion efficiency in motors, since it is this prolonged phase of combustion that might not go to completion in a rocket motor. In this connection, one would anticipate that the outcome in the rocket motor would be quite sensitive to such variables as aluminum agglomeration, propellant stoichiometry, pressure, convective flow situations and motor stay time. These trends are implied by results of the present experiments, and generally recognized by motor developers.

Regarding the adequacy of the quenching experiment, the more serious limitations are most manifest in the same "tail-off" region that controls combustion efficiency. At low pressures, experiments are appreciably non-adiabatic and the temperature tends to drop off in the flow away from the propellant surface even while the aluminum is still burning (Ref. 13). This is presumably due in part to the very effects one is anxious to study; retardation of reaction rate by depletion of oxidizing species and encroachment of oxide on the agglomerate surfaces. Under some conditions, the agglomerate temperature apparently falls below the oxide freezing point, a situation that virtually arrests agglomerate burning. At this point in the laboratory experiment the simulation of the nearly adiabatic rocket motor environment is totally broken down. This situation appears to have happened in the case of atmospheric pressure tests on UTP 3001 propellant shown in Fig. 14, in which combustion of aluminum seems to have ceased at about 55% burned (top curve). Visual examination of samples shows little change in appearance of agglomerates beyond 5 cm. In an earlier study (Ref. 13) of this same propellant in a similar, but larger, experimental apparatus (lower proportional heat loss), the agglomerate combustion rate was also low, but did not

appear to be arrested. Likewise, there is no evidence of arrested burning of agglomerates in the service rocket motor. Thus the apparent cessation of agglomerate burning in the atmospheric pressure tests on UTP 3001 propellant apparently reflects poor simulation of rocket motor behavior late in agglomerate burning, aggravated in this case by the low pressure of these tests and relatively poor stoichiometry of this propellant (16% binder). As can be seen in Fig. 16, the combustion efficiency is much better at 0.7 MPa (100 psi), and a similar pressure dependence is evident with the other propellants noted in Fig. 15 and 16.

In Fig. 14 there are two curves for UTP 3001 propellant. The lower curve resulted from use of a modified method for determination of free aluminum in the quenched sample. The original method depended on determining the weight reduction when aluminum was removed by acid dissolution and washing. The second method amounted to direct determination of the aluminum weight dissolved, by analysis of the acid solution. This method yielded lower values of free aluminum content in the samples. This result implies that the original weight change method measures something more than just free aluminum. As will be noted later, the aluminum lobe of the agglomerate contains a delicate structure of oxide flakes, that breaks up and is lost during acid dissolution and washing. Consequently the weight change method measures the sum of free aluminum and flake oxide. This appears to account for the difference in indicated free aluminum as determined by the two methods, and provides also an estimate of flake oxide weight. Since the other data in the figures (14-16) are all by the weight difference method, it may be assumed that the free aluminum is consistently less than the indicated values.

One further experimental problem, applicable particularly to short quench distances and fast-burning samples, is related to determination of the actual time-to-quench. As noted in Ref. 12, large agglomerates do not come up to speed as fast as small ones when they leave the propellant surface. (Fig. 17 shows the result from Ref. 12.) Further, the actual distance to quench depends on undetermined details of the alcohol behavior during the test. The first of these problems is common to all quench experiments at short quench distances. The second problem is being attacked by a modified design that controls the location of the alcohol surface. In the present work, testing at high pressure would have been more extensive if these problems could have been resolved. Such tests did provide comparative results at different pressures, and provided information on pressure effects on the detailed nature of agglomerates and oxide products, described in the

following.

Nature of Agglomerates

In discussing combustion of aluminum agglomerates, it is often assumed for convenience that they are aluminum droplets, or aluminum droplets with oxide lobes. Experimental investigators are generally aware that the agglomerates are much more complex (Ref. 14, 15). These added complexities may not be important during much of the burning period of the agglomerate, but they merit study for at least two reasons. First, they provide information about how agglomerates are formed. Second, the complexities become important in the later, slow burning part of the agglomerate burning history, and the transition to residual oxide droplets.

The external appearance of quenched agglomerates was shown in Fig. 12. The trend with burning time is qualitatively independent of the initial agglomerate size, pressure, and propellant formulation, except under marginal conditions noted before, when the agglomerate droplet temperature drops low enough to allow flame collapse and oxide freezing. Examination of the interior of normal agglomerates reveals a relatively complex structure (Ref. 7). Cleaved agglomerates show voids, of non-characteristic shape, size and location (Fig. 18). Voids are larger in low pressure tests and early in burning, and usually include one under the oxide lobe (making it somewhat like a bubble early in burning). Agglomerates from atmospheric pressure tests are fairly soft, while agglomerates from tests at higher pressure are brittle and don't cut easily. These trends have not been studied thoroughly (e.g., as a function of propellant composition). Void volume is generally less than 15% of agglomerate volume.

Another feature of the interior of the aluminum lobe of the agglomerate is revealed by careful acid etching to remove the aluminum. It is found that the interior contains an intricate structure of oxide flakes (mentioned above and in Fig. 11, in the discussion of free aluminum analysis). These structures are not recognizable in cleaved samples, but are evidently responsible for the brittle quality of agglomerates from quench tests at elevated pressure. The flake structure is much more extensive in agglomerates from tests at elevated pressure.

The inhomogeneous nature of the aluminum section of the agglomerate poses two practical questions. Does it have any significant effect on combustion? Is it telling us something about formation of agglomerates? The answers are speculation at present. As indicated in Fig. 9-11, the agglomeration event involves

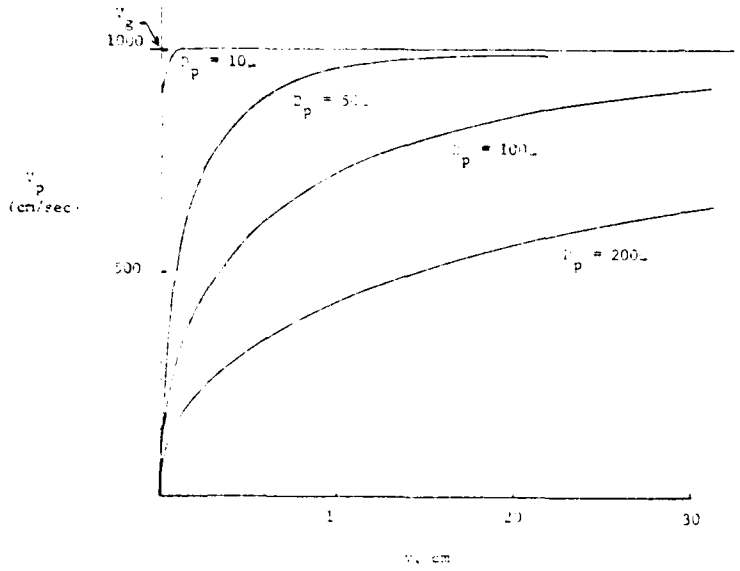

Fig. 17 Agglomerate velocity vs distance from the burning surface (calculated, see Ref. 12).

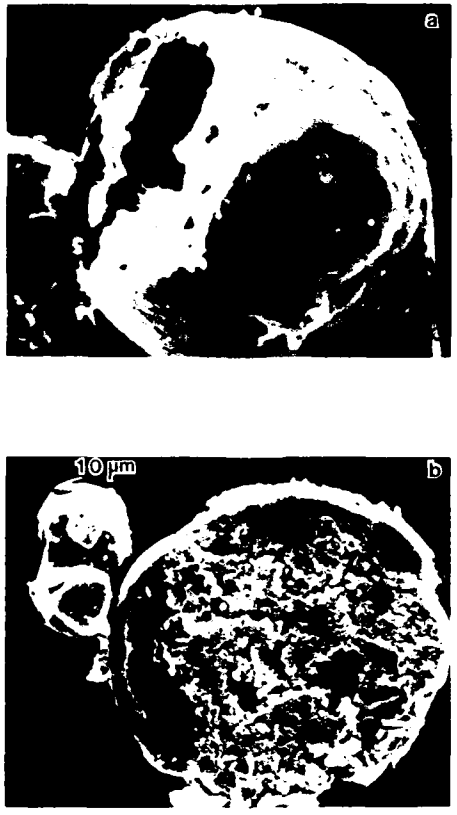

Fig. 18 Agglomerates cleaved to show interior.

a) Soft agglomerate from atmospheric pressure test.

b) Brittle agglomerate from test at 2.8 MPa.

the melt-down and coalescence of a very complex structure, under the influence of surface tension forces of the molten aluminum. It seems likely that this event would trap some solid oxide shell structures in the interior of the agglomerate, and that this insoluble oxide would change to thin molten films in the interior of the agglomerate. If the melt-down and coalescence of the accumulate is gradual enough, the aluminum probably withdraws into a sphere with the oxide changing from a solid aggregation on the surface to a molten oxide lobe. At higher pressure, coalescence is more abrupt, and more oxide aggregate is trapped inside the agglomerate. The test results suggest that trapped aggregate is first converted to very thin sheets, which become concentrated as the aluminum burns away. If the agglomerate is quenched, the films apparently freeze into the flake arrays noted above and in Fig. 11. It is surely these flakes that make agglomerates brittle, and account for the contradictory results of the two free aluminum analysis methods noted in Fig. 14. In fact, the difference in indicated free aluminum for the two UTP 3001 curves in that figure is presumably the mass of the sample that is flakes. These results indicate that about 45% of the oxide in the sample is in the form of flakes (UTP 3001 at 1 atm). As a rough calculation, one may assume that half of the aluminum in these samples is in oxide form, that 10% of the oxide formed during burning goes to the oxide lobe, and that the "flake oxide" remains in flake form during burning. These assumptions and the observed ratio of flake to total agglomerate oxide indicate that the flake is about 5% of the original agglomerate mass. This appears to be consistent with the hypothesis that flake oxide is a relic of all or part of the sintered oxide containment structure of the parent accumulate. In future work, this analysis will be used to make systematic determinations of flake mass, and see if the trend with test conditions is consistent with expected degree of pre-agglomeration oxide formation.

Regarding the voids in the agglomerates, there is no direct evidence as to their source other than the possibility of gas entrapment during coalescence as suggested by agglomerates frozen during coalescence (Fig. 10). Given the complexity of the accumulate, the coalescence event and the gaseous environment, there is no shortage of hypotheses. There is no clear evidence that the voids affect burning, except as they affect agglomerate surface area to mass ratio. They will cause agglomerates to weigh less than would be judged on the basis of visual (motion picture) observations of diameter.

One final feature of agglomerates that needs description is the appearance of

the oxide lobe. For agglomerates quenched early in burning, the lobes are small and generally of a clear glassy appearance. As burning progresses, the oxide lobe gets larger, and changes to a glossy black appearance. Lobes that are of comparable size to the aluminum lobe (i.e., approaching burnout) tend to be black, especially in relatively fuel-rich propellants. It has been suggested that the black appearance is a result of reduction of Al_2O_3 by Al, which apparently gives soluble black suboxide, a behavior observed in laboratory tests on laser heated Al_2O_3 systems in argon atmospheres (Ref. 15). This may not be a crucial aspect of combustion, but may explain the highly visible "black shiny" particles in quenched samples and described in the next section.

In this respect, it is relevant to raise the question of final fate of an agglomerate that is near burnout, and dominated by the oxide lobe (Fig. 19). During burning, the flake oxide is concentrated in the contracting aluminum lobe, and may concurrently be reduced to lower oxides and/or flow into the oxide lobe (or neither). During this burnout stage, the state of the droplet's flame envelope is a matter of speculation. The fragmentation events observed in many studies in non-propellant environments apparently do not occur, because the number of residual oxide droplets produced is comparable to the number of agglomerates burned out. This does not preclude the expulsion of small amounts of material, or retention of some aluminum, lower oxides of aluminum, or other unidentified materials such as carbides. This will be discussed further in connection with the nature of the oxide particle.

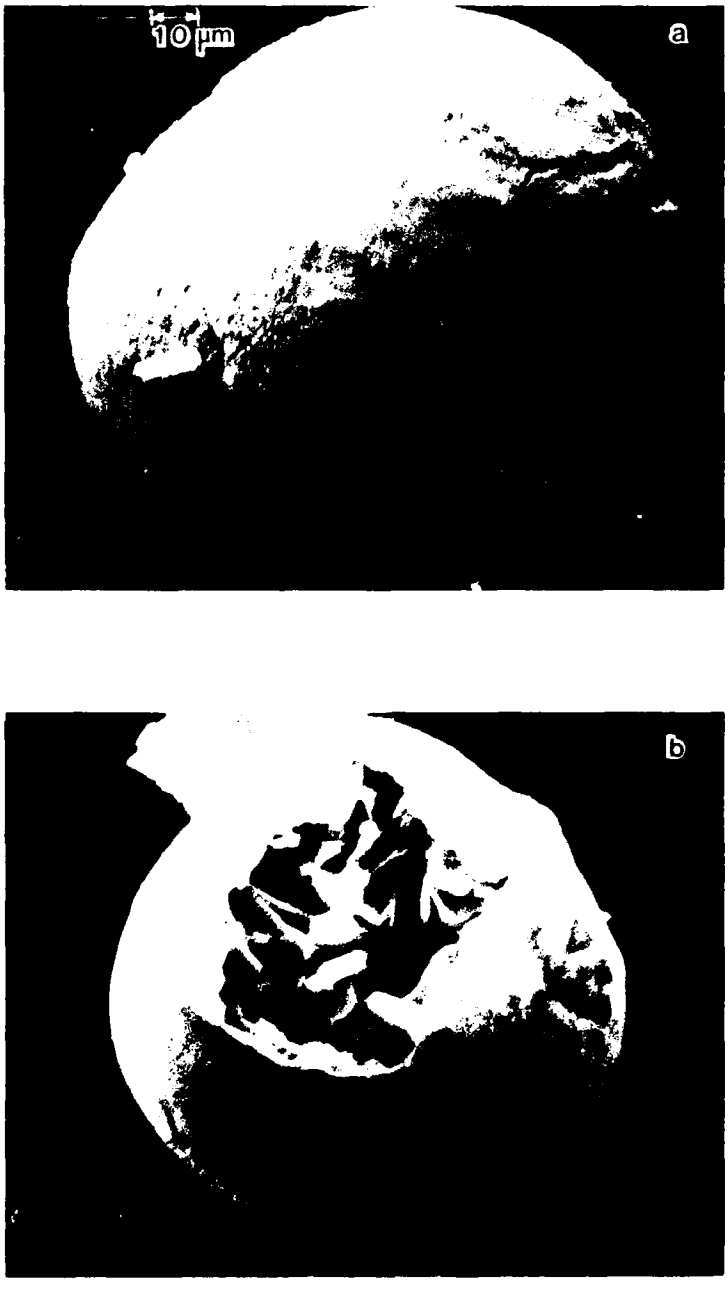

Fig. 19 Agglomerates quenched near burnout. Atmospheric pressure tests.
a) As quenched.
b) Acid-etched.

AD-A114 771 GEORGIA INST OF TECH ATLANTA SCHOOL OF AEROSPACE ENG--ETC F/G 21/9.2
ROCKET RESEARCH AT GEORGIA TECH.(U)
NOV 81 E W PRICE, W C STRAHLE, B T ZINN F49620-78-C-0003
UNCLASSIFIED AFOSR-TR-82-0368 NL

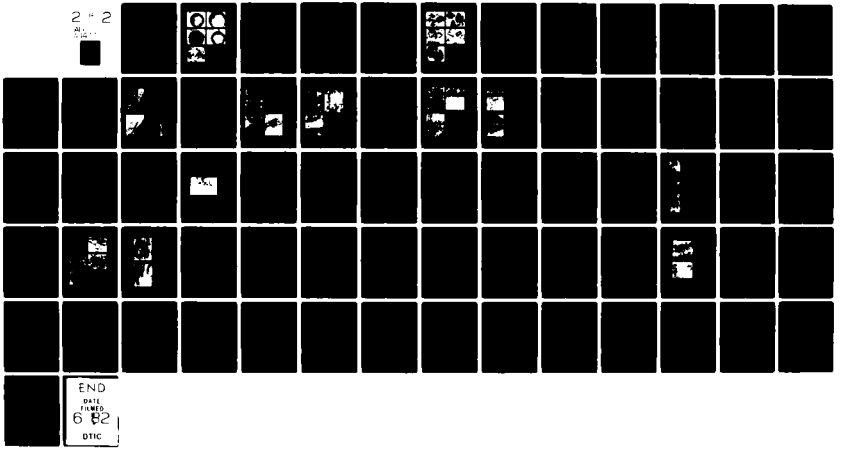

END
DATE FILMED
6 82
DTIC

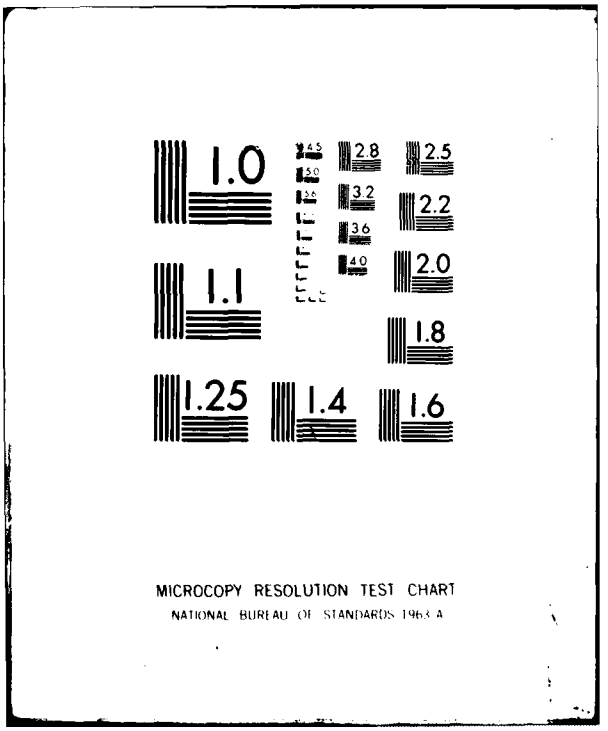
1.0
1.1
1.25
1.4
1.6
1.8
2.0
2.2
2.5
2.8
3.2
3.6
4.0
4.5
5.0
MICROCOPY RESOLUTION TEST CHART
NATIONAL BUREAU OF STANDARDS 1963 A

PRODUCT ALUMINUM OXIDE PARTICLES

It has often been noted (Ref. 15-17) that burning of aluminum droplets leads to two kinds of oxide product droplets, i.e., "smoke" formed in the flame envelope of the aluminum droplet, and "residual oxide" droplets left over when the agglomerates burn out. These are two entirely different populations of droplets, the former being generally less than two microns in diameter and the latter being substantially larger. Being governed by different formation processes, their size distributions are subject to entirely different constraints. In particular, the residual oxide droplet size distribution is linked to the agglomerate size distribution, and hence to all the processes discussed above that govern agglomerate size.

The importance of the combustion-generated size distributions was noted earlier. The effects on combustor stability, component erosion, thrust loss, etc., depend on the details of the size distribution. The effects cannot be fully characterized in practice without consideration of subsequent population changes in the combustor and nozzle flow, a subject beyond the scope of the present study. However, calculations of populations in the flow field cannot be made properly without use of correct starting populations, which are the combustion-generated ones discussed here. Particular attention was paid here to the residual oxide droplet population because, although it represents only 10-20% of the total oxide, its role in motor performance problems is relatively large, relatively unpredictable, and closely related to other aspects of the present study.

Kinds of Oxide Particles and Size Trends

Quenched samples yield a variety of particles other than agglomerates. After all the smoke particles were washed away (separated from the larger particles by repeated sedimentation-decanting operations) the remaining particles consist of (listed in order of decreasing size) agglomerates, black shiny spheres, white spheres, and transparent spheres. The external appearance of these particles is illustrated in Fig. 20 (except agglomerates discussed earlier) The transparent oxide particles represent a very small portion of the mass; they are all in the $< 35\ \mu m$ diameter size. The size distributions of the white oxide and black shiny particles were determined on many tests, and typical distribution for different quench distances is shown in Fig. 21 (these examples are for the same three tests as Fig.

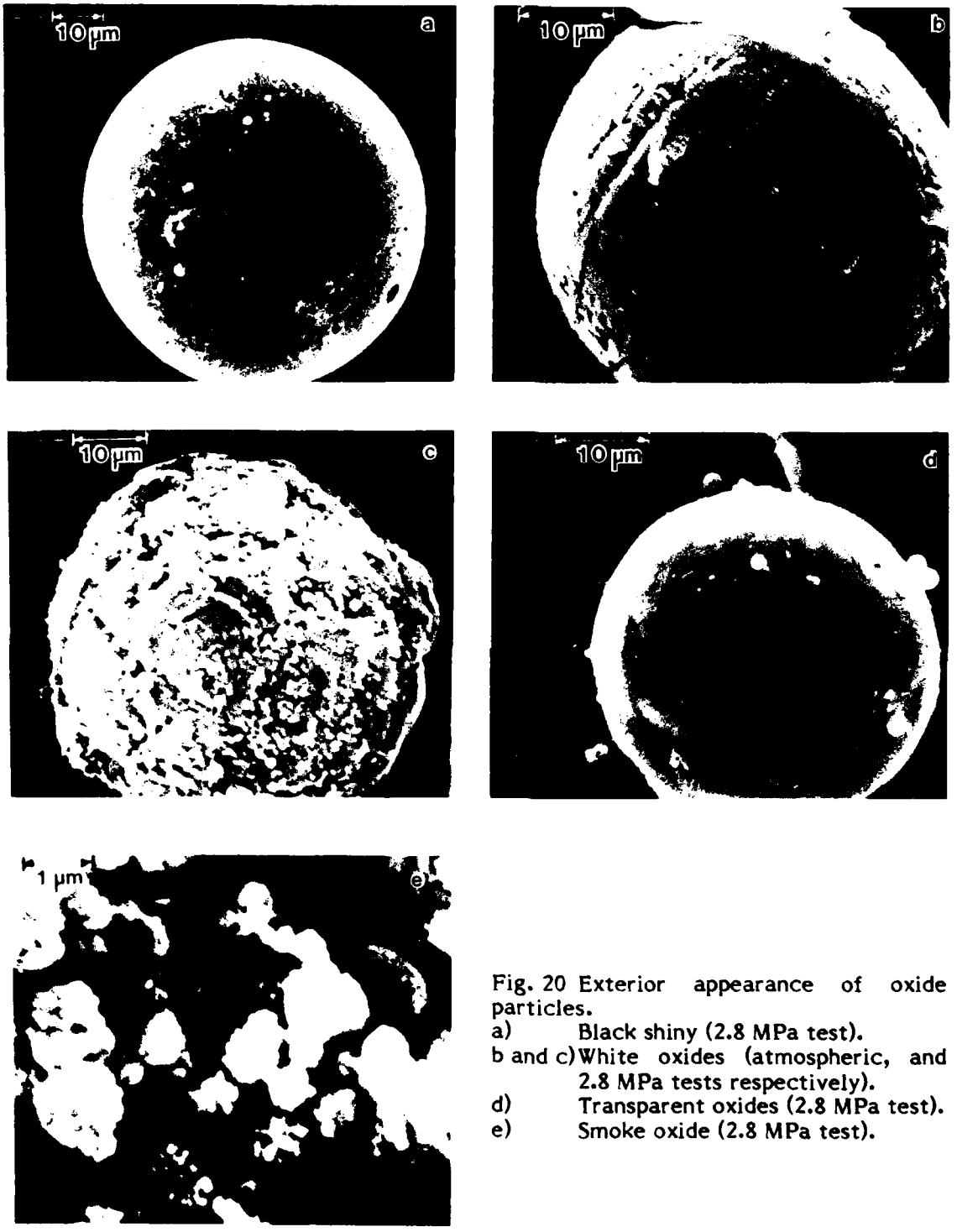

Fig. 20 Exterior appearance of oxide particles.

a) Black shiny (2.8 MPa test).

b and c) White oxides (atmospheric, and 2.8 MPa tests respectively).

d) Transparent oxides (2.8 MPa test).

e) Smoke oxide (2.8 MPa test).

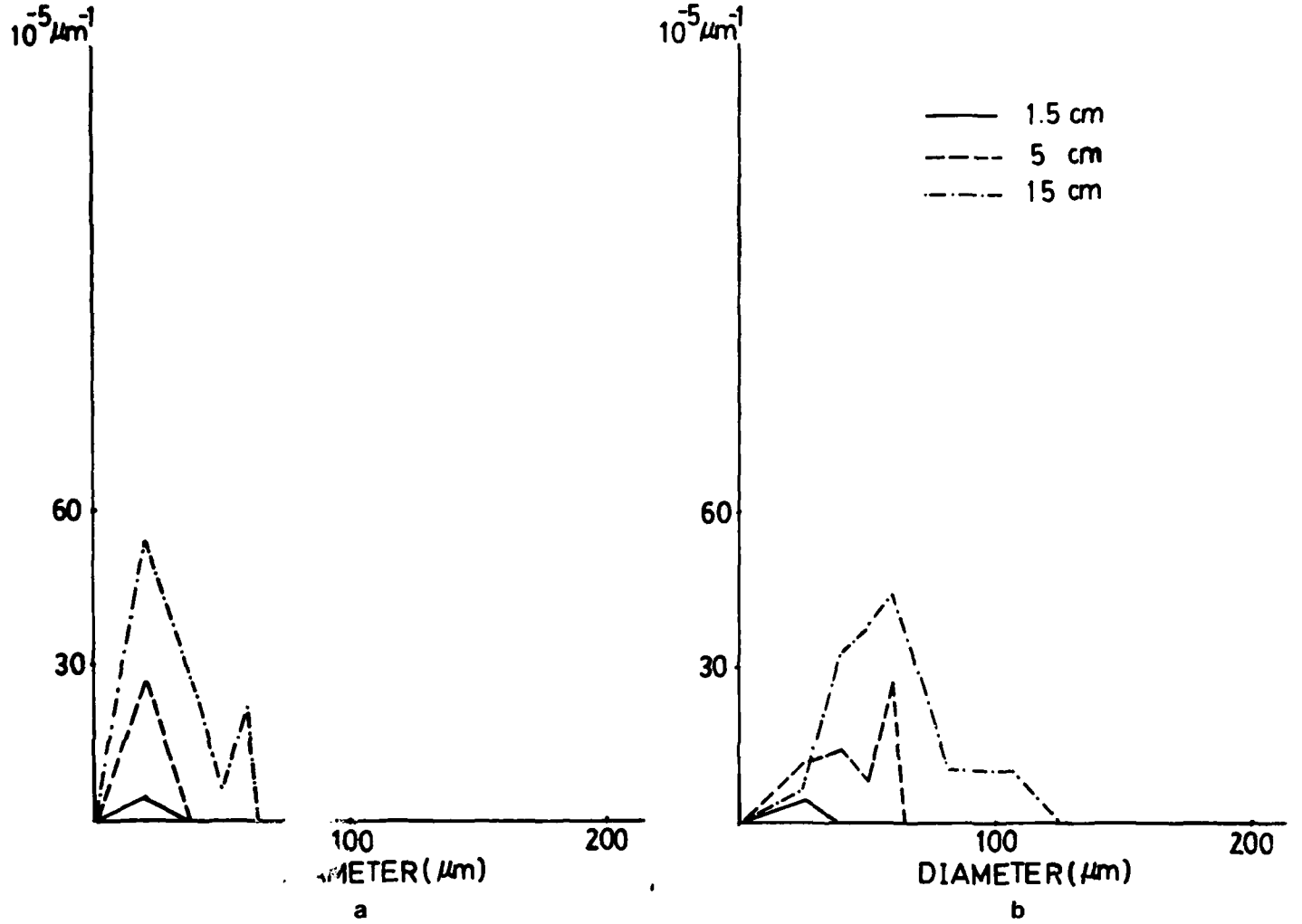

Fig. 21 Size distribution of oxide particles (0.7 MPa test). a) Black shinies, b) White oxide.

13). The size distributions were determined by sieve sizing and weighing the quench sample, and then visually determining the relative portion of agglomerates, black shinies, and white oxides in each size fraction. Overall accuracy of the quench-sieve-classification procedure was not considered good, but adequate to establish certain qualitative features of the size distributions that are critical to understanding the origins of different kinds of oxide particles. In general, it was observed that as quenching distance was increased, the total mass of black shinies increased, but primarily by addition of larger particles. The size of the larger black shinies was comparable to that of oxide lobes on those agglomerates that were near burnout. The number of black shinies in the small end of the size range often decreased with distance from the burning surface. In contrast, the population of the smaller white oxide particles increased over its whole size range. At very long quench distance (longer than in Fig. 21), where the agglomerates are all burned out, the black shinies are few in number, with no small ones. From these trends it was concluded that black shinies are a transition state between agglomerates and oxide particles, reflecting a phase in conversion of the collected oxide (flake, lobe oxide of the "burned out" agglomerates into pure oxide droplets). This was verified by more detailed studies of the particles, described below. The actual conversion process remains a matter of speculation.

Detailed-Nature-of-Oxide-Particles

The nature of the particles was examined by microscopic observation of the exterior surface, and of the interior as revealed by broken particles, and acid-etched particles. Black shinies were also subjected to chemical analysis for free aluminum, and to controlled heating experiments. The exterior appearance of the oxide particles was shown in Fig. 6 and 20. Black shinies are near perfect spheres with glossy surfaces. White oxides are round but have surface features ranging from striations to grainy surface to a cauliflower-like exterior, the latter occurring at higher pressures. Transparent oxides are roughly spherical, and smooth.

When the oxide particles are etched in HCl (3% HCl in water for prolonged periods of time) the transparent oxides show no change. The white oxides (cauliflower ones) show enhancement of surface recesses, no other change. The black shinies show patches of originally glossy surface that have become porous. The free aluminum content of a sample of black shinies was determined to be 2.5%.

Black shinies turned white when heated to 1200°C in oxygen, showed no change in argon. Black shinies heated to 1200°C in argon on a platinum surface showed evidence of drainage of molten aluminum in the manner of agglomerates (Ref. 7).

The nature of the interior of the oxide particles differed substantially (Fig. 22). Broken black shinies exhibited a somewhat amorphous appearance, with very small spherical voids (< 5% of volume, pressure dependent). White oxides exhibited extraordinarily complex interior structure (see Fig. 22) with 5 - 15% void volume, pressure dependent. Transparent oxide particles break like glassy material (Fig. 22) and have no voids.

Relative Mass of Residual and Smoke Oxide

As noted earlier, the portion of aluminum oxide that ends up in the form of the relatively large "residual oxide" class of particles is only about 10-20%, the rest being in fine particle "smoke" form. However, there is a paucity of data on this subject in the literature, that which is available being pertinent mostly to size distributions after flowing through the rocket nozzle. The measurements of free aluminum content in quenched samples described earlier provided also the weight of residual oxide formed up to the point of quench. From those data and the original aluminum mass, the mass of smoke oxide could be determined. Fig. 23 illustrates values of mass fraction of oxide in smoke form corresponding to atmospheric pressure tests used previously for Fig. 14-16. The results indicate that roughly 85% of the oxide is in smoke form. The data suggest that the proportion in smoke form is higher early in burning (short quench distance), but this trend is deemed to be due to systematic errors of measurement that exert undue effect in short quench distance tests. Results in Fig. 23b indicate that the relative portion of oxide in smoke form is not particularly pressure-dependent.

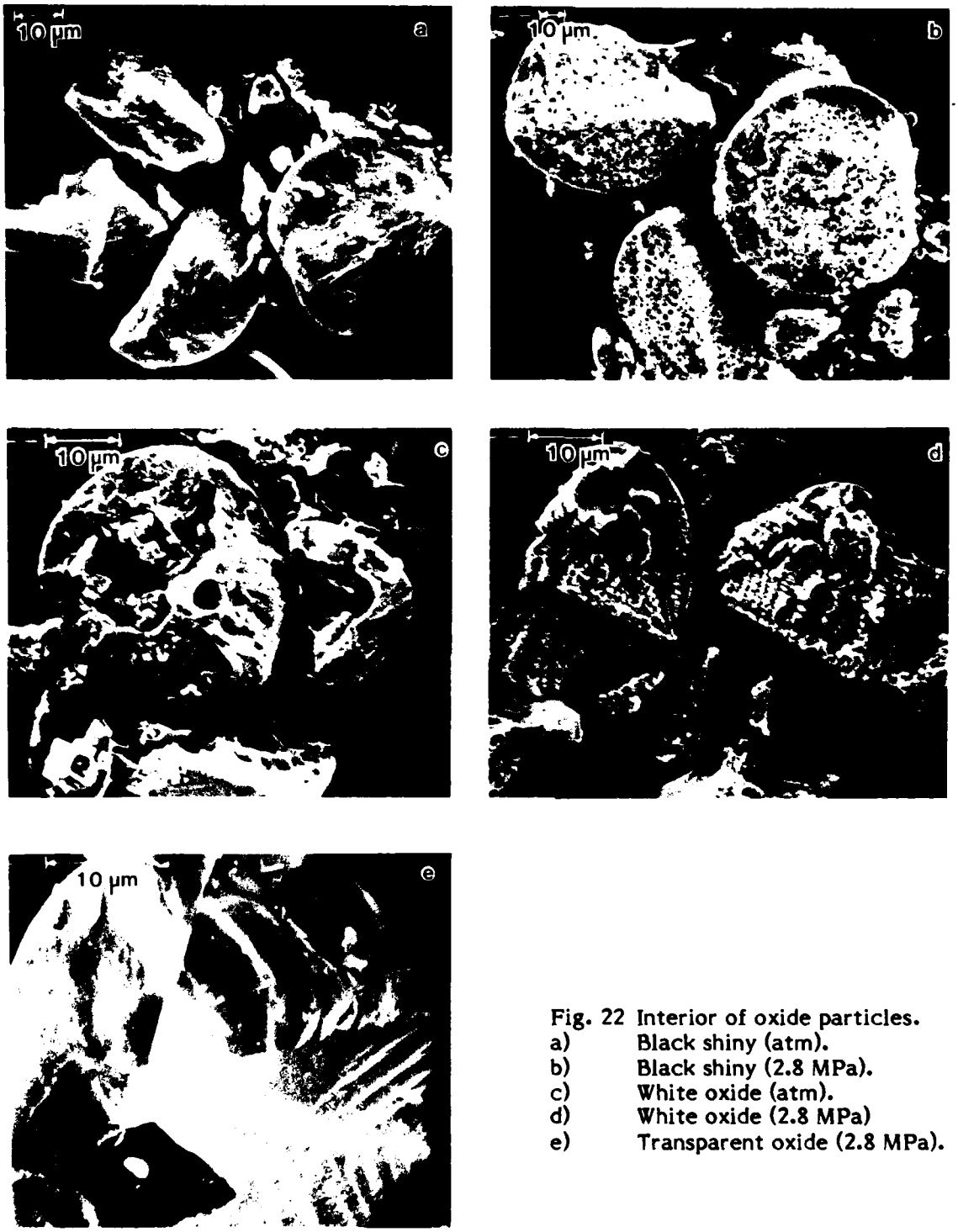

Fig. 22 Interior of oxide particles.
a) Black shiny (atm).
b) Black shiny (2.8 MPa).
c) White oxide (atm).
d) White oxide (2.8 MPa)
e) Transparent oxide (2.8 MPa).

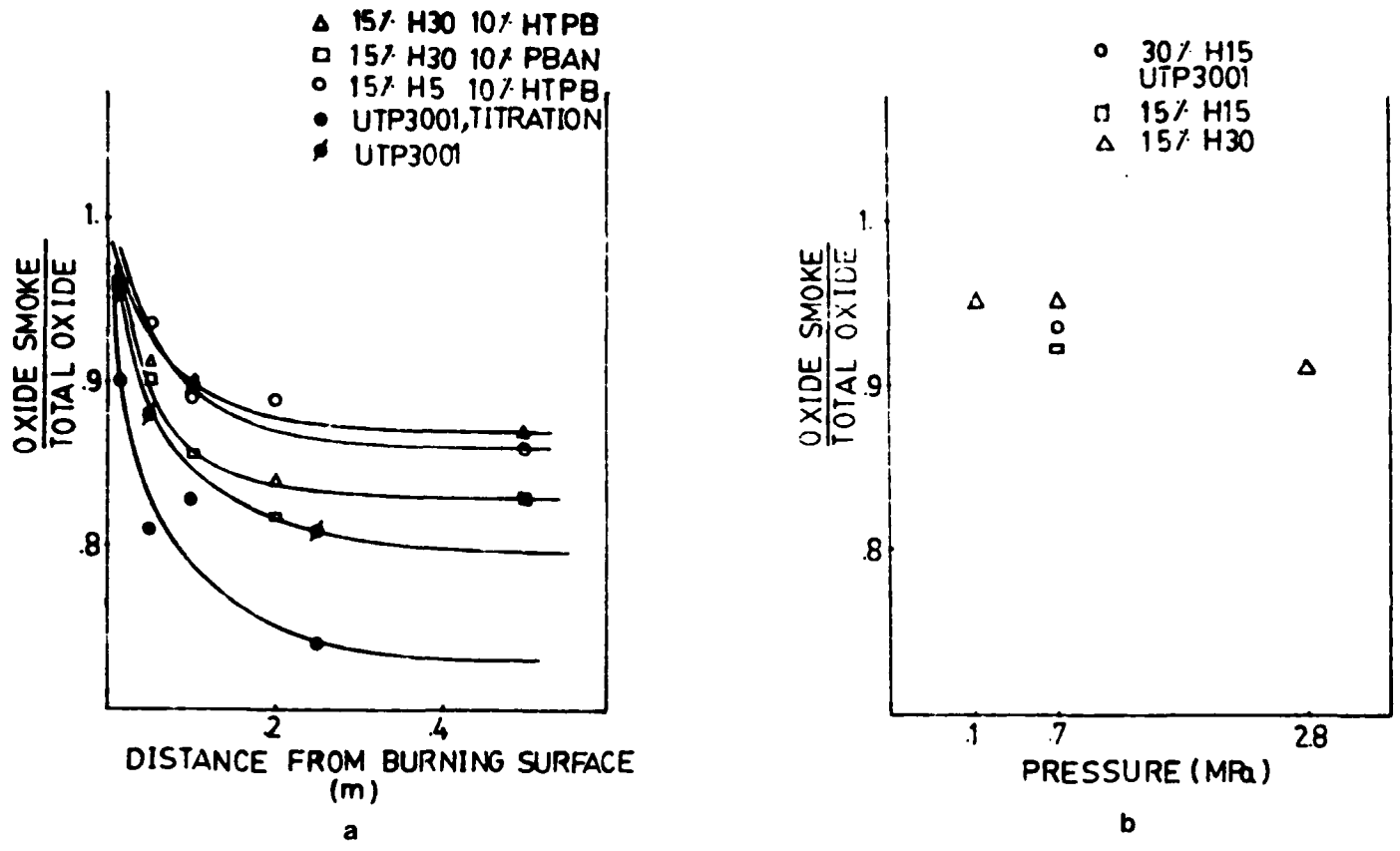

Fig. 23 Mass fraction of oxide in smoke form.
a) Dependence on quench distance (atmospheric pressure tests).
b) Dependence on test pressure (1.5 cm quench distance).

COMBUSTION OF DRY-PRESSED MIXTURES OF ALUMINUM AND AMMONIUM PERCHLORATE POWDERS

Combustion of the aluminum ingredient in composite hydrocarbon binder propellants is a consequence of the availability of oxidizing species provided by decomposition of the solid oxidizer. However, the detailed accumulation-agglomeration-metal ignition process is substantially determined by events other than molecular level oxidation. In order to unravel the roles of different steps in the propellant combustion process, it is helpful to determine just how much of the aluminum "metabolism" is due purely to interaction with the ammonium perchlorate oxidizer. It had been established before that aluminum could survive the environment on the surface of burning ammonium perchlorate for an appreciable time (Ref. 18, 19) without ignition, while there are some recent conflicting claims that intermediate reaction products of AP (present primarily in the AP decomposition-flame zone) might be particularly important to ignition of aluminum (Ref. 20). Previous work on the present project had confirmed a substantial body of literature (e.g., Ref. 21-23) concerning the protective character of the oxide "skin" on aluminum particles. Those collected results had indicated that temperatures in the range 1200 to 2030°C might be required to ignite particles. The AP flame would thus be marginal as an ignition source. However, the ignition requirements referred to in Ref. 21 to 23 were not determined in chemical environments typical of an AP deflagration wave, nor on assemblages of aluminum particles typical of propellant burning surfaces. Thus it was important to determine whether accumulating aluminum on an AP burning surface would adhere there (as implied by results in Ref. 11, 18, 24 and elsewhere), and if it would, whether it would sinter, ignite, and agglomerate.

In order to resolve these questions, combustion tests were run on hard-pressed (175 MPa) samples of Al/AP powder mixes. Tests consisted of interrupted burning by rapid depressurization, and combustion cinemicrophotography. Tests were run with different mixture ratios of Al and AP, different particle size combinations, different kinds of aluminum powder, and different pressures. A summary of test conditions is shown in Table I, and a description and interpretation of results was reported in Ref. 19. These results indicated the following critical points about aluminum behavior and Al-AP interactions:

Table 1
Summary of Tests on Dry-Pressed AP/Al Mixtures*

Sample	85% 10 μm AP 15% 5 μm Al (H-5)	85% 60 μm AP 15% 30 μm Al (H-30)	85% 100 μm AP 15% 30 μm Al (H-30)			85% 100 μm AP 15% 95 μm Al (H-95)		
Pressure								
MPa PSI	Movie	Movie	dp/dt Quench	Movie Hi Mag	Lo Mag	dp/dt Quench	Movie Hi Mag	Lo Mag
4.2 600			✓✓✓ ✓			✓✓✓ ✓		
5.5 800			✓	35	38		5, 9, 13	c
6.9 1000	55	57	✓✓✓	33	4	✓✓✓	1,10,14	

* Check marks denote tests. Number identify the pertinent film.

1. Aluminum particles do not ingite in the AP deflagration zone (propellant-ingredient-size particles).
2. Aluminum adheres to the deflagrating AP surface, and under most conditions accumulates there. Accumulation is very limited where the aluminum particles are comparable in size to the oxidizer particles; those (large) aluminum particles do linger on the surface, but the spacing of the particles is now large enough to reduce chances of a surface particle being joined by underlying particles as occurs with small Al particles.
3. Accumulation of aluminum on the AP surface leads to rigid assemblages on the burning surface that eventually break up and detach. Break-away is usually followed by local inflamation of the accumulate. This appears to occur at break points in the detaching crust, followed by spread into the rest of the crust.
4. The spreading inflamation leads to formation of several large agglomerates, that appear to burn thereafter much in the manner observed with propellants.

The foregoing observations were based on the motion picture tests. Quench tests yielded relatively little evidence of surface accumulation of aluminum, which apparently detached during the depressurization quench.

The test results are interpreted as follows, in the light of earlier tests on behavior of aluminum powders during heating (Ref. 5, 8, 25). Upon being reached by the receding surface of the sample, an aluminum particle adheres to the surface, which is generally believed to consist of a froth layer at a temperature of about 600°C. The particle probably proceeds to higher temperature under the influence of the nearby AP flame, while continuing to reside on the surface. Underlying aluminum particles emerge and join the original ones, concentrating into contacting arrays. The oxide skin on each particle apparently limits aluminum oxidation to a continuing build up of surface oxide. This includes sintering of the particles to each other when they are contacting. As the sintered layer becomes more dense and more heavily oxidized, it becomes resistant to flow of gas from the underlying AP, and also resistant to heat flow from the AP flame to the AP surface. Under these conditions, the layer would be expected to be above the aluminum melting point, and the structural strength would be due to the sintered solid oxide structure that encases the aluminum. This structure in turn is stressed by the gas through

flow, and the stage is set for break-up of the sintered accumulation.

Break-up of the accumulation implies local break up of the oxide that has been "protecting" the aluminum, which promptly increases its oxidation rate and locally heats the sintered structure. Under favorable heat-flow conditions, this can lead to progressive breakdown of adjoining sintered structure, i.e., inflamation. Alternately, aluminum exposed in a break may simply be covered over by new solid oxide, which the AP flame is unable to melt. Both alternatives apparently occur, sometimes in the same test. The inflamation alternative is believed to proceed as follows. A breaking section of the accumulate with exposed molten aluminum self heats due to oxidation of exposed aluminum. This is aided and sustained by limited flow of aluminum under surface tension forces, with associated continual mechanical degradation of any newly forming oxide skin. Heat release goes primarily to heat-up of those particles that are actually reacting, which are insulated from their colder, unignited neighbors by the very oxide that sinters them together. Local self heating melts the protective oxide locally, permitting local coalescence of aluminum "particles" (Fig. 10a), retraction of insoluble oxide from the metal surface, and establishment of a high temperature aluminum vapor flame (photographically manifested by rapidly increased brightness and establishment of the characteristic luminous smoke trail). This state is sometimes reached at more than one site in large accumulates, and leads to a rapid propagative heat-up, oxide melt-down, and inflamation of the accumulate and transformation to one or more burning agglomerates.

While the foregoing scenario is very complex, the observed combustion behavior is hardly amenable to a simple explanation. The interpretation rests on a great deal of information about the real behavior, including not only the combustion of AP/Al samples, but also on behavior of single aluminum particles and powders. The scenario explains why larger unsintered particles don't ignite (no means to break down the oxide skin); why heavier sintering and non-ignition can occur at lower pressure (low oxidizer concentration and poor heating from the oxidizer flame permit protective oxidation of break-up surfaces); and why vigorous combustion can occur when typically reluctant ignition is finally achieved (transition to vapor phase burning). The scenario also has major implications for aluminum behavior in propellant combustion:

1. Ignition of accumulating aluminum will generally depend on exposure to high temperature flames resulting from AP-Binder interaction (i.e., the AP flame alone is not enough). Conditions that delay this AP-Binder flame exposure will yield prolonged accumulation and large agglomerates.

2. Vigorous inflamation of accumulates on or near the burning surface is favored by large specific surface of aluminum (small particles), because the eventual breakup and coalescence of the accumulates at the surface is then a highly exothermic event. Large single aluminum particles ignite further from the surface because the protective oxide won't break down at temperatures near the burning surface, even when the particles linger long enough to heat up to surrounding temperature.

3. The size of agglomerates in propellant combustion is generally recognized to be strongly affected by the degree of segregation of aluminum particles in the propellant microstructure, with local concentrations ("pockets") of aluminum tending to form single agglomerates. It is also recognized that this criterion for agglomerate size is modified by the susceptibility of the accumulating aluminum to ignition, which event usually causes the accumulated aluminum to detach from the propellant surface. In this context it is important to keep in mind that the AP flame will not cause ignition, a fact that accounts for the massive accumulations on the surface of AP/Al samples. Under adverse ignition conditions, accumulated aluminum on the burning surface of propellants may also end up on the surface of oxidizer particles of the propellant and remain during all or part of the burning of the oxidizer particle. Under some conditions (notably low pressure), delayed ignition can even give rise to interconnection ("bridging") of local accumulations to give the more massive accumulations observed with AP/Al samples. In that case, correspondingly large agglomerates may be formed.

STUDY OF THE ACCUMULATION-AGGLOMERATION PROCESS USING AP-BINDER SANDWICHES WITH ALUMINUM FILLED BINDER

One of the primary problems in the study of accumulation and agglomeration of aluminum in a propellant is the chaotic nature of the propellant on the dimensional scale of the relevant processes. In effect, it is impossible to describe what was tested or what happened. On the other hand, some success had been achieved in a companion project to the present one, through testing sandwiches of AP and binder. A sandwich consists of two layers of pre-pressed sheets of ammonium perchlorate (oxidizer) with a layer of binder (fuel) of controlled thickness cured between the sheets. Such systems do not provide the intermittency of microstructure present with granular mixes but they simplify the geometry of the combustion zone and separate the ingredients of the propellant into precisely definable regions providing a better understanding of the flame structure and greater resolution by experimental methods. Using aluminum in the binder lamina provides a means to conduct controlled accumulation-sintering-agglomeration experiments in a combustion environment simulating critical aspects of real propellants.

The investigation of aluminum combustion in sandwiches consisted of preparing sandwiches with various combinations of binder, aluminum and oxidizer in the fuel lamina; edge burning the sandwiches at various pressures; and observing combustion behavior by photography and by microscopic study of quenched samples (quenched by rapid depressurization). Fig. 24 gives the matrix of test conditions used. Only a limited number of tests with photography were run, but quench tests were run at all the indicated conditions, and two tests were run at some test conditions to determine reproducibility.

Results of Sandwich Quench Tests

All test results described below were for binder lamina thickness between 60 and 90 μm. With pure binder laminated sandwiches, it is observed on quenched samples that the binder is slightly recessed at low pressure (1.4 MPa) and is protruding at high pressures (6.9 MPa) (Fig. 25) (Ref. 18, 26, 27). The AP burning rate adjacent to the binder is retarded, with the maximum regression of the surface occuring at about 100 μm from the interface. There are bands of relatively smooth AP surface running along the edges of the interfaces in all samples. These features

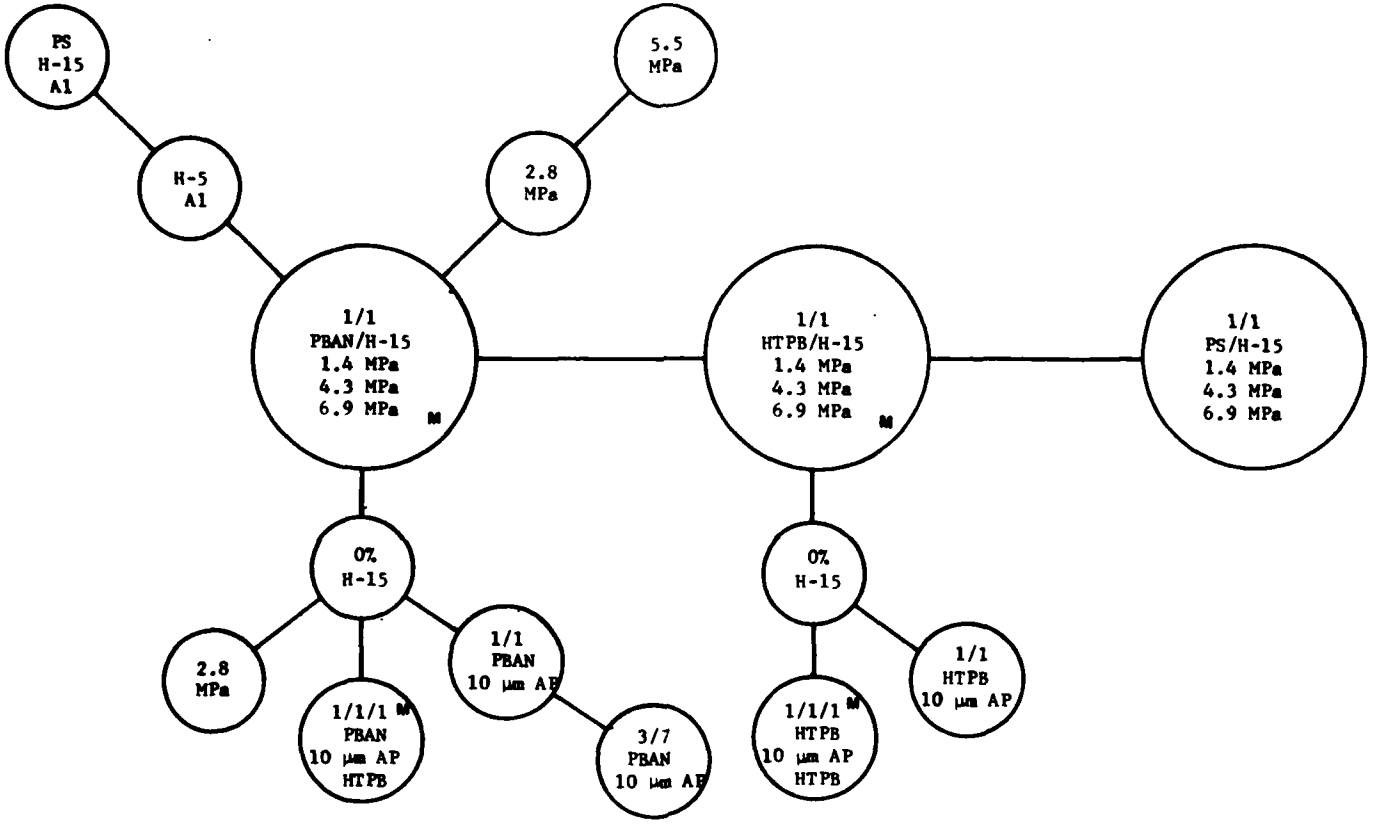

Fig. 24 Summary of conditions for sandwich burning tests (large circles denote primary burning tests (large circles denote primary conditions, small circles denote variants on primary conditions). (M denotes combustion photography.)

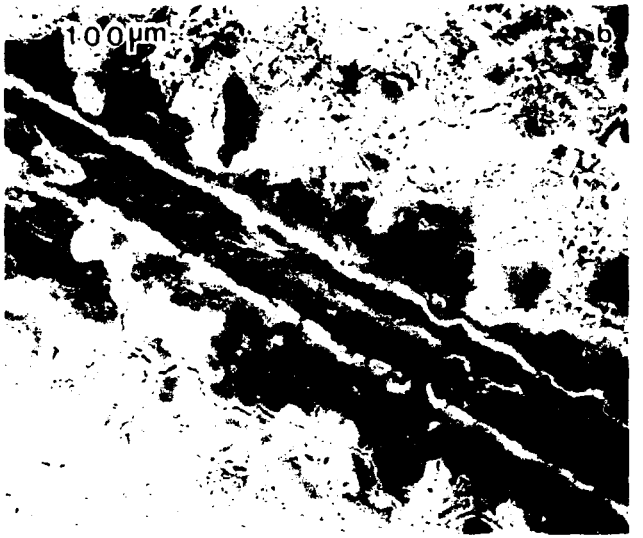

Fig. 25 Examples of quenched AP/PBAN sandwiches.
a) 1.4 MPa, b) 4.1 MPa, c) 6.9 MPa.

did not change with type of binder except that polysulfide has a drier appearance.

The general effect of addition of aluminum to the binder lamina is illustrated in Fig. 26 by samples with a 1/1, PBAN/H-15 Al lamina. The accumulated aluminum is visible on the binder lamina, and has the appearance of being wetted by molten binder. The volumetric loading of aluminum in the lamina is less than 50%, but the surface generally appears to have a higher concentration of aluminum. As noted later, some test conditions lead to occasional presence of dry accumulates and occasional agglomerates on the quenched surface, and some conditions lead to small accumulates or single aluminum particles on the oxidizer surface. In the example shown, the binder lamina is slightly recessed. The smooth bands on the AP surface adjoining the AP-binder interfaces are equally evident with aluminized laminae, and were present under all test conditions in this study. A tendency for the leading edge of the AP surface to be at a location some distance from the interface (i.e., interface AP protruding) was noted above for unaluminized sandwiches, and occurs also with aluminized binder (all tests with binder-Al, all pressures). Use of aluminized binder increased the burning rate in some tests (increased in the case in Fig. 26). In the following, the effect of various test variables are described in terms of the features noted above for aluminized PBAN sandwiches.

a) Effect of Pressure

In the sample case used in Fig. 26 (1/1, PBAN/H-15, at 4.1 MPa), increasing the pressure reduced the amount of distinguishable aluminum on the binder surface, as well as the amount scattered on the AP surface (almost none at 6.9 MPa). The wetted appearance of the aluminum concentrated on the binder lamina is evident at all pressures, with occasional areas of dry-sintered particles at low pressure. The surface profiles of the aluminized PBAN sandwiches (i.e., details near the fuel laminae) were alike over the pressure range 1.4 - 6.9 MPa, and similar to the unaluminized PBAN sandwiches at lower pressures. The trend of the nonaluminized laminae to protrude at higher pressure (Fig. 25) did not occur for the aluminized PBAN sandwiches (Fig. 27). In general, the overall sandwich burning rate appeared to be higher with aluminized PBAN sandwiches, a feature reflected in the overall sandwich profiles, which have more "Vee" shaped profiles.

The above observations of pressure dependence do not all apply for other binders, or other additions to the binder, as noted later.

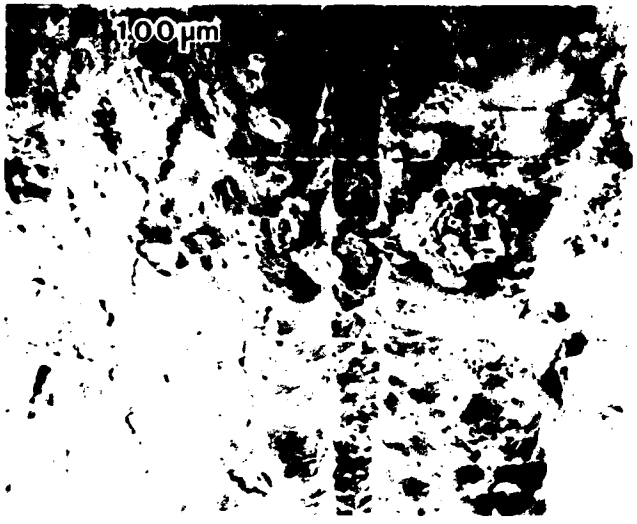

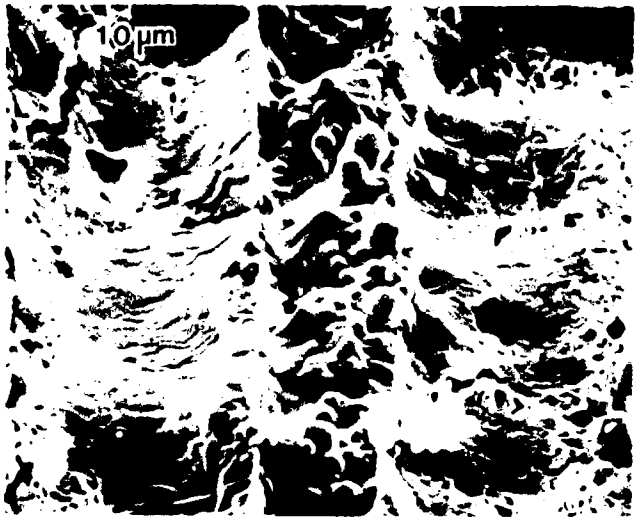

Fig. 26 Examples of quenched sandwich similar to Fig. 25b, but with fuel lamina 1/1, PBAN/H-15 Al, 4.1 MPa.

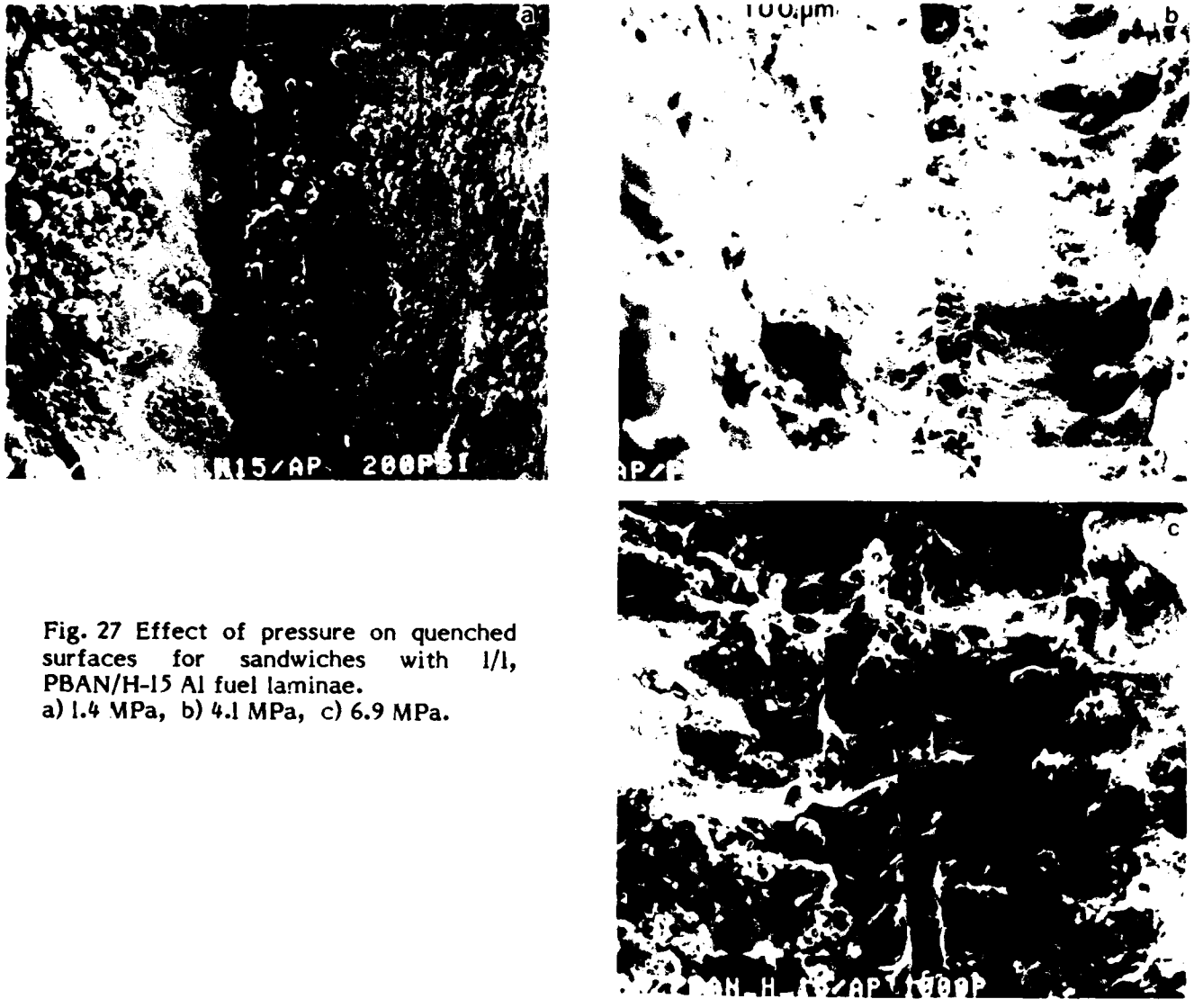

Fig. 27 Effect of pressure on quenched surfaces for sandwiches with 1/1, PBAN/H-15 Al fuel laminae.
a) 1.4 MPa, b) 4.1 MPa, c) 6.9 MPa.

b) Effects of Aluminum Variations

Changes in aluminum (with PBAN binder) had only moderate effect on quenched samples. Use of pre-stretched H-15 in place of as received H-15 (1/1, Binder/Al) produced no effect (although a substantial change was evident in the combustion photography tests described later).

Reducing the aluminum loading to 3/7, Al/Binder resulted in a somewhat lower aluminum concentration on the binder surface, and gave a somewhat smaller enhancement over the non-aluminized burning rate at pressures > 3.5 MPa (as compared to 1/1 Binder/Al).

Use of finer aluminum particles (H-5) in place of H-15 increased the level of accumulation at all pressures.

c) Effect of Binder

Changes in binder resulted in unexpectedly large effects on aluminized sandwiches. At low pressure these differences from PBAN sandwiches were not conspicuous, except for a drier, denser looking aluminum accumulation with polysulfide binder. Above 3.5 MPa, the effect of binder was more conspicuous, as shown in Fig. 28. In particular, the sandwiches with HTPB binder had aluminum accumulation that appeared to be flooded with binder melt. The HTPB/Al lamina and immediately adjoining AP protruded conspicuously at 6.9 MPa. The protrusion was significantly larger than observed in the tests with PBAN/Al fuel laminae or binder laminae alone.

d) Effect of AP in Binder

Introduction of 10 μm AP into a pure PBAN lamina in a 1 to 1 ratio (replacement of Al by AP) resulted in a binder surface that still looked wet, but irregular on a scale comparable to the oxidizer particle dimensions. No distinguishable AP particle surfaces were evident. The binder laminae were recessed slightly at all pressures (Fig. 29), as in the case of aluminized PBAN laminae, and pure PBAN binder at lower pressures. The very localized protrusion of AP immediately adjoining the fuel laminae (Fig. 25-28) is absent with the PBAN/AP lamina (Fig. 29). Instead, at a high pressure there is a wider plateau-like region of protruding AP unique to these samples (Fig. 29 b, c) and the AP/Al/Binder samples noted in the next section. The extent of protrusion of this region was more than with pure binder laminae for PBAN binder, less for HTPB

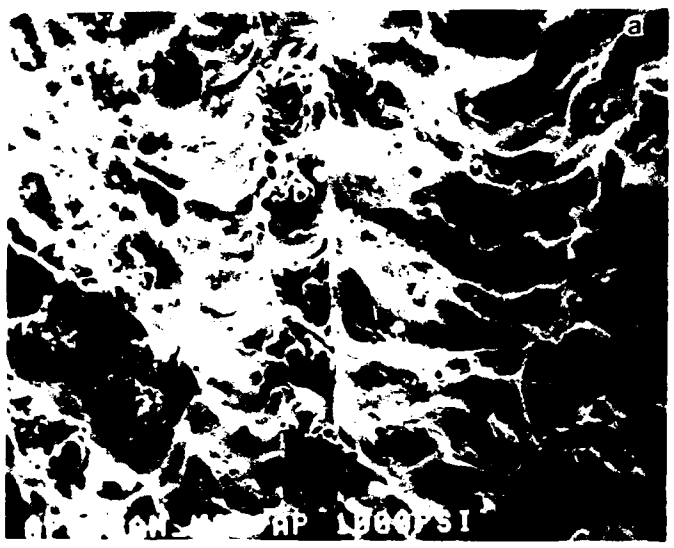

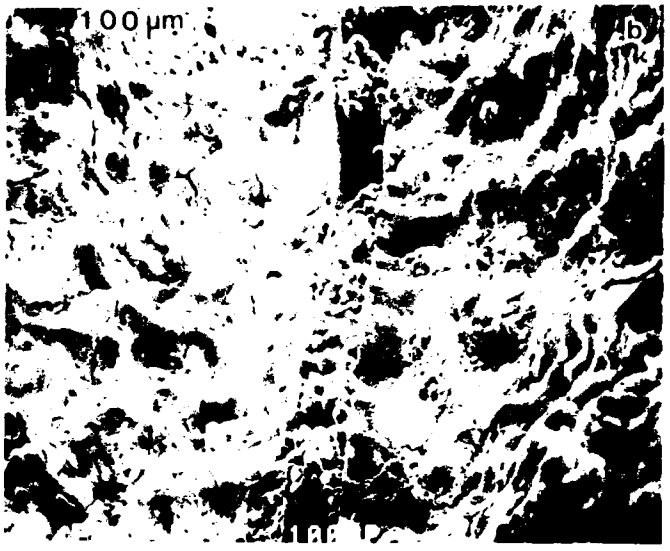

Fig. 28 Effect of type of binder on quenched aluminized sandwiches at 6.9 MPa (1/1, Binder/H-15 Al).
a) PBAN, b) PS, c) HTPB. Compare with Fig. 25c.

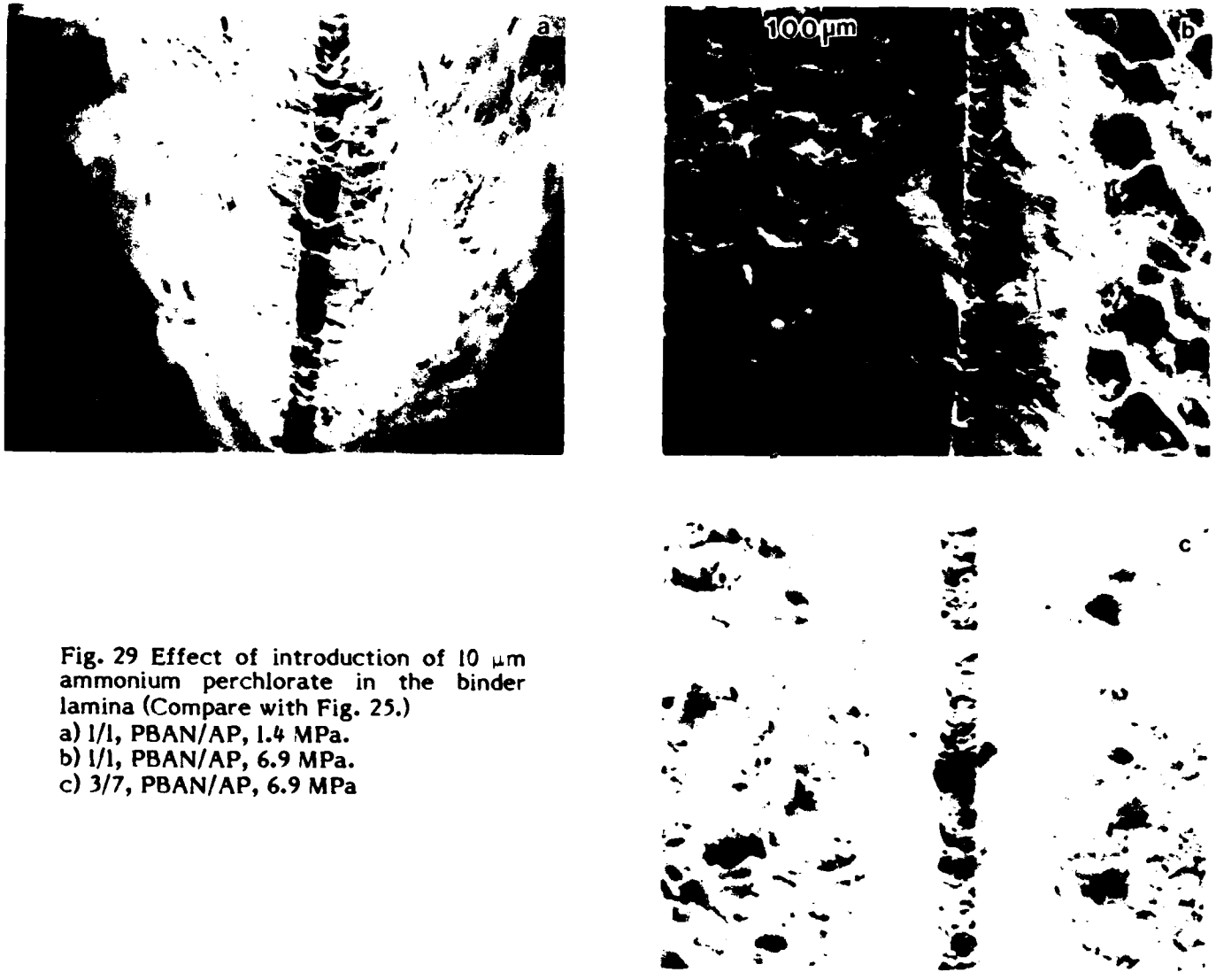

Fig. 29 Effect of introduction of 10 μm ammonium perchlorate in the binder lamina (Compare with Fig. 25.)
a) 1/1, PBAN/AP, 1.4 MPa.
b) 1/1, PBAN/AP, 6.9 MPa.
c) 3/7, PBAN/AP, 6.9 MPa

binder (Fig. 30). The test with a 7/3, AP/PBAN sandwich at high pressure exhibited less overall protrusion of the interfacial regions, and the interface was no longer the most protruding point in the interface region of the profile (Fig. 29c, not shown in Fig. 30).

e) Effect of Al and AP on the Binder

When a 1/1/1; Binder/AP/Al filled lamina was used, the lamina surface had less accumulated aluminum compared to the one with no fine AP at all pressures. The aluminum still had a wet appearance with both binders. But at 6.9 MPa with HTPB binder, the singular protruding feature of the lamina region with only aluminum (Fig. 28c) was absent when fine AP was added too. In general, the Binder/AP/Al sandwiches gave surface profiles closely resembling those obtained with sandwiches having 1/1 Binder/fine AP filled lamina.

Combustion Photography

The test conditions for which combustion photography was used are denoted by the symbol "M" in Fig. 24. From these few tests it was evident that aluminum left the surface primarily as ignited particles and agglomerates (6.9 MPa). Agglomerates were larger, and fewer original particles were present with HTPB binder than with PBAN binder. Addition of fine AP resulted in a reduction of agglomerate size, but did not seem to change the amount of unagglomerated aluminum leaving the surface. There was an appearance of distinguishable diffusion flame sheets or flamelet arrays extending from each AP/Binder interface. It is judged that these are smoke (carbon) trails from the true flames. Aluminum ignition tends to occur in these (presumably hot) regions, in the manner noted by previous investigators (Ref. 18). However, this was not completely systematic in these thin binder sandwiches. Some agglomerates appeared to form up and ignite while straddling the fuel lamina. Such agglomerates are probably of a size comparable to the lamina width. In the case of the HTPB/Al sandwiches at 6.9 MPa, the protruding lamina was easily visible and the top edge appeared to sway locally from one side to the other. In this situation, most of the aluminum emerged burning from one side or the other, not from the tip of the lamina.

In general, the photographic tests were too limited to make generalizations except for the following points:

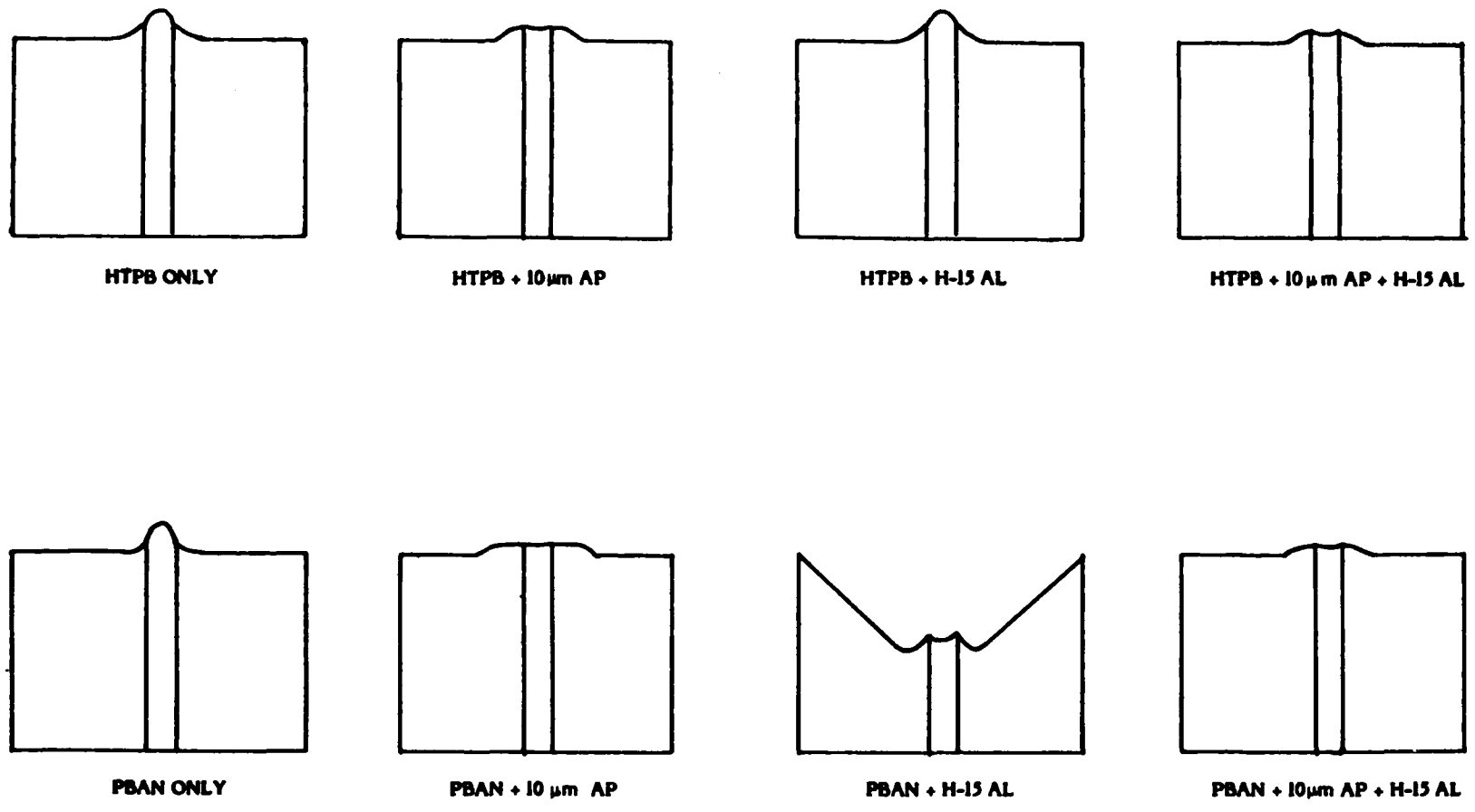

Fig. 30 Sandwich surface profiles for two binders and different combinations of AP and/or Al in the binder laminae.

a) There was extensive agglomerate formation at the sandwich surface. No unignited material was evident leaving the surface.

b) Agglomerates were smaller with PBAN binder than with HTPB binder.

c) Replacement of a 1/1, PBAN/Al lamina by a 1/1/1 PBAN/Al/AP lamina resulted in smaller agglomerates.

d) Separate AP/Binder flame sheets were evident for the two AP-fuel interface planes of the sandwiches, manifested by fluctuating smoke sheets.

e) Ignition of aluminum was favored in proximity of the AP/Binder flame, but with thin sandwiches the agglomerates were of comparable size to the fuel laminae and sometimes ignited and detached from a symmetrical position relative to the fuel lamina.

f) The test in which "pre-stretched" aluminum was used in place of as-received aluminum (H-15) exhibited substantial reduction in size of agglomerates.

Discussion of Sandwich Tests

The original objective of the aluminized binder sandwich tests was to provide a more controlled experiment for observation of aluminum accumulation, sintering, agglomeration and ignition. In particular, it was desired to examine the condition of the aluminum on the burning surface of thin binder lamina, a critical aspect of the behavior that had received only limited attention in a previous study (Ref. 18). Relative to this behavior, the principal result was the notable difference in appearance of the accumulated aluminum with different binders. HTPB binder resulted in a binder-flooded appearance; PBAN binder resulted in obvious aluminum accumulation, with appearance of wetting of particle surfaces and bridging between particles by binder melt; PS binder resulted in a dry-looking accumulation of aluminum. These results, observed on quenched samples, did not provide clues to subsequent development of agglomerates, except in the context of photographic observations of burning. The motion pictures showed that the size of agglomerates was greater with the "flooded look" of the HTPB sandwiches. Since HTPB appears to be the more thermally stable of the binders tested (Ref. 8, 28), this suggests that the binder melt plays an important role in protecting the aluminum from ignition while it is concentrated and heated on the burning surface. The fact that use of sintering-resistant pre-stretched aluminum reduces agglomeration suggests that concentration and heat-up of the aluminum do not assure agglomeration, i.e., that a

final particle-to-particle sintering step is necessary for agglomeration. Likewise, the reduction of agglomeration by addition of fine AP to the aluminized binder lamina suggests that improvement of ignition conditions can block agglomeration. These speculations are consistent with propellant experience; additional combustion photography tests are needed to fully interpret the quenched surface observations.

The original plan for the sandwich tests covered only the study of aluminized binder lamina samples. However, the conspicuous effect of binder type on both surface profiles and aluminum wetting led to a series of tests on nonaluminized sandwiches, to determine to what extent the presence of aluminum was involved. The tests with fine AP additions were then conducted because of observations of the effect of fine AP in propellant testing (Ref. 11, 20 29). Interpretation of the results of these further tests cannot be made yet, but the key results regarding surface profiles of the whole series of sandwich tests merit recapitulation.

1. Surface profiles with and without aluminum were similar with PBAN binder, except that the mildly protruding binder at higher pressure was changed to a mildly recessed profile when aluminum was added. A corresponding increase in sample burning rate resulted, accompanied by a corresponding "V" shaped overall sample profile.

2. With HTPB binder the effect of addition of aluminum had the opposite effect at high pressure. The extent of protrusion of the fuel lamina and adjoining AP was conspicuously increased (compared to nonaluminized HTPB sandwiches). The enhancement of sample burning rate observed with PBAN binder was absent with HTPB binder.

3. Addition of fine AP to PBAN binder laminae resulted in mildly recessed binder laminae at all pressures, as with the addition of aluminum. The corresponding increase in burning rate at higher pressure did not occur. Instead, the usually narrow region of protruding AP adjoining the lamina interfaces was widened. Similar effects were observed with HTPB binder.

4. Addition of both fine AP and aluminum to the binder laminae produced profiles similar to those with only AP added. The primary difference from sandwiches with aluminized binder was the widened region of AP protrusion at 6.9 MPa, and reduction of the unique height of protrusion of the lamina region with HTPB binder.

MODIFICATION OF ALUMINUM TO CONTROL AGGLOMERATION

Background

In view of the obvious importance of the role of the oxide skin on aluminum particles in controlling the onset of sintering, agglomeration and ignition of aluminum, it is reasonable to seek beneficial modification of the oxide. A method explored by Kraeutle (Ref. 30) was to enhance the oxide by further oxidation, by holding powders at elevated temperature in oxidizing atmospheres. This modification method was called "pre-oxidation", and was conducted at temperatures below the aluminum melting point.

A method explored earlier in the present project (Ref. 19, 31) was called "pre-stretching" the oxide, by heating particles through the aluminum melting point. The oxide skin deforms to accomodate the relatively greater thermal expansion and phase change expansion of the aluminum. The oxide deformation is presumably by both inelastic stretching and cracking. In the presence of a low concentration of oxygen, the cracked areas will close rapidly by further oxidation. Upon cooling, the particles shrink, the oxide skin wrinkles or exhibits depressions (Ref. 31), but the oxide surface area is believed to remain sufficient to enclose the aluminum when the particle later melts in the combustion zone. This argument was developed from growing understanding of ignition behavior of aluminum powder, and was evaluated earlier in the project using the hot stage microscope to produce and test the pre-stretched oxide particles (Ref. 31). In those tests the tendency of aluminum powders to sinter and agglomerate when heated was sharply reduced by pre-stretching the oxide.

In subsequent combustion studies on this program, modified aluminum has been carried as one of the test variables, thus giving a systematic demonstration of the potential of modificiation of the oxide skin as a means of controlling agglomeration. For those combustion studies aluminum with pre-stretched oxide was produced in greater quantity by heating the powder in a half open quartz tube to 700°C, using a tube furnace flushed with a nitrogen flow (with some entrained air). The "pre-stretched" aluminum was subsequently sieved to eliminate any large agglomerates or sintered accumulates formed during the "pre-stretching" process. Since the smallest sieve mesh is 37 μ, it is probable that some small accumulates were included, but the mean particle diameter was not significantly altered.

The "pre-stretched" aluminum was compared with as received, and pre-

oxidized aluminum in a series of "propellant" formulations. The formulations included dry pressed AP/Al, and AP/Al/Wax samples. Sandwiches were also prepared consisting of an aluminum filled PBAN lamina between AP slabs. The results of some of these tests have been reported in interim reports (Ref 27, 31), but will be repeated here for completeness.

Combustion of AP/Al Samples

Samples were prepared from mixturs of AP and Al powders by dry pressing mixtures of 85%, 100 μm AP and 15% Alcoa 123 Al to pressure of 170 MPa for 20 minutes. Similar samples were made with pre-stretched Alcoa 123 Al, and samples with pre-oxidized Alcoa 123 Al (provided by Karl Kraeutle of Naval Weapons Center). Tests were run at 6.9 MPa (1000 psi), and observations were made by combustion photography.

Tests on the samples with untreated aluminum exhibited massive accumulation and sintering of aluminum on the burning surface, with ignition occurring only during break-up of detaching accumulate layers. Very large agglomerates formed. Results with the pre-oxidized and with the pre-stretched aluminum were alike. In the tests with pre-stretched aluminum, only small accumulates were evident, with more or less continual detachment of small fragments. Aluminum ignition was only occasional. This result supports the mechanistic argument that led to "pre-stretching" experiments (Ref. 19, 31), and suggests a means of controlling accumulate size, using a modification of aluminum powder that is economically viable in production, possibly by simply changing process control variables in the original powder manufacture. The observation of only limited ignition of the pre-stretched aluminum supports the earlier argument that conditions in the AP flame are not conducive to ignition of aluminum unless some mechanical breakage of the hot sintered accumulate exposes aluminum, and thus provides the opportunity for localized exothermic reaction.

Combustion of AP/Al-Binder/AP Sandwiches

Sandwiches were prepared using the usual method (Ref. 26, 27) of laminating a thin layer of binder between two AP slabs. In this case the binder was a 1/1 mixture of PBAN and Valley Met H-15 aluminum. Samples were prepared using as received and pre-stretched H-15, and combustion tests were run at a pressure of 6.9 MPa (1000 psi) and observed by high speed cinephotography. The sandwiches

prepared with as-received H-15 burned with large slow moving agglomerates, and the ignition and detachment of agglomerates was noticably intermittent, almost periodic. The sample with pre-stretched aluminum burned with small agglomerates and single ignited particles that left the surface in a more or less continuous manner. In this test the pre-stretched aluminum was shown to substantially reduce agglomeration thus improving the combustion behavior of the aluminum. In contrast to the tests on dry-pressed AP/Al samples, use of pre-stretched aluminum in sandwich tests led to improved aluminum ignition, presumably because ignition is induced by the hot AP-Binder flame instead of by aluminum exposure during accumulate break-up.

Combustion of AP/Al/Wax Samples

A set of propellant samples were prepared by dry pressing 30% Valley Met H-30 aluminum, 7% carnauba wax, and 63% 100 μ AP. One sample was prepared using as received H-30, a second sample used pre-stretched H-30, and a third sample used "pre-oxidized" H-30. A fourth sample was prepared in a manner that illustrated the differences in aluminum behavior more graphically in a single motion picture, by using as-received and pre-stretched aluminum in different parts of the same sample. As in the AP/Al tests, dry pressed samples are prepared by mixing the ingredients, pouring the ingredients into a die and pressing the mixture in a hydrauiic press to obtain a compact disc of propellant. The fourth sample was prepared by using a piece of card stock to divide the die into two halves. One half of the die was loaded with the mixture containing as received aluminum while the other half contained the mixture with pre-stretched H-30. The mixture was carefully tamped down and the card separator was carefully removed. The sample was then hydraulically pressed to obtain a disc of propellant. After careful cutting, a 10 mm x 6 mm x 1.6 mm sample was obtained, one half containing as-received H-30 and one half with pre-stretched H-30. Motion pictures of these "half and half" propellants are comparable to split frame motion pictures, i.e., a direct comparison of the combustion behavior of the aluminum is possible.

Motion pictures were filmed for each of the samples burning at 6.9 MPa (1000 psi). The sample with as received H-30 exhibited relatively unfavorable Al combustion characteristics. The surface was covered with large filigrees, aluminum ignition was sporadic, and moderately large to large agglomerates were formed. Significant improvement was seen with the samples with pre-stretched

and pre-oxidized H-30. The surface was rough but fewer filigrees were evident. The aluminum left the surface (ignited) in small agglomerates or single particles. Viewing the "half and half" sample was quite convincing. In any single frame, the region above the half of the sample with as-received aluminum was dark with two or three large burning agglomerates. The region over the other half of the sample surface (pre-stretched aluminum) was nearly a continuous white field of burning particles (Fig. 31).

Combustion of the samples prepared with "pre-oxidized" H-30 was indistinguishable from the "pre-stretched". Both modifications of the aluminum resulted also in higher sample burning rates.

Summary of Aluminum Modification Tests

Combustion photography was used to compare aluminum behavior in tests on three kinds of samples:

Dry-pressed mixtures of AP and Al powders.

Dry-pressed mixtures of AP, Al, and Carnauba wax powders.

Sandwiches with aluminum in the binder lamina.

Both pre-oxidation and pre-stretching treatments of aluminum particles resulted in reduction of accumulation of aluminum on the burning surface, and major reduction of the size of aggregates leaving the surface. In those tests where an AP-hydrocarbon flame was present, the changes resulting from use of modified aluminum led to more prompt ignition of accumulating aluminum and to correspondingly smaller agglomerates. In the tests on AP/Al samples (no hydrocarbon fuel), aluminum ignition was not improved, apparently because conditions in the combustion zone of the AP are not conducive to ignition of the aluminum. In general, the results are consistent with those obtained earlier by Boggs, et al (Ref. 32), with pre-oxidized aluminum, although detailed comparison cannot be made of the two aluminum modifications because of differences in other test sample variables.

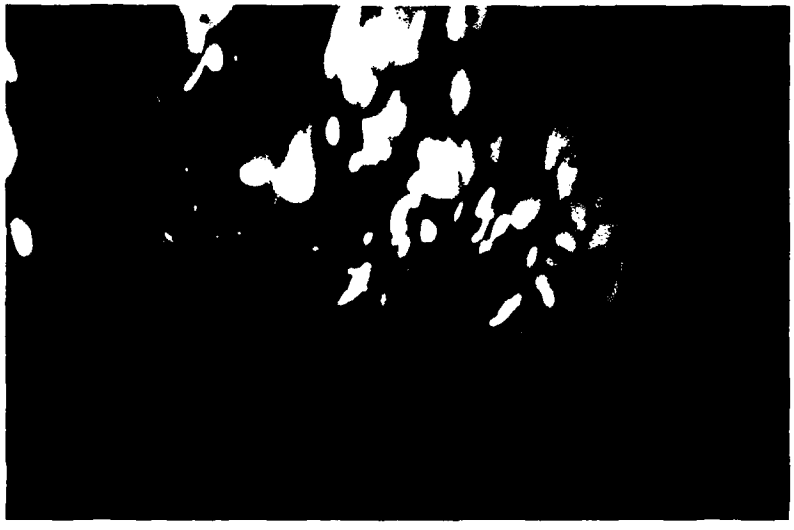

Fig. 31 Comparison of aluminum combustion with dry pressed AP/Al/Wax samples: pre-stretched on the right and as-received aluminum on the left.

STUDIES OF A FAMILY OF PROPELLANTS PREPARED AT THIOKOL-ELKTON

Background

Variation of composition and ingredient particle sizes is probably the most critical factor available in conduct of propellant combustion research. The high cost of preparation of propellant mixes, unfortunately, tends to limit the systematic use of this critical variable as an investigative tool in research and often forces the use of samples prepared by improvised means of unevaluated relevance (e.g., use of samples prepared by dry pressing powder mixes). During the present study, a family of samples became available, which has a systematic variation of composition, prepared by state-of-the-art method (Ref. 33). These same formulations were studied by the suppliers (Ref. 11, 33) using a variety of combustion experiments. In the present program this series of propellants was studied by combustion photography, and by scanning electron microscope analysis of sample surfaces quenched by rapid depressurization. The objectives were three-fold: first, it was desired to establish a basis of comparison of test results on conventional propellants with work on the present program using samples prepared by various improvised methods; second, it was desired to take advantage of the available range of systematic variations of formulations; and third, it was desired to provide an independent set of test results that could be compared with those of the propellant supplier (for reproducibility or possible mutual improvement of experimental methods). In the following, information regarding the propellants, tests, results, and interpretation is summarized.

Propellant Formulations

The range of test variables covered in this investigation is given in Table 2. The actual composition of the propellants can be obtained from Ref. 11 and 33; they are high solids HTPB propellants with variations on a baseline propellant having 18% aluminum and a trimodal AP blend. One or two variables were changed at a time to study the effect of these variations on the combustion behavior of the propellant. All the propellants studied are low burning rate composite propellants. The sample designated 1780-1 was used here as a baseline formulation. Not all the formulations in the supplier's original program were available, and not all those supplied were tested in the present investigation. Choices were based in part on anticipated results, and in part on supplier's test results.

Table 2

Range of Major Propellant Variables Investigated

HTPB BINDER	
LEVEL:	9 to 14%
ALUMINUM	
LEVEL:	18 to 22.4 %
SIZE:	7.5 to 84 μm
AMMONIUM PERCHLORATE	
LEVEL:	55 to 71%
SIZE:	6 to 400 μm
MODALITY:	
Bimodal:	400/fine
Trimodal:	400/200/fine
HMX	
LEVEL:	0 to 15%
SIZE:	6 and 9 μm
ALTERNATIVE:	RDX

Experimental Procedures

Combustion Photography: The experimental set up and the procedure are similar to those described in Ref. 34. The sample dimensions were 10 mm x 6 mm x 1.6 mm. Ektachrome 7241 high speed color film was used for motion pictures. The film framing rates and the aperture f-stop setting varied with test pressure, and are given in Table 3. The samples were externally illuminated by a Xenon lamp under all test conditions. Test conditions are tabulated in Table 4.

Quench Procedure: Quenching was accomplished by rapid depressurization of the combustion vessel by diaphragm rupture. The experimental set up and technique are described in Ref. 35. The sample dimensions were maintained the same as in combustion photography for ease of comparison of results. The quenched samples were then prepared for study under a scanning electron microscope. Quench test conditions are tabulated in Table 5.

Results

Combustion Photography: Combustion photography provides details regarding the combustion efficiency, nature of accumulates on the burning surface, size of agglomerates leaving the surface, burning rate, etc.. The combustion photographs were initially compiled into edited motion pictures for three different pressures and then spliced together into one picture for easy comparison of combustion of different samples. The results of combustion photography allow a comparison of combustion behavior as a function of size of aluminum, % binder, size of AP particles, addition of HMX, usage of DDI curative in propellant and pressure. The pictures were examined for:

(a) Degree of accumulation of aluminum on the surface.

(b) Duration of retention of accumulated aluminum on the surface.

(c) Qualitative estimate of the size range of agglomerates leaving the burning surface.

(d) Ignition characteristics of agglomerates.

(e) Burning rate of sample.

(f) Brightness of field of view which in turn is a measure of the vigorousness of combustion.

(g) Qualitative estimate of unignited aluminum leaving the burning surface.

Behavior in each test was ranked in Table 6, and can be interpreted by comparison with behavior of the baseline propellant No. 1780-1 as described below, in terms of

Table 3

High Speed Camera Settings for Combustion Photography

Pressure MPa (psi)	Film Speed f/sec	F-Stop
1.4 (200)	3000	5.6
3.45 (500)	3400	8.0
6.9 (1000)	4000	11.0

Table 4

Test Conditions for Combustion Photography

PRESSURE / FORMULATION	1.4 MPa (200 psi)	2.62 MPa (350 psi)	3.45 MPa (500 psi)	6.9 MPa (1000 psi)
BASELINE	X	X	X	X
AL EFFECT (SIZE)				
Fine Al	X		X	X
Coarse Al	X		X	X
BINDER EFFECT				
High Binder	X		X	
DDI	X		X	
Catalyst Fe_2O_3			X	
AP SIDE EFFECTS				
400/200/71	X		X	
400/71			X	
400/41			X	
HMX	X		X	X

Table 5

Conditions for Quench Tests of Propellants

1.	6.9 MPa Quenches of all formulations.
2.	Quenches of baseline formulation at progressively lower pressures of 6.9, 5.2, 3.45, 2.42, 1.41, 0.7 MPa.
3.	Quenches of 400/200/71 (no fine AP) at the same series of pressures as in 2.
4.	Quenches of DDI curative propellant at the same series of pressures as in 2.

accumulating insight into the aluminum behavior and the observed results ranked in the table.

At a pressure of 1.4 MPa (200 psi) the combustion of the baseline formulation is as follows. As the burning surface recedes, the ingredient aluminum particles accumulate on the surface due to the concentration of the surface aluminum particles with the underlying particles, and retention on the surface by the surface tension forces of the molten binder, in the absence of favorable ignition conditions. The accumulation is moderate in the case of the baseline propellant. Past studies (Ref. 6, 32, 36, 37) indicate that as this accumulation progresses, a sintered filigree of particles forms and as accumulation progresses further, a part of the filigree is eventually exposed to the hot diffusion flame. This results in local breakdown of the sintered oxide skin of the filigree, followed by a spreading inflamation and coalescence into an agglomerate. In the case of the baseline propellant of the present study, most of the accumulated aluminum ignites on the propellant surface and ignition-coalescence is rapid. Some of the burning agglomerates reside on the burning surface for a short time before being swept away by the gas flow. The agglomerates leaving the burning surface range in size from single particles to about 350 μm. The field of view is moderately bright both close to the burning surface and in the far field, with a moderate amount of smoke in the combustion zone. No unignited aluminum is evident leaving the burning surface. To the extent possible in still photographs, the foregoing details are illustrated in Fig.32.

The propellant combustion behavior is not significantly different at 3.45 MPa except that the degree of accumulation is less and hence smaller agglomerates leave the burning surface.

The results of all tests are tabulated in comparative terms in Table 6 a (1.4 MPa tests) and Table 6 b (3.45 MPa). The numbers 1 - 5 used in these tables rank the indicated combustion behavior on a scale of 1-5.

It is observed from the analysis of this combustion photography that the general trend is for a bright combustion field, short residence time, smaller agglomerates, and high burning rate to go together. Conditions which favor this complex of behavior are:

a) Small (i.e., < 15 μm) aluminum particle size: Relatively fine aluminum provides more surface area and finer sintered structure of accumulates, which results in more vigorous inflamation at the moment of accumulate breakdown. However, under adverse ignition conditions, the large surface area can lead to more

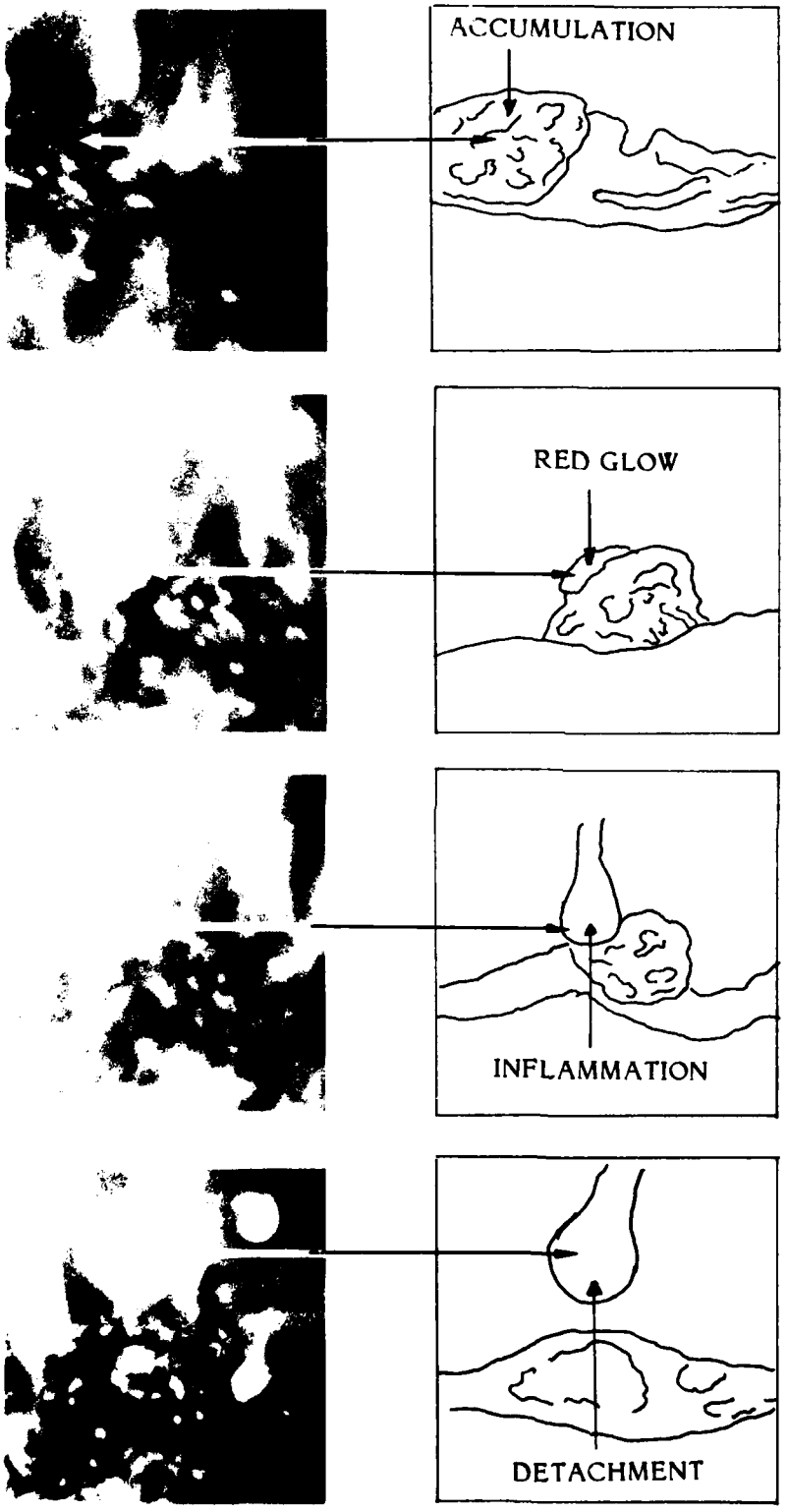

Fig. 32 Combustion field for sample 1780-1 at 1.4 MPa.

Comparative Results of Tests Run at 1.4 MPa

CHARACTERISTICS / FORMULATION	Degree of Accumulation	Retention on Burning Surface	Ignition		Aggl. Size		Brightness		Smoke	Burning Rate	Unburned Aluminum Leaving Surface
			Surface or Gas	Quick or Slow	Range	Avg. Size	Near Field	Far Field			
BASELINE	3	2	S	Q	3	3	2	2	2	—	1
AL EFFECT											
Fine Al	3*	2	S	S & Q Crusts	3	2	3	3	2	Higher	1
Coarse Al	5	3	S & G	S	2	2	1	1	3	Smaller	2
BINDER EFFECT											
High % Binder	4	3	S	S	4	4	1	1	3	Lower	1
DDI Curative	3	2	S	Q	3	2	2	2	2	Lower	1
AP SIDE EFFECT											
400/200/90 μm AP	2	1	S	Q	2	1	1	—	2		1
HMX	3	2	S	Q	3	2	1	1	2	Higher	1

* (Crusting occasionally)

Comparative Results of Tests Run at 3.45 MPa

CHARACTERISTICS / FORMULATION	Degree of Accumulation	Retention on Burning Surface	Ignition		Aggl. Size		Brightness		Smoke	Burning Rate	Unburned Aluminum Leaving Surface
			Surface or Gas	Quick or Slow	Range	Avg. Size	Near Field	Far Field			
BASELINE	3	2	S	Q	3	3	2	2	2	—	1
AL EFFECT											
Fine Al	3*	2	S	Q	3	2	3	3	2	Higher	1
Coarse Al	4	3	S & G	S	2	2	1	1	3	Lower	2
BINDER EFFECT											
High % Binder	4	3	S	S	4	4	1	1	3	Lower	1
DDI Curative	2	2	S	Q	3	2	2	2	2	Lower	1
Fe_2O_3 Catalyst	3	2	S	Q	3	2	3	2	2	Higher	1
AP SIDE EFFECT											
600/200/90 μm	2	1	S	Q	2	2	3	2	2	Higher	1
400/90 μm	2	1	S	Q	1	1	3	—	2	Lower	1
400/50	3	2	S	Q	2	2	2	2	2	Higher	1
HMX	3	2	S	Q	3	3	1	1	2	Higher	1

* (Crusting occasionally)

extensive sintering and larger agglomerates, as observed here with the finest aluminum particle size.

b) Low binder to oxidizer ratio: The "bright burning" complex is apparently favored by the more oxidizer-rich environment and perhaps even more by the less prolonged surface retention and protection from oxidizing species, due to reduced binder presence in the surface accumulates.

c) Close proximity of the oxidizer-binder flame to the accumulating aluminum: Whether due to higher pressure or to propellant microstructure, proximity to these high temperature flamelets appears to precipitate early ignition of aluminum, and hence less accumulation and agglomeration and more vigorous combustion.

SEM Studies of Quenched Burning Surfaces

The general appearance of quenched surfaces is illustrated by the series in Fig. 33 for 1780-1 formulation at 5 pressures. The coarser oxidizer particles are conspicuous at lower pressures, with the intervening areas showing a binder surface that looks like it was a melt prior to quench. The aluminum concentrated in the binder is evident at lower pressure, while the fine oxidizer particles are either not evident, or not distinguishable from aluminum particles. The larger oxidizer particles generally have concave surfaces, especially at high pressure. The profiles of the oxidizer surfaces have a close resemblance to the profiles obtained in aluminized sandwich burning tests. The region adjoining the binder is protruding and has a smooth surface. Further from the interface, the sloping surface flattens out and transitions to a central area that has a frothy surface appearance, sometimes raised (low pressure). Under some conditions (low pressure), collections of aluminum particles were contained in the central froth region (Fig. 34). At pressures higher than 3.45 MPa the surfaces of the oxidizer particles were deeply concave and exhibited no froth or aluminum. In general, the array of accumulated aluminum on the burning surface reflected its original distribution in the propellant microstructure. The fine oxidizer did not manifest its presence. "Pocket" concentrations of aluminum occurred in spite of the presence of the fine AP. These trends were generally true over the whole pressure range, but the aluminum concentration became flooded with binder melt at higher pressure.

The principal effects of propellant variations on samples quenched at 6.9 MPa were the following:

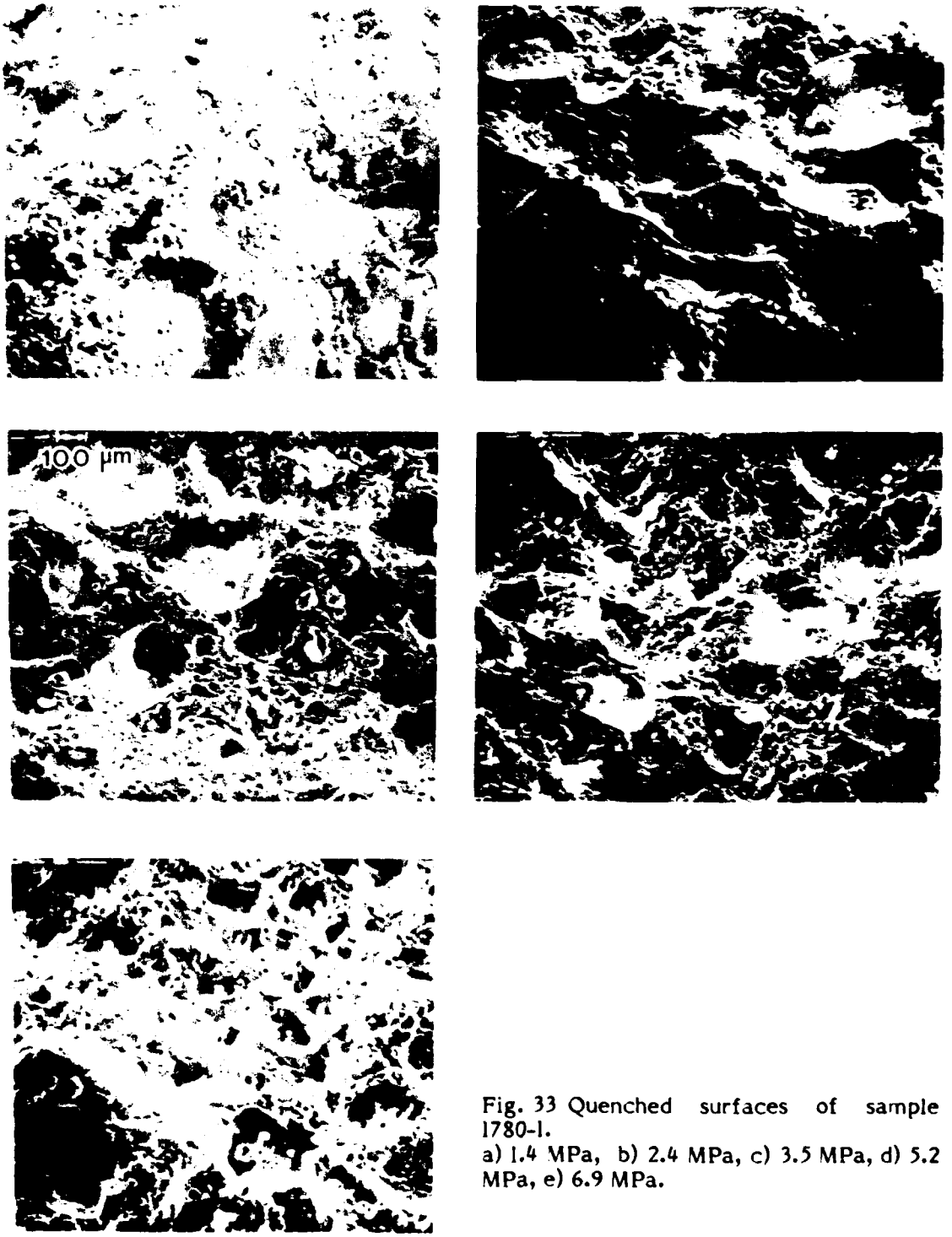

Fig. 33 Quenched surfaces of sample 1780-1.
a) 1.4 MPa, b) 2.4 MPa, c) 3.5 MPa, d) 5.2 MPa, e) 6.9 MPa.

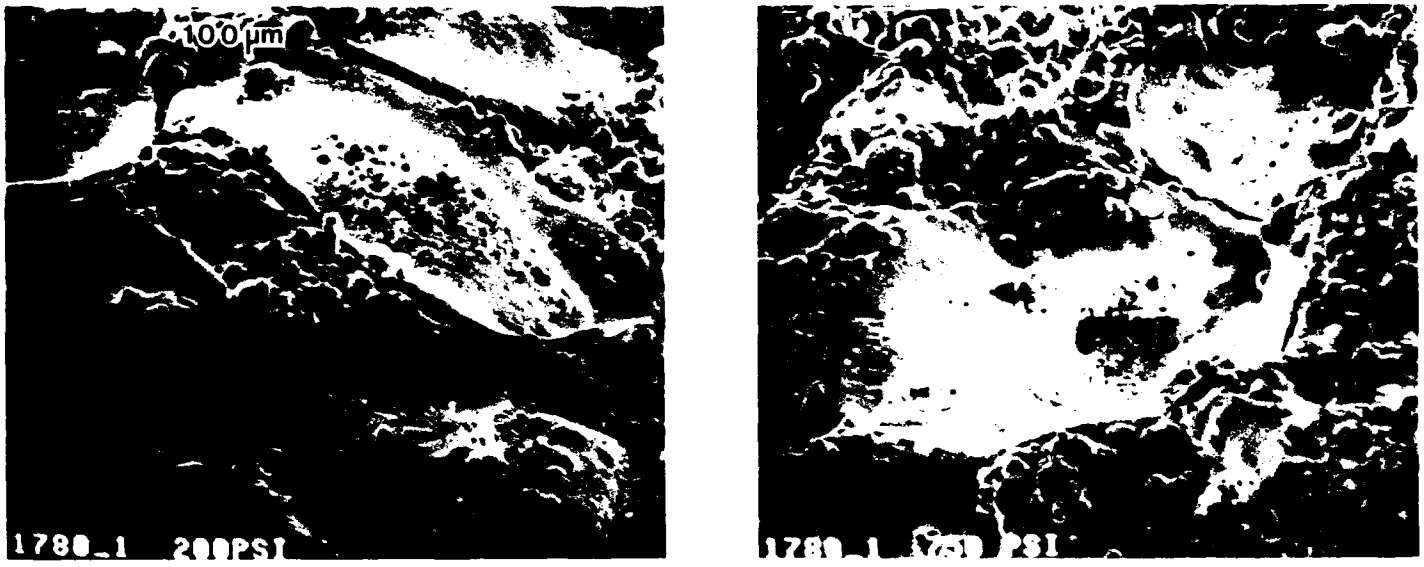

Fig. 34 Aluminum accumulation on the surface of an oxidizer particle, sample 1780-1.
a) Heavy at 1.4 MPa, b) not at 5.2 MPa.

a) Replacement of fine AP by an intermediate size resulted in a surface accumulation of aluminum that was of a filigree nature. This result is a consequence of the fact that pockets in the propellant microstructure were eliminated by being filled with the intermediate size AP particles, leaving the relatively finer aluminum particles in less concentrated clumps. The aluminum looked appreciably less flooded.

b) The sample with fine aluminum showed local areas of formation of aluminum crust, larger than typical pocket accumulations.

c) The samples with a moderate amount of HMX tended to give a more wet looking binder surface, with very small holes in the binder surface.

d) The sample with coarse aluminum showed very little accumulated aluminum on the surface, localized only to individual pockets, containing 4 - 10 particles.

The reader is reminded that the description of the sample surface may reflect changes that took place during quench. It seems likely that the drier aluminum accumulates may detach during quench, and the binder may experience some local flow of the molten surface. The holes in the binder with HMX may be blown during quench, and the froth on the oxidizer surface may be disrupted. These are all believed to be of only moderate importance to surface appearance, except for the possible detachment of accumulates in transition (which limits their observation to the relatively poor resolution obtainable from the combustion photography).

Discussion

The results indicate the relevance of the early comments on propellant microstructure to the formation of surface accumulates and agglomerates. Pocket-forming oxidizer particle blends form agglomerates of pocket size. In this respect, the presence of a moderate amount of fine AP does not prevent pocket size accumulates, but apparently aids ignition of aluminum enough to give somewhat more vigorous inflamation and burning. Using fine aluminum seems to have aided sintering, which in turn led to some very large agglomerates, a behavior that was not prevented by presence of fine oxidizer. The presence of aluminum accumulations in the middle of oxidizer burning surfaces has been observed in previous studies (Ref. 11, 24, 36), and is believed to result from a failure of the pocket accumulation to ignite at the time of transition as the underlying surface passes from binder to an underlying oxidizer particle. This is consistent with

observations reported in earlier sections regarding survival of accumulates on oxidizer surfaces. In general, this type of behavior is more common under the unfavorable ignition conditions at low pressure. Of particular importance is the effect of filling the "pockets" with oxidizer particles large enough to displace the aluminum into thinner "sponge" elements of binder, oxidizer particles large enough to deflagrate on the surface like the larger particles. This leads to a more tenuous filigree of aluminum accumulation, that forms in close proximity with hot oxidizer-binder flamelets. The result is relatively small and vigorously burning agglomerates.

COMBUSTION OF HIGH ALUMINUM CONTENT SOLID PROPELLANTS

Most rocket propellants with aluminum as a fuel ingredient contain 12 - 18% aluminum. Motor performance calculations generally indicate that optimum performance would be obtained at a higher aluminum content, and particularly so in volume-limited applications where high propellant density is also advantageous. In addition, there is some indication that high aluminum content reduces susceptibility to detonation. However, there are problems with high aluminum content that reduce its actual performance, problems that would have to be minimized before increased aluminum would be advantageous. However, the seriousness of these problems (low combustion efficiency and high two-phase flow losses in the nozzle flow) has remained substantially unevaluated, as have the possibilities of reducing the problems by better "design" of combustion. Results and methods of the present research offered the means to achieve improved combustion and control of product oxide droplet size distribution, and an exploratory study was made. This work was reported in Ref. 38 and is summarized here.

Three types of experiments were conducted on propellants containing 5 - 35% aluminum. These consisted of high speed cinemicrophotography; microscopic studies of quenched burning surfaces; and microscopic and chemical analysis of the efflux from the burning surface (quench-collected in ethanol at various distances from the burning surface). In order to permit a large range of propellant formulations, the propellant was simulated by one of two different processes.

1. Dry-pressing powder mixtures in which polymeric binder is replaced by carnauba wax powder.
2. Hand mixing small samples of conventional ingredients, followed by pressing and then curing.

The modifications in formulation that were tested are shown in the test summaries in Fig. 35 to 37. The charts show a central reference formulation and test pressure, and sequences of values of different variables, changed one at a time from the central reference condition. At least one test was run for each condition in the charts.

A motion picture sequence is available summarizing the combustion photography. The effects of test variables on combustion characteristics are

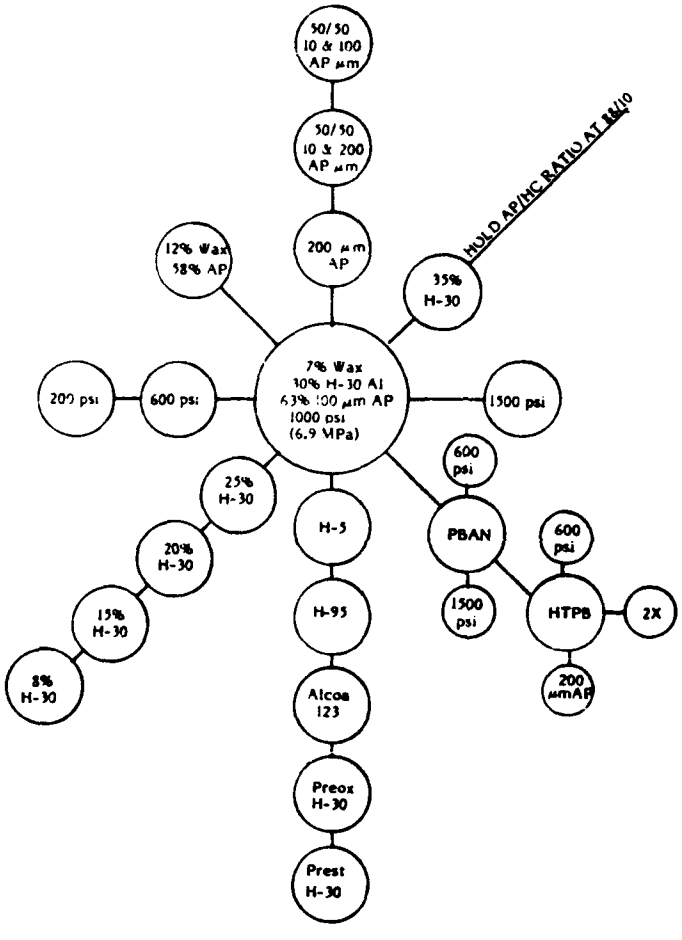

Fig. 35 Test conditions for combustion photography: AP-Wax-Al, "dry pressed" samples. Each small circle indicates one or more tests with indicated modification of test conditions relative to the "reference state" inside the large circle.

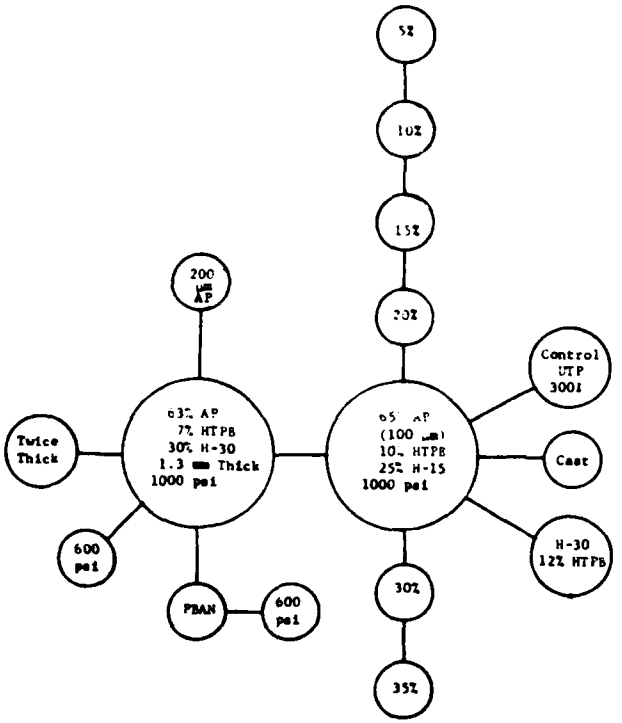

Fig. 36 Test conditions for combustion photography: AP-HTPB-Al, "wet pressed" samples.

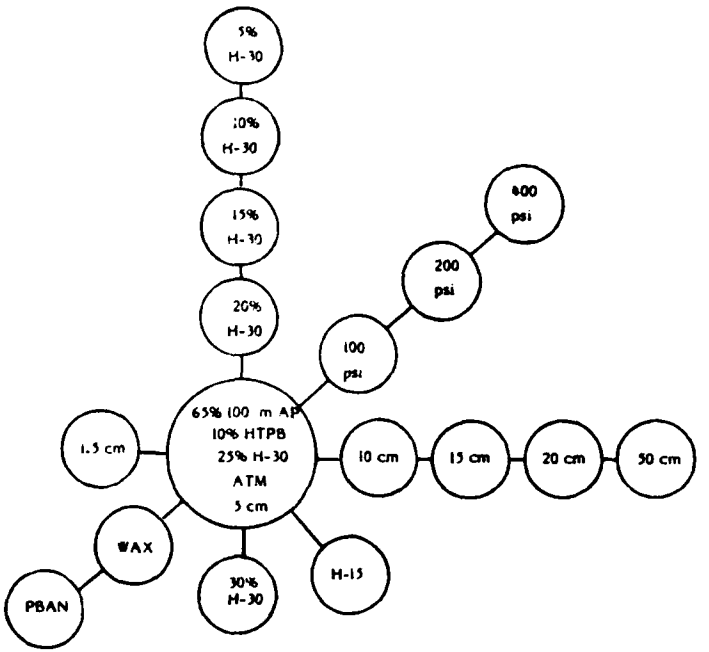

Fig. 37 Test conditions for plume quench samples.

tabulated in Table 7. Fig. 38 shows the effect of aluminum content on the burning surface as revealed by microscopic examination of quenched samples. Fig. 39 shows typical size distribution of aluminum agglomerates from plume quench tests and Fig. 40 shows amounts of unreacted aluminum remaining in plume quench samples for various test conditions (indicative of combustion efficiency). These and other results are presented in more detail in Ref. 38. From the combined results, the following conclusions were drawn regarding high aluminum content propellants.

1. Combustion efficiency of aluminum remains high to 25% aluminum. It is pressure-dependent in the range tested, and would apparently be better at typical rocket motor pressures than in the tests reported here.
2. Burning rate tends to a maximum around 18% aluminum, and the brightness of the combustion field peaks at about the same aluminum content.
3. The size of aluminum agglomerates (and degree of agglomeration) increase with aluminum content, especially above 25% aluminum. Other indicators of slow combustion also follow this trend (burning rate, brightness of field, combustion efficiency at 5 cm).
4. Several measures for improving combustion were found to be effective, including: treatment of aluminum powder to minimize agglomeration; choice of relative size of AP and Al particles so as to isolate groupings of accumulating aluminum particles on the burning surface from each other; choice of propellant and motor conditions conducive to aluminum ignition (particle size control, low binder content, high pressure).
5. An accompanying study (summarized elsewhere in this report and in Ref. 7) shows that the oxide products of burned agglomerates consist of about 85% smoke particles (< 2 μm) and 15% burnout residuals of agglomerates. The size of the latter depends on the size of the parent agglomerate, and increases with % aluminum. The size range is 5 - 80 μm. With a 25% aluminum propellant, the size could probably be kept around 10 -25 μm by appropriate choices of aluminum powder and of ingredient particle size distribution (this is a "projection"). Flow effects may modify the combustion-generated sizes.
6. Combustion behavior appears to be significantly dependent on propellant binder type, content, and/or distribution in the matrix. However,

Table 7
Summary of Effect of Test Variables on Combustion Behavior
As Indicated by Combustion Photography

Behavior / Variables	Accumulation on Surface	Accumulate Attachment to Surface	Ignition of Agglomerate	Size of Agglomerate
Effect of Increase in % Aluminum	Increases	Effect not clearly visible from movie; seems to be no effect. Oscillating sintered Al increases.	More agglomerates ignite on surface and remain longer on surface.	Increases
Effect of Increase in Pressure	Decreases but the effect is not significant between 1000 & 1500 psi.	At low pressure stays attached and glows red. Effect vanishes with pressure.	No significant variation. Mostly surface ignition.	Decreases, but not significantly between 1000 & 1500 psi.
Effect of Increase in Aluminum Particle Size	Increases	Stays attached to the surface longer; and with 95 μm particle intensively.	Ignition in the gas phase to surface ignition mostly.	Increases, but with 95 μm particle very little agglomeration.
Effect of Pre-treatment of Al (pre-oxidizing & pre-stretching)	Decreases considerably	Residence time on surface is reduced.	Ignition mostly in gas phase.	Decreases significantly.
Effect of Increase in Oxidizer Particle Size	Increases	Could not be detected very well.	No significant difference except with 200 μm AP Al agglomerates were spewed in all directions.	Increases
Effect of Addition of Fine AP	Decreases	No significant difference, but spewing of Al in 200 μm AP sample was absent.	No noticable difference.	Decreases
Wet Pressed Effect of Binder				
(a) PBAN	Decreases compared to wax.	Not observable.	Mostly surface ignition.	Decreases compared to wax.
(b) HTPB	Sample did not burn to completion (thickness effect) and sample burned almost like PBAN sample when made twice as thick.			
Second Series Effect of % Al Increase in HTPB Series.	Not observable because of bright field of view in all tests.		Ignition mostly after leaving surface in all samples.	Increases gradually.

Table 7 (Continued)
Summary of Effect of Test Variables on Combustion Behavior
As Indicated by Combustion Photography

Behavior Variables	Burning Rate	Brightness Near Burning Surface	Additional Remarks
Effect of Increase in % Aluminum	Peaks between 15 & 20% Al loading.	Peaks at 15 and 20% Al loading.	Amount of unburned Al leaving surface increases.
Effect of Increase in Pressure	Increases gradually.	Increases	Amount of unburned Al decreases, but not very significantly.
Effect of Increase in Aluminum Particle Size	Decreases	Decreases	Amount of unburned particle increases and is considerable with H-95.
Effect of Pre-treatment of Al (pre-oxidizing & pre-stretching)	Increases	Increases. Pre-oxidized gives higher burning rate.	Very little unburned Al leaving surface.
Effect of Increase on Oxidizer Particle Size	Decreases	Decreases	More unburned Al leaving surface.
Effect of Addition of Fine AP	Increases	Increases	Less unburned Al leaving the burning surface.
Wet-Pressed			
Effect of Binder			
(a) PBAN	Increases	Increases considerably.	Less unburned Al leaving surface.
(b) HTPB	Sample did not burn to completion (thickness effect), and sample burned almost like PBAN sample when made twice as thick.		
Second Series			
Effect of % Al Increase in HTPB Series	Peaks between 15 & 20% Al loading.	Peaks about 20% Al loading.	Very little unburned Al leaving the surface.

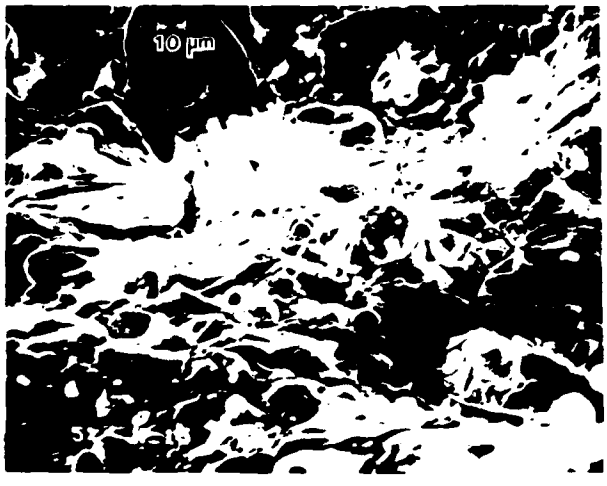

a

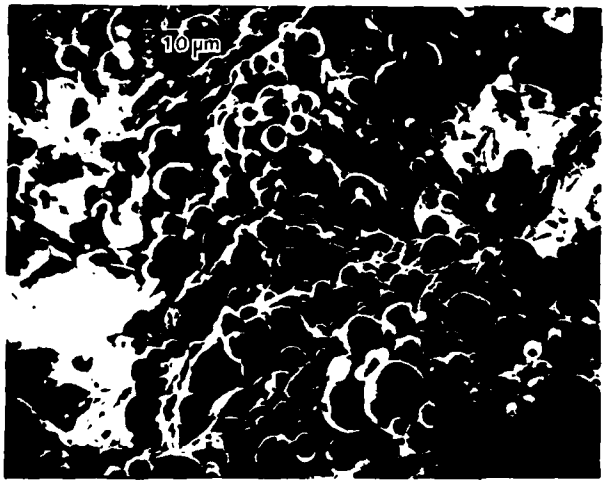

b

Fig. 38 Aluminum accumulation on the burning surface of AP-HTPB-Al sample quenched by rapid depressurization at 6.9 MPa. (a) Low % aluminum (5%). (b) High % aluminum (35%).

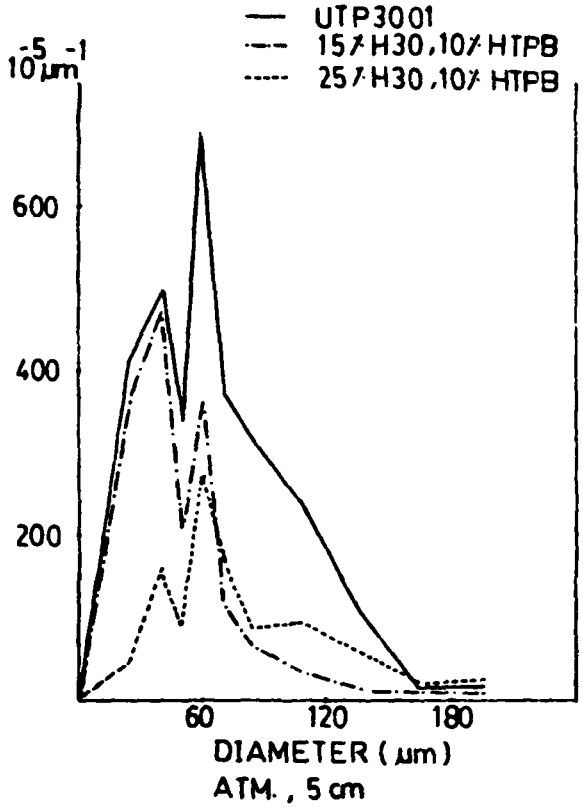

Fig. 39 Size distribution of particles in plume quench samples. Atmospheric pressure tests, quench distance = 5 cm.

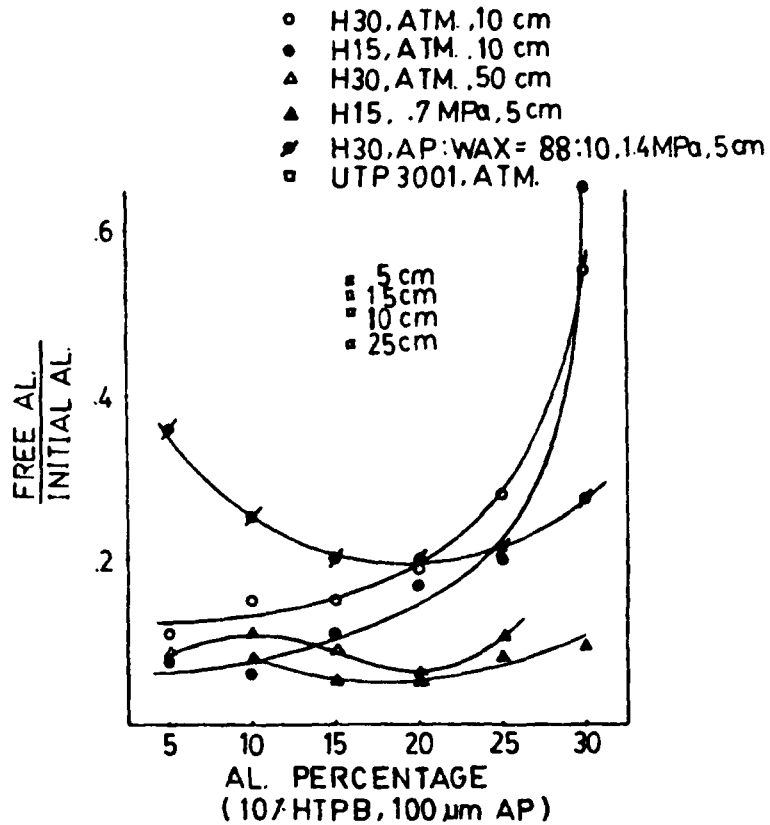

Fig. 40 Mass fraction of unreacted aluminum in plume quench samples (weight difference method of Al determination).

this variable was not adequately evaluated because of the improvised methods for propellant processing available in the study.

In general, the results suggest that combustion efficiency can be held to conventional levels with aluminum contents up to about 25%, provided propellant ingredients are tailored for that purpose. In the process, combustion-generated aluminum oxide size distributions can be kept comparable to present ones. This conclusion needs further support by tests on propellants with conventional binders and processing.

REFERENCES

1. Price, E. W., et al, "Combustion of Solid Propellants and Low Frequency Combustion Instability," NOTS TP 4244, June 1967.
2. Povinelli, L. A., and R. A. Rosenstein, "Alumina Size Distributions from High-Pressure Composite Solid Propellant Combustion," AIAA J., Vol. 2, No. 10 (1964), pp. 1754-1760.
3. Miller, R. R., "Some Factors Affecting the Combustion of Aluminum in Solid Propellants," ICRPG 2nd Combustion Conference, CPIA Publication 105, Vol. I, May 1966, p. 331-335.
4. Cohen, N. S., "A Pocket Model for Aluminum Agglomeration in Composite Propellants," AIAA/SAE/ASME 17th Joint Propulsion Conference, AIAA Paper 81-1585.
5. Price, E. W., "Combustion of Aluminum in Solid Propellant Flames," 53rd Meeting of AGARD Propulsion and Energetics Panel, 1979, AGARD-CP-259, pp. 14-1-14-15.
6. Hubbartt, J. E., E. W. Price, W. C. Strahle and B. T. Zinn, "Rocket Research at Georgia Tech," AFOSR Interim Scientific Report, November 1978.
7. Price, E. W., C. J. Park, R. K. Sigman and J. K. Sambamurthi, "The Nature and Combustion of Agglomerates," 18th JANNAF Combustion Meeting, CPIA Publication 347, October 1981.
8. Price, E. W., and R. K. Sigman, "Behavior of Aluminum in Solid Propellant Combustion," AFOSR-TR-77-0050, November 1976.
9. Caveny, L. H., and A. Gany, "Aluminum Combustion Under Rocket Motor Conditions," 53rd Meeting of the AGARD Propulsion and Energetics Panel, 1979, AGARD-CP-259, pp.13-1-13-13.
10. Price, E. W., "Relevance of Analytical Models for Perturbation of Combustion of Solid Propellants," AIAA J., Vol. 7, No. 1, (1969), pp. 153-154.
11. Brundige, W. N., and L. H. Caveny, "Combustion of Low-Burn-Rate HTPB Propellants in an Acceleration Field - Part III," 18th JANNAF Combustion Meeting, CPIA Publication 347, October 1981.
12. Price, E. W., et al, "The Fire Environment of a Solid Rocket Propellant Burning in Air," AFWL-TR-78-34, March 1979.
13. Price, E. W., E. A. Powell and R. K. Sigman, "Further Studies of the Fire Environment of a Solid Rocket Propellant Burning in Air," AFWL-TR-79-55,

April 1980.

14. Micheli, P. L., and W. G. Schmidt, "Behavior of Aluminum in Solid Rocket Motors, Vol. I" AFRPL-TR-77-29, December 1977.
15. Kraeutle, K. J., and H. H. Bradley, Jr., "Combustion of Aluminized Propellants: The Influence of Pressure and Propellant Combustion on Formation of Aluminum Combustion Residue," 14th JANNAF Combustion Meeting, CPIA Publication 292, Vol. I, December 1977, pp. 209-219.
16. Price, E. W., J. E. Crump, H. C. Christensen and R. Sehgal, "Comments on 'Alumina Size Distributions from High-Pressure Composite Solid-Propellant Combustion'," AIAA J., Vol. 3, No. 9 (1965), pp. 1790-1791.
17. Brzustowski, T. A., and I. Glassman, "Vapor-Phase Diffusion Flames in the Combustion of Magnesium and Aluminum: I. Analytical developments, and II. Experimental observations in oxygen atmospheres," AIAA Progress in Astronautics and Aeronautics: Heterogeneous Combustion, edited by H. G. Wolfhard, I. Glassman, and L. Green, Jr., Academic Press Inc., New York, 1964, Vol. 15, pp. 75-158.
18. Boggs, T. L., D. E. Zurn, W. C. Strahle, J. C. Handley and T. T. Milkie, "Mechanisms of Combustion," NWC-TP-5514, July 1973.
19. Price, E. W., W. C. Strahle, B. T. Zinn, J. E. Hubbartt, D. H. Neale, R. K. Sigman and B. R. Daniel, "Rocket Research at Georgia Tech," AFOSR Interim Scientific Report, November 1979.
20. Schmidt, W., and R. Poynter, "Zirconium/Aluminum Combustion," AFRPL-TR-80-8, March 1980.
21. Mellor, A. M., and I. Glassman, "Augmented Ignition Efficiency for Aluminum," Combust. Sci. Technol., Vol. 1, No. 6 (1970), pp. 437-447. (See also: same title, Princeton University, Dept. of Aerospace Sciences Technical Report No. 791, 1967.)
22. Frolov, Yu. V. P. F. Pokhil, and V. S. Logachev, "Ignition and Combustion of Powdered Aluminum in High-Temperature Gaseous Media and in a Composition of Heterogeneous Condensed Systems," Fizika Goreniya i Vzryva, Vol. 8, No. 2 (1973), pp. 213-236.
23. Glassman, I. "Combustion of Metals: Physical Considerations," ARS Progress in Astronautics and Rocketry, Vol. 1, Solid Propellant Rocket Research, Academic Press, New York, 1960, pp. 253-258.
24. Boggs, T. L., et al, "Combustion of Solid Propellants and Low Frequency

Combustion Instability," Progress Report, 1 October 1967-1 November1968, NWC-TP-4749, June 1969.

25. Prentice, J. L., and K. J. Kraeutle, "Metal Particle Combustion," Progress Report, 1 May 1967-30 September 1968, NWC-TP-4658, January 1969.
26. Price, E. W., J. C. Handley, R. R. Panyam, R. K. Sigman, and A. Ghosh, "Combustion of Ammonium Perchlorate-Polymer Sandwiches," AIAA J., Vol. 19, No. 3, (1981), pp. 380-386.
27. Price, E. W., R. K. Sigman and R. R. Panyam, "Combustion Mechanisms of Solid Propellants," Annual Technical Report 1 August 1979-31 July 1980 for Office of Naval Research, Georgia Institute of Technology, September 1981.
28. Cohen, N. S., R. W. Fleming, and R. L. Derr, "Propellants and Combustion — I, Role of Binder in Solid Propellant Combustion," AIAA/SAE 8th Joint Propulsion Specialist Conference, AIAA Paper 72-1121. (See also: AIAA J., Vol. 12, No. 2 (1974), pp. 212-218.
29. Miller, R. R., M. T. Donohue, R. A. Young, and J. R. Martin, "Control of Solids Distribution in HTPB Propellants," AFRPL-TR-78-14, April 1978.
30. Kraeutle, K. J., "The Behavior of Aluminum During Subignition Heating and Its Dependence on Environmental Conditions and Particle Properties," 9th JANNAF Combustion Meeting, CPIA Publication 231, December 1972, pp. 325-340.
31. Price, E. W., W. C. Strahle, B. T. Zinn, J. E. Hubbartt, R. K. Sigman, and B. R. Daniel, "Rocket Research at Georgia Tech," AFOSR Interim Scientific Report, Georgia Institute of Technology, November 1980.
32. Boggs, T. L., K. J. Kraeutle, and D. E. Zurn, "The Combustion of As-Received and Preoxidized Aluminum in Sandwich and Propellant Configurations," 9th JANNAF Combustion Meeting, CPIA Publication 231, December 1972, pp. 341-345.
33. Brundige, W. N. "Space Motor Combustion Technology, Phase I. Data Base Development," AFRPL-TR-80-52, December 1980.
34. Boggs, T. L., J. E. Crump, K. J. Kraeutle, and D. E. Zurn, "Cinephotomicrography and Scanning Electron Microscope as Used To Study Solid Propellant Combustion at the Naval Weapons Center," NWC-TP-5944, May 1977.
35. Varney, A. M., "An Experimental Investigation of the Burning Mechanisms of Ammonium Perchlorate Composite Solid Propellants," Ph.D. Thesis, Georgia

Institute of Technology, 1970.

36. Price, E. W., K. J. Kraeutle, R. K. Sigman, J. E. Crump,T. L. Boggs, D. E. Zurn, "Behavior of Aluminum in Solid Propellant Combustion, NWC-TP-6120, in press.

37. Crump, J. E. J. L. Prentice, and K. J. Kraeutle, "Role of Scanning Electron Microscope in the Study of Solid Propellant Combustion: II. Behavior of Metal Additives," Combust. Sci. Technol. Vol. 1 (1969), pp. 205-223.

38. Price, E. W., J. K. Sambamurthi, R. K. Sigman and C. J. Park, "Combustion of High Aluminum Content Solid Propellants," 18th JANNAF Combustion Meeting, CPIA Publication 347, October 1981.

C. Publications

1. Price, E. W., R. K. Sigman, and J. C. Handley, "Microstructure of the Combustion Zone," 15th JANNAF Combustion Meeting, CPIA Publication 297, February 1979, Vol. II, pp. 163-177.

2. Hubbartt, J. E., E. W. Price, W. C. Strahle, B. T. Zinn, "Rocket Research at Georgia Tech," AFOSR Interim Scientific Report, November 1978.

3. Price, E. W., W. C. Strahle, B. T. Zinn, J. E. Hubbartt, D. H. Neale, R. K. Sigman, and B. R. Daniel, "Rocket Research at Georgia Tech," AFOSR Interim Scientific Report, November 1979.

4. Price, E. W., W. C. Strahle, B. T. Zinn, J. E. Hubbartt, R. K. Sigman, and B. R. Daniel, "Rocket Research at Georgia Tech," AFOSR Interim Scientific Report, November 1980.

5. Price, E. W., "Combustion of Aluminum in Solid Propellant Flames," 53rd Meeting of the AGARD Propulsion and Energetics Panel, Oslo, Norway, April 1979, AGARD Conference Proceedings No. 259.

6. Price, E. W., "Velocity Coupling in Oscillatory Combustion of Solid Propellants," AIAA Journal, Readers' Forum, Vol. 17, No. 7, July 1979, pp. 799-800.

7. Price, E. W., C. J. Park, R. K. Sigman, and J. K. Sambamurthi, "The Nature and Combustion of Agglomerates," 18th JANNAF Combustion Meeting, CPIA Publication 347, October 1981.

8. Price, E. W., J. K. Sambamurthi, R. K. Sigman and C. J. Park, "Combustion of High Aluminum Content Solid Propellants, 18th JANNAF Combustion Meeting, CPIA Publication 347, October 1981.

9. Price, E. W., "Metalized Propellants," chapter for AIAA book on "Fundamentals of Combustion of Solid Propellants," submitted for publication 1981.

D. Professional Activities

1. Participant, AGARD Symposium on Solid Rocket Motor Technology, Oslo, Norway, April 1979.

2. Organizer-Chairman, JANNAF Workshop on Aluminum Combustion, 1980.

3. Participant, JANNAF Workshop on Aluminum Combustion, 1980.

4. Participant, JANNAF Workshop on Velocity Coupling, 1979.

5. Presentations, JANNAF Combustion Meeting (see Publication list).

6. National Publications Committee, AIAA, 1971-1981.

7. Member, AIAA Pendray Award Committee, 1978-81, Chairman, 1978.

TASK IV

ROCKET MOTOR AEROACOUSTICS

W. C. STRAHLE

TASK IV
ROCKET MOTOR AEROACOUSTICS

A. Research Objectives

The following were the objectives of this Task:

1. To demonstrate that the fluctuating pressure field in a rocket motor may be calculated if the state of the turbulence of the interior flow is known.

2. To turn No. 1 around and attempt to deduce some of the turbulence structure from measurement of the pressure fluctuation field.

B. Progress and Significant Accomplishments

Introduction

Vibration of solid rocket motors occurs on a routine basis with one cause, clearly identifiable, being the fluctuations in chamber pressure. These fluctuations will occur even for stable motors because of the turbulence of the main flow in the motor. It is desirable to keep the vibration levels as low as possible to avoid detrimental interaction with other components of the vehicle system. Moreover, it is desirable that the vibration levels be predictable in order to set rational design criteria for the rest of the system.

There are several potential causes for interior pressure fluctuations, but one which has been incompletely explored is the turbulence of the main flow. Several computational schemes for turbulent flow are currently available to enable a reasonable estimate for the turbulence levels as a function of chamber position, at least with propellant grains of simple geometry. However, the calculation of the pressure field, given the velocity fluctuation levels, has not been

attempted. It was the purpose of this program to enable calculation of the pressure field and to compare the calculations with measurements.

Experiment

Two primary pieces of experimental hardware were used in this program, as shown in Fig. 1. One was a long tube, connected to vaccuum, terminated by a choked nozzle. It operates by sucking a flow into the inlet and, by virtue of its length, contains mostly a fully developed turbulent pipe flow. The second apparatus is a tube, also connected to vaccuum, but constructed of porous walls and closed at the head end. This apparatus sucks in air from the side walls and exhausts through a choked nozzle. Therefore, this system is a rocket motor simulator, which models a center perforated grain configuration. In this configuration the mass flow distribution as a function of axial length was altered by taping discrete lengths of the porous walls.

Four different types of measurements were applied to these configurations. They were

1. Multiple flush mounted microphones
2. Twin hot film anemometers mapping out space-separated correlations of axial velocity fluctuations.
3. Axial traverses of static pressure fluctuations while driving acoustic waves in the cavity with an acoustic driver
4. Radial pitot pressure traverses for both the mean and fluctuating pitot pressure.

The primary measurement was the wall pressure fluctuation since this is a vibration source. The theory outlined below, however, relates this wall pressure fluctuation to the correlation of velocity fluctuations; hence, the hot film measurements were made. The axial pressure traverses under acoustic excitation were made because the side wall and end plane acoustic impedances are required in the theory. Finally, the

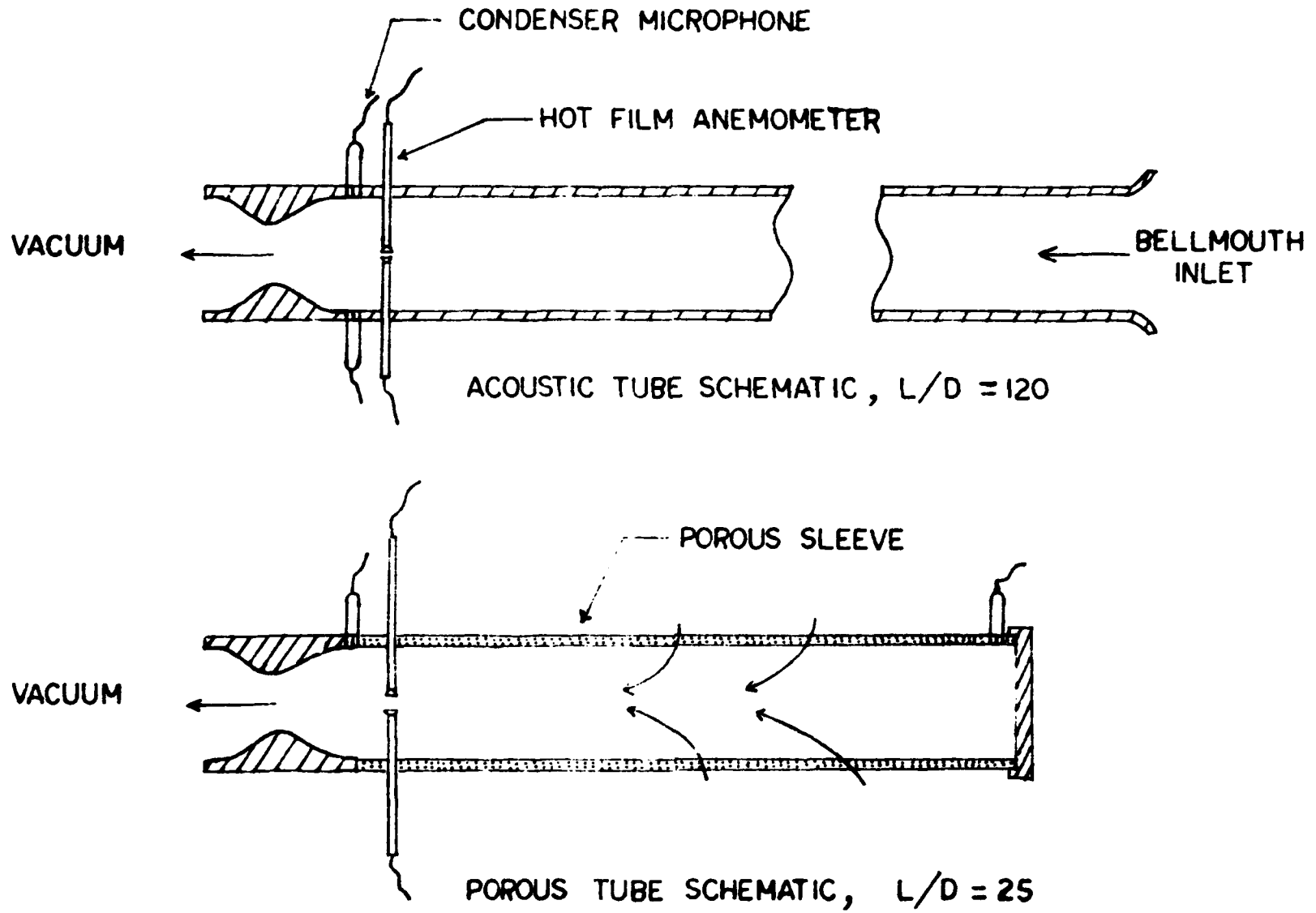

Figure IV-1. Schematic of Experimental Configurations.

pitot pressures were measured for two reasons. First, mean velocity profiles were obtained. Secondly, there was a need to investigate the connection between wall pressure fluctuations and flow-interior pressure fluctuations.

Theory

The theory of aeroacoustics applied to these configurations is documented in Refs. (1) and (2). Briefly, it follows from the Bernoulli enthalpy approach to aeroacoustics which identifies two kinds of pressure fluctuations. First, there is a propagational acoustic motion concentrated at frequencies centered about natural mode frequencies, which is driven by the entire volume of turbulence. Secondly, there is a broadband pressure fluctuation corresponding to the random vorticity field, which is convected at roughly the flow velocity. These two fields are superimposed to produce the overall pressure seen at the wall.

According to the theory, the pressure field should be roughly independent of radial position for both the propagational component and hydrodynamic component of the pressure field. As seen below, future modifications of the theory will be required for the hydrodynamic component because there is some problem with radial variation near the wall that is as yet unaccounted for by the theory.

The theory requires that both axially and radially separated cross-correlation of axial velocity fluctuations be known in order that the pressure field may be computed. Hence, such measurements were made. The theory also showed how to separate the hydrodynamic and propagational components of pressure by separating two microphones in space. This was also accomplished experimentally.

Synopsis of Results

Figure 2 shows three things for the long tube experiment. First there is the pressure spectrum at the half-radius point which is deduced by simultaneous hot film and pitot pressure measurements. Secondly, there is the spectrum of pressure measured at the wall by a flush mounted microphone. Thirdly, there is the cross spectrum of two flush mounted microphones which are space-separated a distance which is large compared with a correlation length scale of the turbulence. This latter measurement produces only the acoustic components of the sound because the broadband component is uncorrelated at the two space-separated positions. The peaks in this cross spectrum are at the natural mode frequencies for longitudinal oscillations in the tube. The wall spectrum is seen to contain the acoustic information plus a broadband component. The large surprise in the program, however, was the discovery of the large disparity between the wall pressure and the interior pressure which is dominated by broadband noise, as seen in Fig. 2. The theory, as presently constructed would say that the two should agree.

Calculation by the theory for the long tube, after the necessary acoustic impedance measurements and turbulence measurements were carried out, show the results of Fig. 3. The theory falls in between the pressure spectra measured at the wall and that measured in the interior. Moreover, the theory predicts that the acoustic motions should be seen in the pressure spectrum. They are seen in the wall spectrum (Fig. 2) but they are not in the interior spectrum. Similar results were obtained for the porous tube experiments.

The fact that the wall spectrum was close to the space-separated cross spectrum means that a) the acoustic motions are being impressed faithfully on the wall, as expected but b) the theory is deficient in the discrimination of wall and interior pressure for the broadband component of pressure. At the conclusion of the program the reason for this discrepancy had not been discovered. It is believed that the neglect of

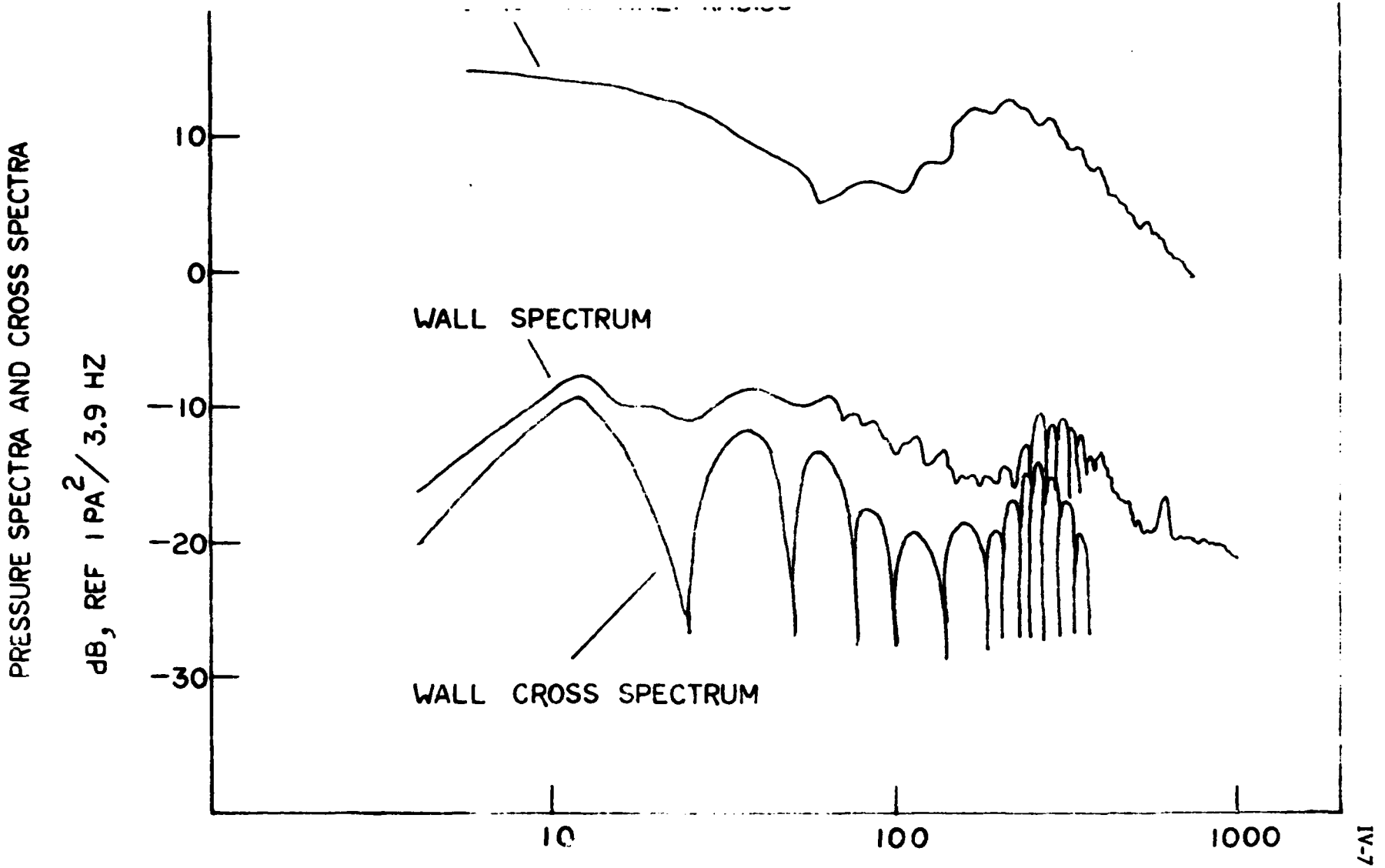

Figure IV-2. Various auto spectra and cross-spectra of pressure measurements for the long tube apparatus.

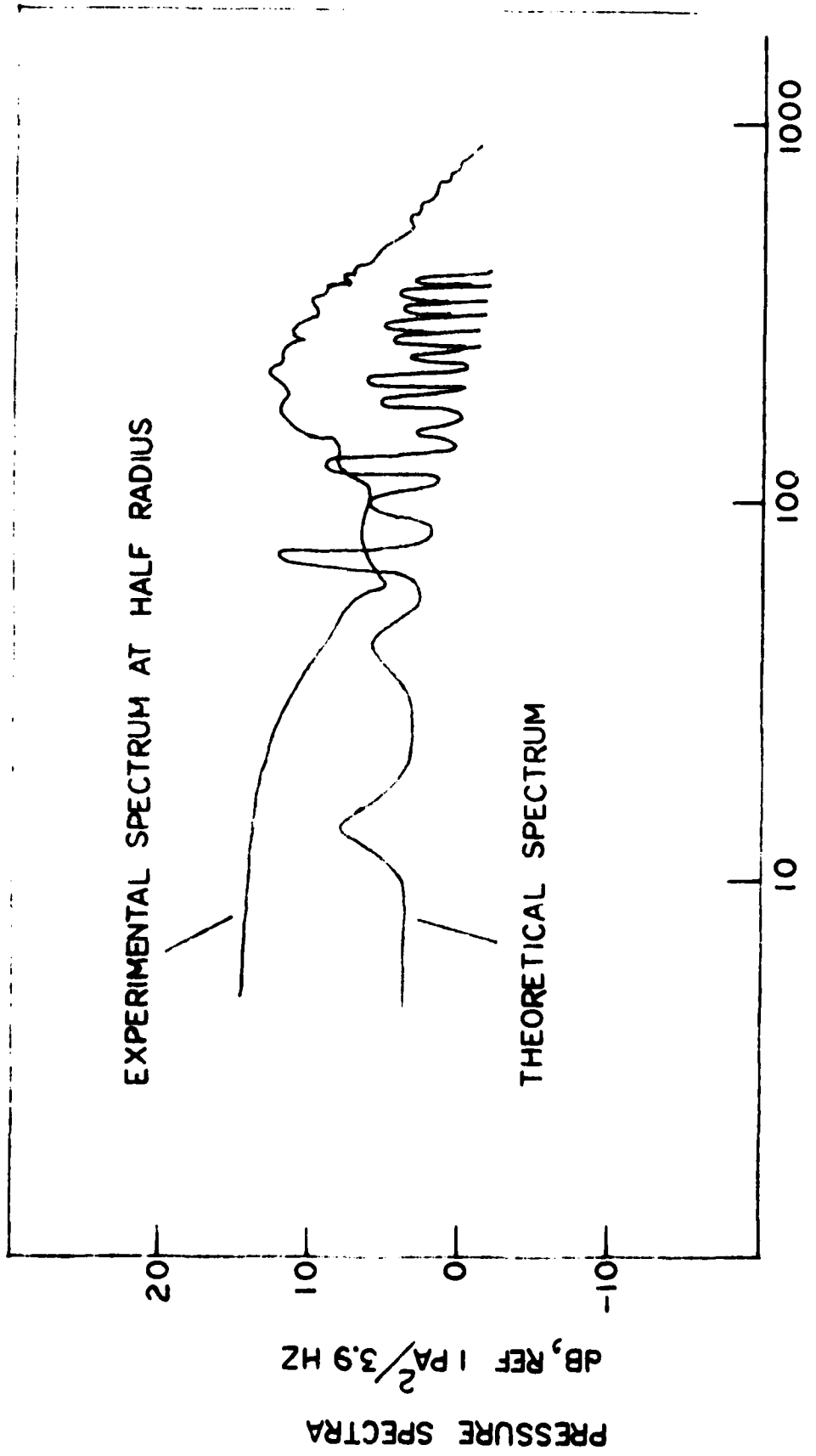

Figure IV-3. Comparison of theory and experiment for the long tube apparatus.

viscous effects in the theory is the culprit and future work should investigate this area.

C. Publications

1. Strahle, W. C. and Neale, D. H., "Turbulence Generated Pressure Fluctuations in a Rocket-Like Cavity," AIAA Journal, 19, pp 360-365 (1981).

2. Hegde, U. G. and Strahle, W. C., "Investigation of Turbulence Generated Pressure Fluctuations in Some Interior Flows," AIAA Paper No. 82-0175, (1982).

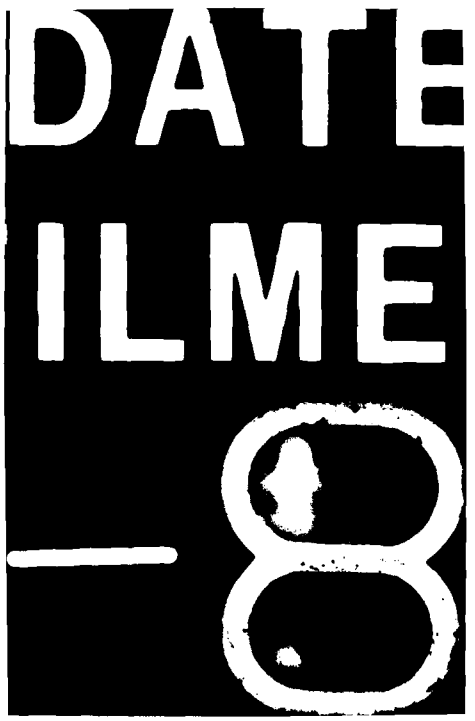
DATE:
ILME
8